October 2019

Spatial and Temporal Mapping of Distributed Precipitation, Surface and Groundwater Stable Isotopes Enables Insights into Hydrologic Processes Operating at a Catchment Scale

Alison Cole

SPATIAL AND TEMPORAL MAPPING OF DISTRIBUTED PRECIPITATION, SURFACE AND GROUNDWATER STABLE ISOTOPES ENABLES INSIGHTS INTO HYDROLOGIC PROCESSES OPERATING AT A CATCHMENT SCALE

A Thesis Presented

By

Alison A. Cole

Submitted to the Graduate School of the
University of Massachusetts Amherst in partial fulfillment
of the requirements for the degree of

MASTER OF SCIENCE

September 2019

Geosciences

SPATIAL AND TEMPORAL MAPPING OF DISTRIBUTED PRECIPITATION, SURFACE AND GROUNDWATER STABLE ISOTOPES ENABLES NEW INSIGHTS INTO HYDROLOGIC PROCESSES OPERATING AT A CATCHMENT SCALE

A Thesis Presented

By

ALISON A. COLE

Approved as to style and content by:

_____

David F. Boutt, Chair

_____

Stephen Burns, Member

_____

Julie Brigham-Grette, Member

_____

Julie Brigham-Grette, Chair, Department of Geosciences University of Massachusetts-Amherst

DEDICATION

To the most supportive people I know and to the ones who always send their unconditional love, my friends and family.

ACKNOWLEDGMENTS

I would like to thank my advisor, Dave F. Boutt for his years of guidance and support. I would also like to extend my thanks to the members of my committee Stephen Burns and Julie Brigham-Grette on all stages of this project. I also have to thank all the undergraduates and especially Marsha that helped with all of the sample collecting and analyses, this project would not have been completed if it hadn't been for their constant help and support.

I also want to thank the 10B for funding this research and providing expenses for all the necessary materials. I wish to express my sincerest thanks to all the individuals who volunteered their participation in this project. And a special thanks to Travis Drury in his effort in recruiting participants for our precipitation sampling network.

Finally, I have to thank all my friends who have constantly supported me (you know who you are) and encouraged me during my three years in Amherst. You have truly made these years fly by and I am so grateful for your friendship. This thesis would not have been finished without all the love I received from my family and friends. This is for you. And lastly, I have to thank my family who were always there when I needed extra support, love to you all.

ABSTRACT

SPATIAL AND TEMPORAL MAPPING OF DISTRIBUTED SURFACE AND GROUNDWATER STABLE ISOTOPES ENABLES INSIGHTS INTO HYDROLOGIC PROCESSES OPERATING AT THE CATCHMENT SCALE

SEPTEMBER, 2019

ALISON A. COLE, B.S., HOBART AND WILLIAM SMITH COLLEGES

M.S., UNIVERSITY OF MASSACHUSETTS-AMHERST

Directed by: professor David F. Boutt

Isotopic analyses of $\delta^{18}O$ and $\delta^{2}H$ of water through the hydrologic cycle have allowed hydrologists to better understand the portioning of water. Recently there have been strides to use the stable isotopes of meteoric waters in continental environments to make better interpretations related to climate and relationships between precipitation, surface water, and groundwater. In this study 11 precipitation (394 samples), 516 surface water (1917 samples), and 409 groundwater sites (1405 samples) across Massachusetts was used to create an isoscape for each respective water. All samples have been collected by volunteers throughout Massachusetts. Using these samples state meteoric water line: $\delta^{2}H = 7.7*\delta^{18}O + 9.8$, surface water line: $\delta^{2}H = 5.7*\delta^{18}O - 4.2$, and groundwater line: $\delta^{2}H = 6.5*\delta^{18}O + 2.9$ was created for the state of Massachusetts. The state meteoric water line was determined from a larger precipitation database consisting of 558 samples. The $\delta^{18}O$ values of the 558 precipitation samples across Massachusetts range from -23.6 to -1.30‰. The $\delta^{2}H$ values range from -183 to -6.7‰. The d-excess values range from -9.7 to 44‰. The $\delta^{18}O$ values of the 1,917 surface samples across Massachusetts ranged from -13.0 to -3.48‰, $\delta^{2}H$ values range from -84.3 to -16.3‰, and

deuterium excess (d-excess) values range from -9.72 to 24.9‰. The $\delta^{18}O$ values of the 1405 groundwater samples across Massachusetts ranged from -12.2 to -5.07‰. The $\delta^{2}H$ values range from -80.1 to -35.5‰. The d-excess values range from -0.2 to 35.2‰.

The $\delta^{18}O$ isoscape for each of the above-mentioned waters shows an isotopic separation along an east-west topographic gradient where isotopes were enriched in the eastern portion of Massachusetts and depleted in the western portion of Massachusetts. Precipitation, surface water, and groundwater show unique isotopic variability. The isotopic variability of precipitation is primarily due to seasonality, moisture source and differences in topography across Massachusetts due to the good agreement between climatic and environmental parameters. The $\delta^{18}O$ and $\delta^{2}H$ isotopic variability of surface water is due to a biasing of precipitation as well an enrichment due to an open water system as the surface water dataset correlates with surface water type and precipitation isotopic values. The $\delta^{18}O$ and $\delta^{2}H$ isotopic variability of groundwater is due to the dampening of surface water and precipitation because of hydrogeologic processes and the biasing of surface waters that have gone through open water isotopic variability. This dataset will elucidate isotopic variability in Massachusetts and provide a better understanding on how modern water is propagated through the hydrologic cycle. It will also become an important tool for both local and regional water management and water resources.

TABLE OF CONTENTS

Page

LIST OF TABLES

Table Page

LIST OF FIGURES

Figure Page

CHAPTER 1

INTRODUCTION

1.1 Stable Isotopes as a Hydrological Tracer

The exploration of the stable isotopes of water, oxygen and hydrogen isotope measurements, have increasingly improved our understanding of the behavior of water isotopes on both a large and small scale. They have been widely used as tracers to better understand hydrological and meteorological processes. Numerous studies have used stable isotopes in hydrological (Birkel et al., 2018, Yeh et al., 2014; Kendall and Coplen, 2001; West et al., 2014; Good et al., 2015; Landwehr et al., 2014; Jasechko et al., 2017; Jasechko et al., 2014), meteorological (Dutton et al., 2005; Gonfiantini et al., 2001; Puntsag et al., 2016; Ren et al., 2017; Celle-Jeanton et al., 2004; Earman et al., 2006; Lachniet et al. 2009), and paleoclimatology reconstruction studies (Landais et al., 2017; Risi et al., 2010; Dansgaard, 1953; Jouzel, 2003; Wang et al., 2008; Cruz et al., 2005a). Recently there have been strides to use the stable isotopes of meteoric waters in continental environments to make better interpretations related to climate and relationships between precipitation, surface water, and groundwater (Sprenger et al., 2018; Koeniger et al., 2016; Hervé-Fernández et al., 2016; Berry et al., 2017) both spatially and temporally through the use of isoscapes. In recent years there have been strides in isotopic studies both on a global and local scale. Such strides are described below.

In 2018, Sprenger et al. looked at the differences in the isotopic composition of mobile and bulk water and found that bulk soil water isotopes have an evaporative signal

but mobile water isotopes do not. The difference between mobile and bulk soil water isotopic composition motivated McDonnell (2014) to create the "two water world" hypothesis. This hypothesis states that mobile water is related to groundwater recharge and other sources that sustain streamflow and water of a slower flow region related with plant water uptake (Sprenger et al., 2018). It was determined that the differences between bulk and mobile waters are time variant and are linked to the volume and age of the mobile water. This study suggested that pore spaces varies depending on the soil properties and the soil water content but also sheds light on the activation of preferential flow paths and interactions between macropores and the soil matrix. Through measured and simulated data, it is suggested that the age of the water at pore scale influences the evaporative signal of soil water, where the younger mobile water is similar to the recharge signal but the water from a slower recharge region shows an evaporative signal due to soil evaporation.

Through the creation of isoscapes, local processes such as the one mentioned above, can provide spatial and temporal information that can be beneficial to water resources and management. Isoscapes are the end result of spatial and temporal distribution of isotopes, they are useful in describing environmental conditions across space and time (Bowen, 2010). They allow us to determine the interconnectivity in various systems, such ecological, hydrological, biogeochemical, or meteorological systems. In 2001, Kendall and Coplen created an isoscape for $\delta^{18}O$ and $\delta^{2}H$ in river waters across the United States. They used precipitation isotope data from the Global Network for Isotopes in Precipitation (GNIP) which was established by a collaboration between the International Atomic Energy Agency (IAEA) and the World Meteorological

Organization (WMO). Surface isotope data were collected from selected US Geological Survey (USGS) water-quality monitoring sites. Through extensive analyses of $\delta^{18}O$ and $\delta^{2}H$ in both precipitation and surface waters this study revealed distinct spatial and temporal differences in $\delta^{18}O$ and $\delta^{2}H$ of both river and meteoric waters. State Meteoric Water Lines were created based on geographic regions across the US. A regional pattern within the State Meteoric Water Lines were noted suggesting the large geographic areas are controlled by the humidity of the local air mass which conveys an evaporative enrichment and thus in the stream samples within the area. Spatially the $\delta^{18}O$ and $\delta^{2}H$ in river waters are in good agreement with each other but also reveal a distinct correlation with topographic contours and appear to be primarily reflecting the isotopic signal of precipitation.

In 2014 West, et al. presented the first isoscape for South Africa, an important intersection of oceans and climate systems and a center for socio-economic development. An isotopic study was performed on groundwater and tap water and the use of global models was used to determine how variable the isotopic composition of precipitation is across South Africa. Isotopic analyses of groundwater and tap water revealed a consistent spatial distribution of $\delta^{18}O$, $\delta^{2}H$, and deuterium excess for both but also showed an offset between groundwater and tap water, especially in major wildlife reserves across South Africa. When groundwater isotopes were compared with modeled isotopic compositions of precipitation across South Africa, these comparisons highlighted large differences which may have important implications for the estimation of the isotopic composition of precipitation in the area.

In 2017 Jasechko et al. used 20 years of spatial and temporal data of the stable isotopes of water in groundwater, river water, and precipitation to determine seasonal bias in groundwater recharge and young streamflow in the Nelson River basin of west-central Canada. A comparison of groundwater and precipitation was used to quantify seasonal bias in the groundwater recharge ratio. Amount-weighted precipitation isotopic compositions for long-term annual for temperatures less than and greater than 0 °C were calculated. These coefficients, along with the groundwater isotope data, were used to create an equation that would approximate differences in the groundwater recharge ratio. Values less than one imply that summer recharge ratios exceed winter recharge ratios or that groundwater recharge is biased by summer recharge, and values greater than one imply that winter recharge ratios exceeds summer recharge ratios or the groundwater is biased by winter recharge (Jasechko et al., 2017). It was determined that cold-season recharge ratios are greater than warmer season recharge ratios and that precipitation which falls within the past two or three months make up about one-quarter of river discharge.

The use of stable isotopes can not only provide insight on modern day processes but they can also provide a more thorough understanding of how changes in atmospheric circulation, changes in the size of the Arctic ice sheet, and changes in temperature affects the underlying mechanisms of the hydrologic cycle. In 2016 Puntsag et al. examined a 43-year record of precipitation isotope values. These values were collected at the Hubbard Brook Experimental Forest in New Hampshire, US. With this long-term precipitation isotopic dataset, Puntsag and others were able to look at how changes in the arctic vortex could potentially alter the source and isotopic values of precipitation. Over

the 43 years record they noted a positive trend in the deuterium excess values and a negative trend in both the $\delta^{18}O$ and $\delta^{2}H$. These trends were linked to increases in the interaction with air masses from the Atlantic Ocean and Arctic. It was suggested by an increase in scientific evidence that the extreme cold events that occurred during the fall and winter in the northeastern US are due in part by Arctic warming. This pattern is primarily due to Arctic warming, which is causes a decrease in the temperature gradient between the Arctic and mid-latitudes and leads to larger swells in the jet stream, pulling in more cold air southward into the mid-latitudes and the northeastern US.

1.2 Background

1.2.1 Massachusetts Climatology and Climatic Zones

Massachusetts is located in the northeastern portion of the United States and borders the Atlantic Ocean. It occupies 27,340 square kilometers where most of the state lies north of 42° latitude. Its north-south width is approximately 80.5 kilometers and 160.9 kilometers in the eastern portion (CoCoRahs) and its east-west length is approximately 321.9 kilometers including the Cape portion of the state. In elevation, Massachusetts ranges from less than 152.4 meters to 1062.8 meters above sea level where the western portion is characterized as mountainous, the central portion as rolling hills and coast as flat land with marshes and small lakes and ponds (CoCoRahs).

Massachusetts lies in the prevailing westerlies, a region that is dominated by westerlies, generally eastward air movement and drier continental airflow (Weider and Boutt, 2011 and CoCoRahs). Most of the precipitation events are sourced from colder regions: Arctic, Mid/North Atlantic and the Pacific. Massachusetts tends to see

precipitation events that originate from the Arctic, Mid-Atlantic, North Atlantic, Pacific, Continental, and the Gulf, Figure 1.1(Puntsag et al, 2016) which can be seen in figure 1.1.

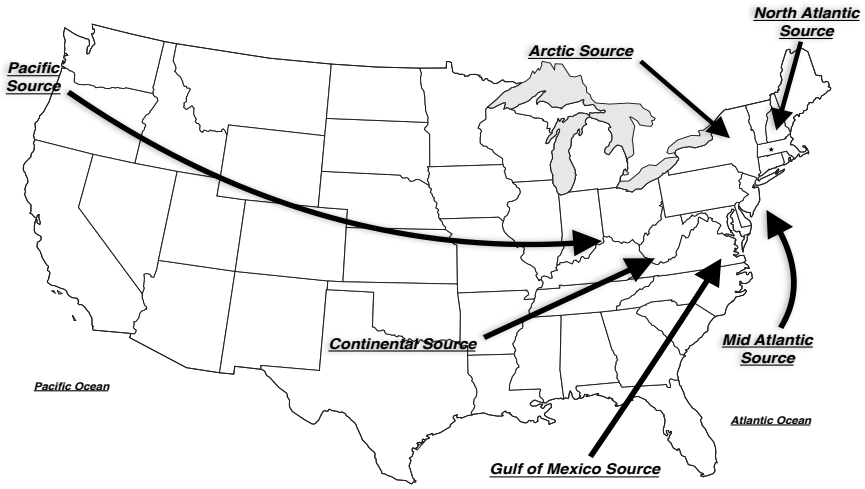

Figure 1.1: Massachusetts typically sees air masses that originate from six difference sources: Continental, Gulf of Mexico Mid-Atlantic, Pacific, North Atlantic and Arctic (Adapted from Puntsag et al., 2006).

Massachusetts receives approximately 1000 millimeters of rain annually and on average temperatures range from as high as 26°C and low as -8°C. This temperature variability is due to variance in topography. Because of this snowfall amount varies across the state making it difficult to determine a snowfall average (CoCoRahs).

The National Climatic Division Center divided the state into three climatological divisions: Climate Zone 1, Climate Zone 2, and Climate Zone 3 (NCDC). Throughout this paper these zones will be shortened to CZ1, CZ2 and CZ3. Though, according to the Koppen-Geiger Classification, Massachusetts has four climatological divisions with the fourth climate zone encompassing the coast and Cape Cod. For this study, we have

grouped together Climate Zone 4 with Climate Zone 3, thus dividing Massachusetts into only three Climate Zones.

Climate zone 1, the western division, encompasses an area from longitudes of -69.56 W to approximately -72.81 W and has an elevation over 304 meters It is characterized as a temperate forest (Jasechko et al., 2014) with an average annual temperature of about 46 °F. It covers approximately one fourth of the entire state and includes the low mountains of the Berkshires and parts of the Taconic Range (CoCoRahs). Climate zone 1 is considered the wettest and receives about two inches more of precipitation than climate zone 3, the coastal division. The mountainous nature of the western division is one reason this zone is considered the wettest zone (CoCoRahs).

Climate zone 2, the central division, covers roughly 50 percent of the state. It encompasses an area from -72.81W to approximately -71.38W. This zone is also considered a temperate forest and has an annual average temperature of 49 °F. Its average rainfall varies little to none compared to the western division. The elevation in the central division ranges from 152.4 to 304 meters.

Climate zone 3, the coastal division, includes the portion along the Atlantic Ocean from -72.81W to approximately -70.0W. The elevation in this division is less than 152.4 meters and consists of mostly flat land with numerous marshes. This zone is humid subtropical and is considered the driest zone during the summer months but the wettest during the winter months. Average annual amounts of snowfall increase from the coast westward. It has an average annual temperature of 50 °F (CoCoRahs).

1.2.2 Surficial Geology

Massachusetts is primarily composed of stratified glacial fluvial, outwash plains, glacial till and bedrock (Boutt, 2017; Weider and Boutt 2011; Stone et al. 2006). Today, most of the New England aquifers are dominated by sand and gravel as these aquifers are the most productive and yields more water than the underlying bedrock (Weider and Boutt, 2011; Boutt, 2017). The surficial landscape of Massachusetts was shaped by the retreat and melt of the last two continental ice sheets at the end of the Pleistocene. As the ice retreated, it deepened the valleys and moved large quantities of sediment and deposited it on top of pre-existing bedrock (Weider and Boutt, 2011; Stone et al. 2006). As the ice melted seasonally, it deposited sediment as stratified deposits in valleys at/or beyond the ice margin (Randall, 2001; Weider and Boutt 2011). This sediment mostly consists of subglacial till and debris-laden basal ice (Weider and Boutt, 2011). Coarse grained ice contact deposits are commonly found in broad lowlands and only occupy a small portion of the valley floor (Weider and Boutt 2011; Boutt, 2017; Stone et al., 2006). In major valleys where glacial lakes existed, lacustrine material is overlain by prograding deltas (Weider and Boutt, 2011). Bordering the valleys where highlands and high valleys exists, surficial materials are dominated by tills and tend to be located at higher elevations. These surficial deposits are primarily composed of poorly sorted silt, sand and gravel, surficial and unconsolidated materials and is overlain by lacustrine sediments and glacial-fluvial material reworked by streams (Weider and Boutt, 2011; Stone et al, 2006). Thicker tills have a higher clay content, a lower porosity and hydraulic conductivity and are normally found in drumlins or in the subsurface (Weider and Boutt, 2011). Figure 1.2 illustrates the glacial and post glacial deposits commonly

found in New England and emphasizes the relationship between coarse-grained deltaic deposits and fine grained marine deposits in the subsurface (Weider and Boutt, 2011; Stone et al., 1992).

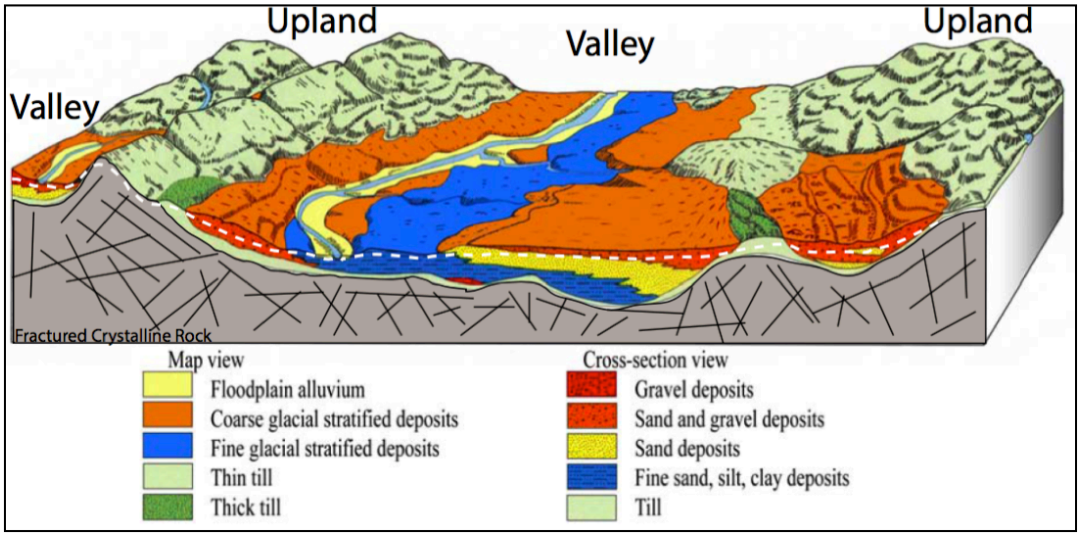

Figure 1.2: Schematic diagram of the surficial topography of Massachusetts (Stone et al., 2006) as created by the retreat of the last two ice sheets at the end of the Pleistocene.

The bedrock topography of Massachusetts consists of sediment packages, which tend to be thickest in the North-South trending valleys and follows the grain of the underlying low-porosity fractured crystalline and metamorphic bedrock (Weider and Boutt, 2011; Stone et al., 2006). In the south-eastern portion of Massachusetts localized areas of outwash derived sediment occur. Some of these coastal regions are heavily influenced by marine-derived sediments (Weider and Boutt, 2011). In New England the porosity of glacial till ranges from 10-20%, in stratified glacial fluvial the porosity ranges from 25-50% and bedrock has a small range in porosity; the percentage indicates the amount of water than can be stored. The permeability of till is roughly 10^{-6} to 10^{-4} m^2 while the permeability of stratified glacial fluvial is 10^{-3} to 10^{-1} m^2 (Fetter, 2000; Boutt, 2017).

1.2.3 Application of Stable Isotopes of Water and Atmospheric Influences

The interpretation and analysis of the stable isotopic composition of environmental water (precipitation, surface water, groundwater), $\delta^{18}O$ and $\delta^{2}H$, are an important tool in examining the hydrologic processes on a global and regional scale (Dansgaard 1964; Kendall and Coplen, 2001; Bowen 2010; Puntsag 2016). These analyses provide a better understanding for quantifying the spatially integrated effects of the water cycle and processes that occur in both the watershed and atmosphere (Bowen et al., 2011) as well as determining the relative amount of precipitation and groundwater in surface waters (Kendall and Coplen, 2001). Oxygen and hydrogen measurements of precipitation, surface water, and groundwater illustrate the effects of climate, topography, elevation, and various environmental parameters (Dansgaard, 1964; Welker, et al. 2012; Askers et al., 2017; Evaristo et al., 2015, Lee et al., 2010).

Several studies have established that a variety of climatological, geological, biological, and hydrological effects on the stable isotopic composition of water (Bowen, 2010; Ren et al., 2017; Gonfiantini et al., 2001; Reddy et al., 2006; Sprenger et al., 2018; Puntsag et al., 2016; Askers et al., 2017; McGuire and McDonnell, 2010; Mueller et al., 2014; Botter et al., 2010). Such studies have determined a negative relationship between $\delta^{18}O$ and elevation (Gonfiantini et al., 2001; Celle-Jeanton et al., 2003; Landwehr et al., 2014, Abach et al., 1968; Windhorst et al., 2013), a positive relationship between $\delta^{18}O$, temperature, distance inland, and latitude (Ren et al., 2017; Akers et al., 2017; Wu et al., 2015; Dutton et al., 2005; Ingraham and Taylor, 1991; Welker, 2000; Liu et al., 2010),

and a correlation between water vapor source and $\delta^{18}O$ (Puntsag et al., 2016; Timsic and Patterson, 2014).

Understanding the stable isotopes of water relies heavily on accurate and high precision measurements of $\delta^{18}O$ and $\delta^{2}H$ (Brand et al 2009; Wassenaar et al 2012). The concentrations of these isotopes are considered ideal tracers as they are part of the water molecule and can be easily sampled and preserved in groundwater, surface water, precipitation. Most importantly hydrogen and oxygen can preserve vital historical information (location, time, phase of precipitation) thus becoming a primary tool for hydrological, atmospheric, and meteorological studies (Timsic and Patterson, 2014; Bowen et al., 2007; Reddy et al., 2006). The stable isotopes of water are presented in the δ notation and represent the difference in heavy to light isotopes of water relative to the Vienna Standard Mean Ocean Water (VSMOW) (Sprenger et al., 2015; Craig, 1961; Gonfiantini et al., 1995). Although the delta notation is a dimensionless quantity the values are in per mil because of the low variation in the natural abundance of water stable isotopes (Coplen, 2011; Sprenger et al., 2016). High δ values indicate a higher $^{18}O/^{16}O$ and $^{2}H/^{1}H$ ratio relative to the Vienna Standard Mean Ocean Water. Low δ values indicate a lower $^{18}O/^{16}O$ and $^{2}H/^{1}H$ ratio relative to the Vienna Standard Mean Ocean Water. For the purposes of this paper, the term "enriched" will be used to describe water samples that have a high amount of heavy isotopes and "depleted" will be used to describe water samples that have a low amount of heavy isotopes. To determine the $\delta^{18}O$ and $\delta^{2}H$ of a water sample equation 1 is used:

$$\delta = \left(\frac{R_{Sample}}{R_{Standard}} - 1\right) \times 1000 \quad (1)$$

where R is the abundance ratio of the heavy and light isotopes (e.g., $^{18}O / ^{16}O$ and $^{2}H / ^{1}H$) and $R_{standard}$ is the VSMOW.

In a dual isotope plot, $\delta^{18}O$-$\delta^{2}H$, the relationship between $\delta^{18}O$ and $\delta^{2}H$ is defined as the global meteoric water line (GMWL) (Craig, 1961) and is described by the following equation:

$$\delta^{2}H = 8\ \delta^{18}O + 10 \quad (2)$$

This equation represents the relationship of $\delta^{18}O$ and $\delta^{2}H$ of surface waters globally and is an approximation of the mean world annual amount-weighted precipitation (Timsic and Patterson, 2014). This relationship is a result from Rayleigh processes, which is directly affected by temperature and pressure conditions during phase changes between liquid water and water vapor (Dansgaard, 1964).

More recently, the stable isotopes of water are analyzed together with deuterium excess (d-excess), equation 3, which was originally proposed by Dansgaard, 1964.

$$\text{d-excess} = \delta^{2}H - 8 * \delta^{18}O + 10 \quad (3)$$

D-excess is the y-intercept of the GMWL and is dependent on relative humidity, temperature, and kinetic isotope effects during evaporation (Coplen et al., 2001). Because of this, d-excess values are sensitive to evaporative processes and can be used to measure the contribution of evaporated moisture and allow for additional assessments of environmental conditions during the time of vapor formation or rainout. High d-excess values indicate more evaporated moisture has been added and low values indicate samples fractionated by evaporation (Timsic and Patterson, 2014; Coplen et al., 2001).

The line condition excess (lc-excess) is the deviation from the local meteoric line rather than the GMWL and is a good indicator of evaporative fractionation (Birkel et al., 2018). It is defined by: Lc-excess = $\delta^{2}H - a\delta^{18}O - b$ where *a* and *b* are the slope and y-intercept, respectively, of the SMWL

1.3 Research Objectives

Past and present studies on oxygen and hydrogen isotopes of water as a tracer have provided new insight on hydrogeological processes on both the regional and global scale. Surface and groundwater in the Northeast US are heavily impacted by intense land-use changes, urbanization, anthropogenic, natural factors, and climate change. Currently, more emphasis is being placed on managing waters with respect to quality and quantity. Through the use of isoscapes, we have a better understanding of hydroclimatic processes and their effect on water resources across spatial scales (Kendall and Coplen, 2001, Jaseckho et al., 2017, Birkel, et al., 2018, Allen et al., 2019). The use of stable water isotopes has become an inexpensive way to characterize the temporal and spatial variability of stable isotopes at a high resolution (Birkel et al., 2018) and can be used to inform management on both a local and regional scale. What we are lacking are fundamental answers to questions such as: a) What is the nature of surface and groundwater interaction in the northeast US? b) What are the potential impacts of climate change on stream flow generation, groundwater recharge, and groundwater storage? c) How important are extreme precipitation events to groundwater storage? And d) How or does groundwater surface water interconnectivity change spatially? This study aims to examine the relationship between modern precipitation, surface water, and groundwater

stable isotopes across Massachusetts via crowdsourcing and assess the isotopic variability of the waters and correlate this irregularity with each other. We also identify the spatial and temporal trends in seasonal surface and groundwater isotopes and two-week weighted precipitation isotopes and distinguish hydrologic and hydrogeologic trends in surface and groundwater respectively. Using these trends, we discuss and quantify the implications for either precipitation induced variability or variability due to open water systems, topographic differences, hydrogeologic and hydrologic processes in surface and groundwater stable isotopes.

CHAPTER 2

METHODS

2.1 Precipitation Sampling Network and Data Sources

558 precipitation samples were analyzed from 45 selected precipitation sites 11 of which were grouped together to create a precipitation isoscape network, Figure 2..

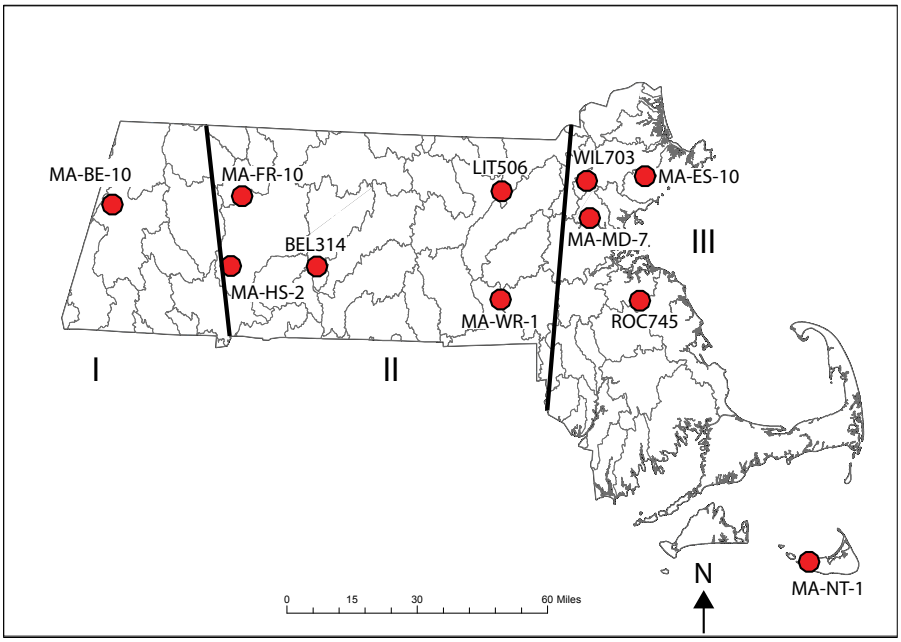

Figure 2.1: Index map indicating locations of volunteers in our precipitation isoscape network.

The 558 precipitation samples are a combination of grab samples taken from students and faculty at the University of Massachusetts-Amherst and eight of the precipitation sites are from the Western Massachusetts Watering Monitoring Program (WMWM) which is conducted by the Massachusetts state hydrologist. These eight sites are sampled monthly during the months of November through February.

For this study, the 11 sampling sites that form our precipitation isoscpae network will be the primary focus in this research as it provides a more consistent sampling

period. Sampling for the precipitation network took place from March 2017 to March 2018 and is still ongoing. Each volunteer was supplied with 30 30 mL high density polyethylene (HDPE) bottles, a small funnel, and a data collection sheet. Volunteers were asked to pour the contents of their rain gauge into a 1-L Nalgene bottle every day for a two-week time increment. At the end of the two weeks, the contents of the 1-L Nalgene bottle were poured into one 30 mL bottle which would result in a two-week composite sample. During the winter months, if there was snow, volunteers would place the snow into a saucepan and dip the bottom of the pan into hot tap water. The melted snow can then be measured by pouring it from the saucepan into the inner cylinder of the rain gauge. Every six months, volunteers would send their precipitation samples to the University of Massachusetts-Amherst. Samples were stored in plastic bags between the time of receipt and analysis. Stable isotope analyses were measured by a Picarro Cavity Ring Down Spectrometer (L2120-I) analyzer conducted at the University of Massachusetts- Amherst using the methods as described in section *2.4*.

Precipitation isotope analyses were screened and samples that had a deuterium excess less than -10‰ were discarded as these may have been compromised by evaporation during storage. A total of 40 precipitation samples were removed from the analysis. After screening the precipitation isotope data we calculated a two-week weighted averages following to remove any bias:

$$\text{Two-week weighted } \delta = P_{(2\text{-weeks})} \times \delta^{2}H \text{ or } \delta^{18}O \quad (4)$$

Where $P_{(2\text{-weeks})}$ is the two-week precipitation amount as provided by the volunteers. We then determined the average annual with a two-week weighted average following

$$\delta^{2}H \text{ or } \delta^{18}O = \sum P_i / \sum \delta^{2}H \text{ or } \delta^{18}O \quad (5)$$

Where P_i is the sum of the precipitation amount of the sampling site.

2.2 Surface Water Sampling Network and Data Sources

1,917 surface water samples from 556 surface water sites, Figure 2., across Massachusetts were analyzed for $\delta^{18}O$ and $\delta^{2}H$. Surface water sites were selected based on their spatial location in order to accurately represent a surface water isoscape for Massachusetts.

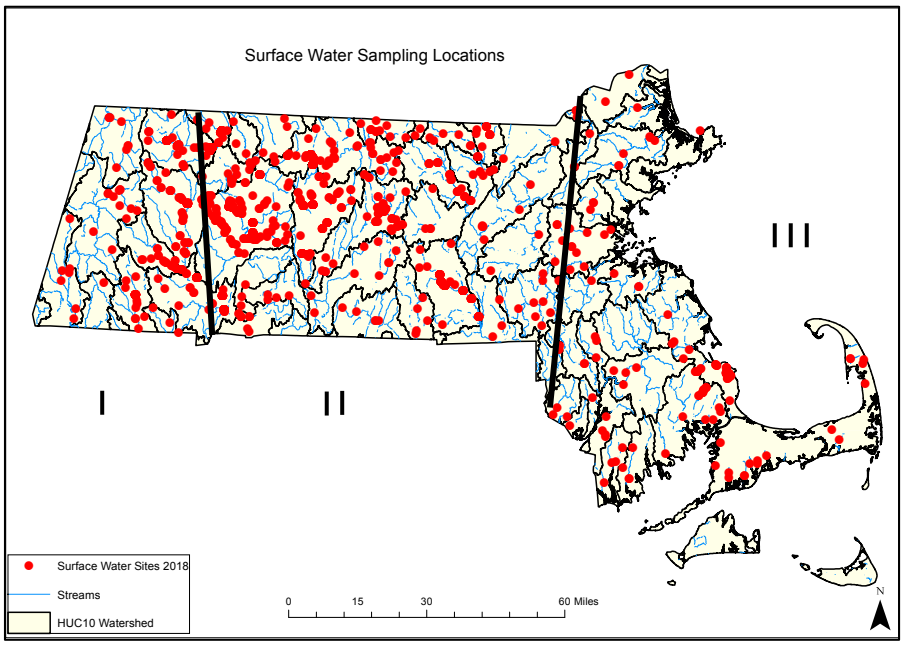

Figure 2.2: Index map showing the locations of surface water samples taken across Massachusetts. Black lines represent the boundaries between climate zones as determined by the National Climate Division Center.

Surface water samples were collected from 2011-2018. Samples were collected from faculty and students from the University of Massachusetts-Amherst, watershed associations (Nashua Watershed, Charles River Water, Blackstone, Quabbin, and Chicopee River Watershed), and the acid rain monitoring (ARM) project which is further

described in *section 4.1.6*. 250 sites are from the ARM project, three sites are from the Connecticut River watershed, 17 sites re from volunteers, 11 sites are from the Nashua River watershed, one site is from the National Ecological Observatory Network, three are from the NWIS, six are from Blackstone, 259 sites are from the University of Massachusetts-Amherst database, and 14 are from the WMWM.

Volunteers were supplied with one or more 15mL high density polyethylene (HDPE) bottles and a data collection sheet. On the day of sampling, volunteers were asked to thoroughly clean out the HDPE bottle with the to be collected water and then refill the bottle to the top to limit the amount of headspace and securely fasten the cap. Samples were returned to the University of Massachusetts where they were prepared for analysis within a few weeks upon arrival. Samples were stored in plastic bags between the time of receipt and analysis. Stable isotope analyses were measured by a Picarro Cavity Ring Down Spectrometer (L2120-I) analyzer conducted at the University of Massachusetts- Amherst and later screened.

2.3 Groundwater Sampling Network and Data Sources

1,406 groundwater samples from 409 groundwater sites across Massachusetts were analyzed for $\delta^{18}O$ and $\delta^{2}H$, figure 2.3.

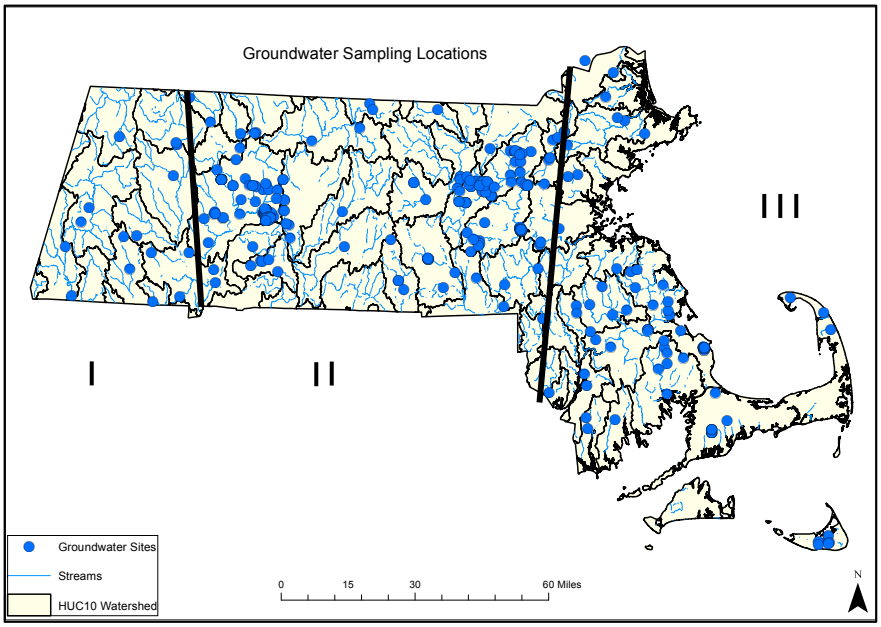

Figure 2.3: Index map illustrating the location of all groundwater samples (409 sites).

Groundwater samples were collected from 2011-2018. 38 sites are from the US Geological Survey Eastern Massachusetts Water Monitoring (USGS-ESWM), six sites are from the US Geological Survey in Nantucket, 79 sites are from the US Geological Survey National Water Information System (USGS-NWIS), four are from the US Geological Survey Snow Pond, 95 sites are from the University of Massachusetts-Amherst database with sampling done by students and faculty, 71 sites are from Safewell (a well testing company for real estate transactions), and 126 sites are from volunteers across Massachusetts.

Each volunteer was supplied with one or more 15mL high density polyethylene (HDPE) bottles and a data collection sheet. On the day of sampling, volunteers were asked to first run the tap water for a couple seconds, thoroughly clean out the bottle with the tap water and the fill the bottle to the top to limit the amount of headspace and securely fasten the cap. Samples were returned to the University of Massachusetts-

Amherst where they were prepared for analysis within a few weeks upon arrival. Samples were stored in plastic bags at room temperature between the time of receipt and analysis. Stable isotope analyses were measured by a Picarro Cavity Ring Down Spectrometer (L2120-I) analyzer conducted at the University of Massachusetts- Amherst and later screened

2.4 Analytical Methods - Picarro

Stable isotope compositions were measured by a wavelength scanned cavity ring-down spectrometry on un-acidified samples by a Picarro Cavity Ring Down Spectrometer (L2120-I) analyzer (Berden et al. 2000). Cavity ring-down spectroscopy is a direct absorbing technique which is conducted with eight pulse or continuous light sources which is significantly more sensitivity than the conventional absorption spectroscopy. The Picarro is equipped with a high precision vaporizer (A0211) and fitted with a CTC PAL auto-sampler. International reference standards (IAEA, Vienna, Austria) were used to calibrate the instrument to the VSMOW scale. To remove possible memory effect between samples, each sample was analyzed six times and the results of the first three injections were discarded. To further reduce memory effect, we adopted a modified version of a technique by Penna et al. 2012 where samples are grouped by water source and location. Three reference waters that isotopically bracket the sample values were run alternately with the water samples: Boulder, Colorado, Tallahassee, Florida and Amherst, Massachusetts, were used for a total of nine times each in every sample tray. The average values for these standards are -16.5‰, -2.6‰, and -7.5‰ respectively. These standards were calibrated with the Greenland Ice Sheet Precipitation (GISP), Standard

Light Antarctic Precipitation (SLAP) and Vienna Standard Mean Ocean Water (VSMOW) from the IAEA (Kendall and Coplen, 2001). The results were calculated based on a rolling calibration so that each sample is determined by the three standards closest in time to that of the sample.

2.5 Analytical Methods - HYSPLIT Model

To examine moisture variability in oxygen and hydrogen for precipitation, HYPSLIT models were performed. Following the trajectory methods from Puntsag et al. 2016 and Welker et al. 2008, the National Oceanographic and Atmospheric Administration Air Resources Laboratory Hybrid Single-Particle Lagrangian Integrated Trajectory (HYSPLIT) model, online version, was used (Draxler, et al. 2003). This model calculates air mass position through time using pressure, temperature, wind speed, vertical motion, and solar radiation inputs (Welker et al. 2008). We used the Global Data Assimilation System (GDAS) 2006-current set archived by the NOAA for meteorological data. Air mass position history was computed within the HYSPLIT model by a Lagrangian three-dimensional air mass velocity algorithm, which is typically used for atmospheric trajectory analyses (Stein et al., 2015). We used 72 h as our total back trajectory run time for air masses at 500m above ground level and at a start of 18 UTC. From Welker et al. (2008) a 72-hour time period adequately identifies precipitation source areas for most of the samples. Previous studies have also suggested that precipitation in North America falls within one to two days after moisture is transported from the Pacific Ocean, Atlantic Ocean or the Gulf of Mexico (Welker, 2008). From Puntsag et al. (2015) the 500 meters above ground level parameter used in

the back-trajectory analysis shows a more easterly component. This represents the surface air being drawn into an approaching frontal system. The end location parameter for the trajectory points was projected back to where the precipitation data was gathered from, the Amherst weather station (42.3861N and -72.5375 W).

CHAPTER 3

PRECIPITATION

3.1 Results

3.1.1 Averages and meteoric water lines

The $\delta^{18}O$ values of the 558 precipitation samples across Massachusetts range from -23.6 to -1.30‰, $\delta^{2}H$ values range from -183 to -6.7‰, and d-excess values range from -9.7 to 44‰. Average $\delta^{18}O$, $\delta^{2}H$ and d-excess values are -7.9 (±4), -50 (±29), and 13 (±6) ‰ respectively. The precipitation data points form a flattened ellipse on the GMWL, figure 3.1. Most of the data points lie along the GMWL with a few plotting off onto the evaporative enrichment line.

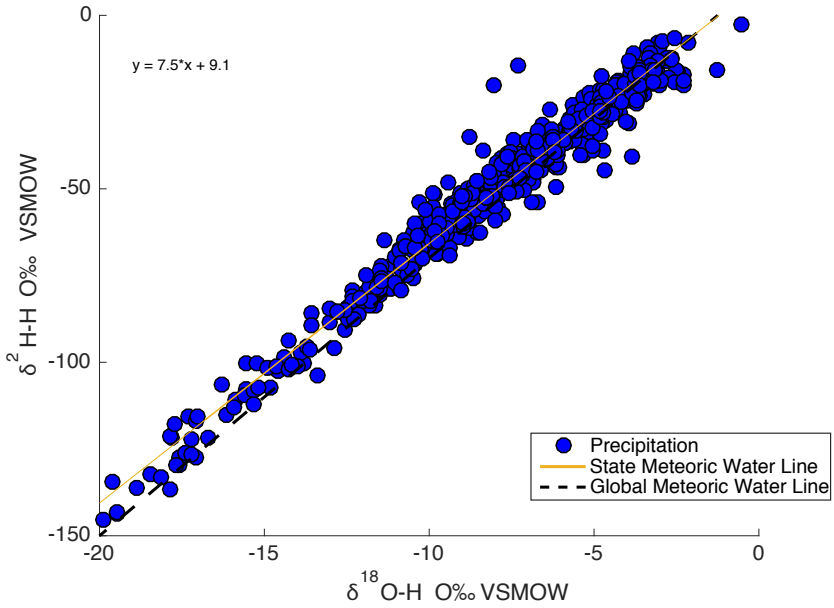

Figure 3.1: Dual isotope plot of the all precipitation data (558 analyses).

The state meteoric water line (SMWL) was generated from the 558 unweighted stable isotope values: $\delta^{2}H = 7.5*\delta^{18}O + 9.1$, figure 3.1. The slope of the SMWL is 7.5 and the y-intercept is 9.1. Only 1% of the 558 precipitation samples had d-excess values

less than 10‰, suggesting that our samples did not undergo significant secondary evaporation during storage.

394 out of the 558 precipitation samples are from our precipitation isoscape network, figure 3.2. $\delta^{18}O$ values range from -18 to -1.3‰, $\delta^{2}H$ values range from -132 to -8.0‰ and d-excess values range from -7.3 to 44‰. Average $\delta^{18}O$, $\delta^{2}H$ and d-excess values are -7.6 (±3), -47 (±24), and 12 (±6)‰ respectively. The precipitation data points form a flattened ellipse on the GMWL. Most of the data points fall on the GMWL with a few plotting off onto the evaporative enrichment line, figure 3.2.

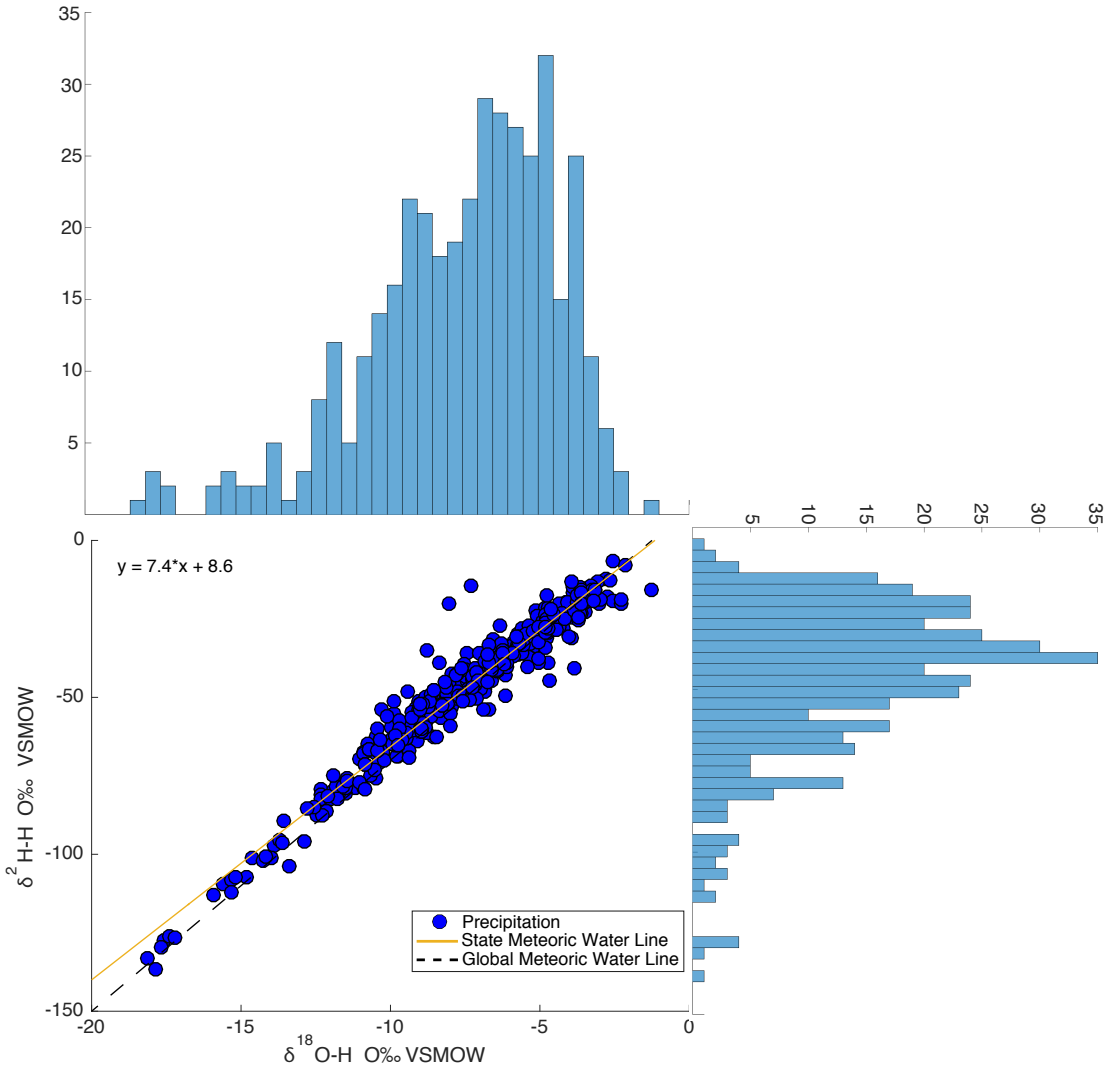

Figure 3.2: Dual isotope plot of samples in the isoscape precipitation network (394 precipitation samples 11sampling sites). The frequency of $\delta^{18}O$ and $\delta^{2}H$ are plotted on their respective axes.

The SMWL generated from the unweighted stable isotope values of the 394 precipitation samples is $\delta^{2}H = 7.4*\delta^{18}O + 8.6$. Figure 3.2 exhibits a bias towards enriched values. To account for this and to better represent the SMWL, the 394 precipitation samples were binned by 0.5‰. After binning the precipitation samples, we determined a new SMWL: $\delta^{2}H = 7.7*\delta^{18}O + 9.8$, figure 3.3. This equation is our official description of the SMWL for Massachusetts and will be referred to throughout this paper and in the figures.

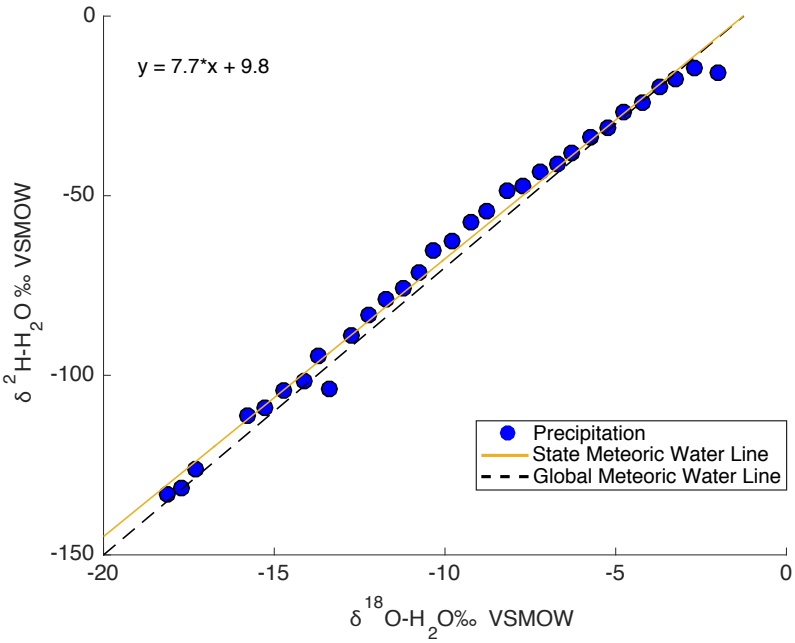

Figure 3.3: The 394 precipitation isoscape samples were binned by 0.5‰. This is the SMWL calculated from the 31 unweighted stable isotope values.

To determine the accuracy of our precipitation analyses, we correlated our precipitation isotope analyses with two precipitation sites from Massachusetts collected by Vachon et al., 2010 where he determined the monthly weighted stable isotopic

averages of two precipitation sites: MA13-Boston, MA01-Cape Cod. Weighted monthly averages from our network were calculated and compared to the weighted monthly averages of MA13 and MA01. Standard deviations between our weighted monthly averages and the weighted monthly averages of MA13 and MA01 ranged from 1.9 to 0.2‰. These values are shown in Table 3.1. Because the standard deviations do not exhibit a large variability and are in good agreement with each other we therefore concluded that our precipitation samples accurately represent the precipitation isotopic composition for the state of Massachusetts.

	MA isoscape	MA01	MA13	STD
Jan	-10.1	-8.5	-9.3	0.8
Feb	-11.7	-7.6	-8.3	2.2
Mar	-12.0	-9.3	-8.3	1.9
Apr	-7.0	-4.1	-5.9	1.4
Ma	-6.0	-4.9	4.7	0.7
Jun	-7.0	-5.4	-9.1	1.9
Jul	-5.0	-4.5	-4.7	0.2
Aug	-5.0	-6.6	-5.1	0.9
Sept	-6.0	-4.7	-4.6	0.8
Oct	-7.0	-6.2	-0.7	0.7
Nov	-8.0	-6.0	-7.2	1.0
Dec	8.0	-8.4	-7.9	0.3

Table 3.1: Comparison of monthly $\delta^{18}O$ for precipitation samples, MA01 and MA13 from Vachon et al., 2007 to average monthly $\delta^{18}O$ in our precipitation isoscape network. All values are in per mil.

3.1.2 Seasonal Patterns

Two week-weighted $\delta^{18}O$ values reported for each of the stations were plotted as a time series, figure 3.4.

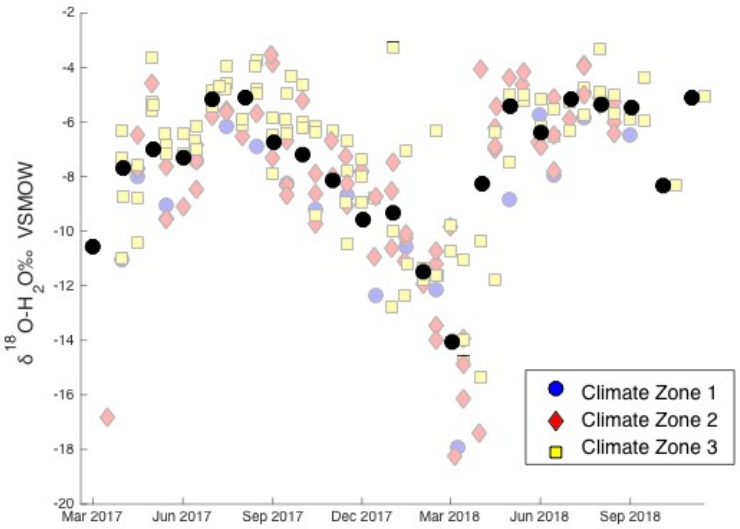

Figure 3.4: Time series of two weighted precipitation $\delta^{18}O$ values (399 analyses). A moving monthly average is illustrated by a black dot. Precipitation samples have been categorized based on climate zones.

From March 2017 to July 2017 $\delta^{18}O$ values increase and then decrease from September 2017 to March 2018, figure 3.4. After March 2018 $\delta^{18}O$ values begin to increase rapidly and then begin to plateau in July 2018. The maximum $\delta^{18}O$ average is noted during late summer months, August and September, and the minimum $\delta^{18}O$ average is noted during late winter/early spring months, February and March, figure 3.4.

Following the methods of von Freyberg et al. (2018), using the equation below, a sine-wave was fitted through the reported precipitation isotope values to better quantify the seasonal isotope cycles.

$$Cp(t) = A_p \sin(2\pi f t - \phi P) + kP \quad (6)$$

In equations 6 and 7, A_p is the amplitude for precipitation (‰), ϕ is the phase of the seasonal cycle, t is the time in years, f is the frequency (yr^{-1}), and k (‰) is a constant which describes the vertical offset of the isotope signal (von Freyberg et al., 2018).

These equations allow us to quantify the amplitude of the seasonal isotope cycles and the coefficients, *a*, *b,* and *c* by using multiple linear regressions where *a*, *b,* and *c* are the amplitude, phase, and offset respectively.

$$Cp(t) = a_p \cos(2\pi f t) + b_p \sin(2\pi f t) + cP \quad (7)$$

The amplitude A_p is then determine by:

$$Ap = \sqrt{a_p^2 + b_p^2} \quad (8)$$

Using these equations, we fit sine curves to the isotope data for all the precipitation isoscape samples, figure 3.5, as well as each individual station. We found the equation of the sine fitted line to be:

$Cp(t) = -2.07 \cos 2\pi \times \frac{1}{365} x \times -1.88 \sin 2\pi \times \frac{1}{365} x + -7.82.$ Precipitation varies approximately -5.4‰ seasonally.

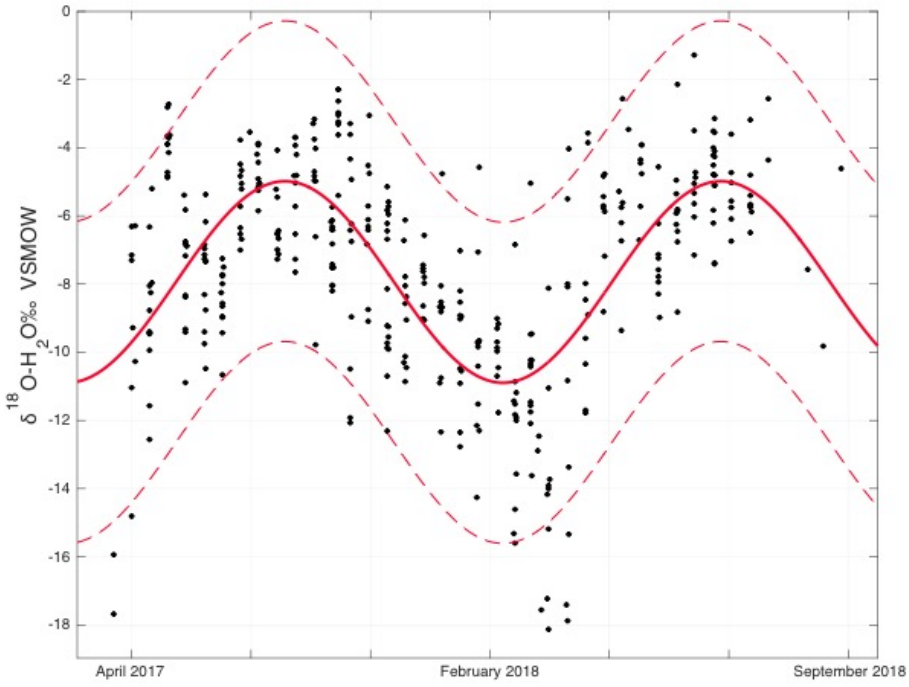

Figure 3.5: Time series of precipitation isotopic analyses with a seasonal fitted red line where the dashed red lines indicate the 95% confidence interval boundary, using nonlinear least squares method where the amplitude is 2.7‰.

Amplitudes and offsets for each of the 11 precipitation sites were determined and compared with the calculated amplitudes and offsets of MA01 and MA13 (Vachon et al., 2007) to determine the accuracy of our calculated values. These values can be seen in Table 3.2. The amplitude for each of our precipitation site ranges from 2.14 to 4.00 (±0.66) and the offset ranges from -6.12 to -9.39‰ (±0.99).

	Seasonal Amplitude	offset (per mil)
MA-BE-10	2.91	-9.39
MA-HS-2	2.79	-8.39
BEL314	2.14	-7.84
MA-FR-10	2.84	-8.97
LIT506	3.77	-8.34
ROC-745	2.48	-7.20
MA-ES-2	2.93	-7.55
MA-MD-07	2.41	-7.21
WIL703	4.00	-8.11
MA-NT-1	3.04	-6.12
MA-WR-1	2.69	-7.73
MA01	1.70	-6.30
MA13	1.90	-6.50

Table 3.2: Seasonal amplitude and offset for each precipitation site along with MA01 and MA13 from Vachon et al., 2007.

Additionally, seasonal local meteoric water lines were determined for winter and summer. Winter months includes October to March and summer months includes April to September. The LMWL for summer generated from the unweighted stable isotope values sampled during the summer months is $\delta^{2}H = 6.6*\delta^{18}O + 2.6$. The LMWL for winter is $\delta^{2}H = 7.4*\delta^{18}O + 11$. Figure 3.6 illustrates the relationship between the winter

and summer LMWLs. The slope, y-intercept, and d-excess of the winter LMWL is larger than the slope and y-intercept of the summer LMWL.

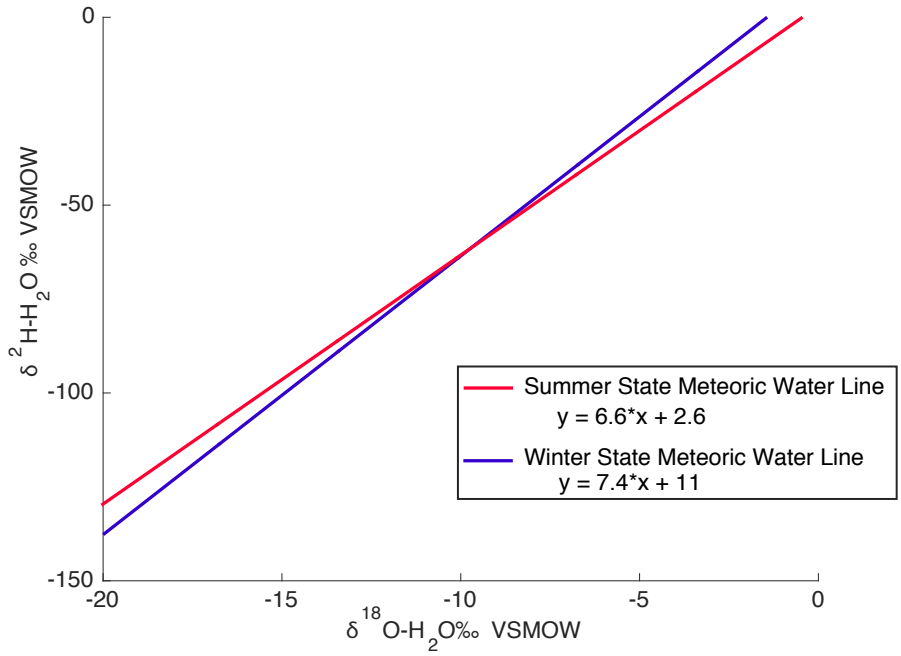

Figure 3.6: State meteoric water lines for both summer and winter.

Median, minimum and maximum $\delta^{18}O$ values were determined over a 12-month period and correlated to determine any statistical significance associated over this period, figure 3.7. Over this 12-month interval, the $\delta^{18}O$ values are variable where on average there is a -5.4‰ range. This same method was performed on the $\delta^{2}H$ values, though it was determined that this plot illustrated similar patterns to that of the box plot of $\delta^{18}O$ values and did not illustrate any new information, figure 3.8. Over a 12-month period $\delta^{18}O$ values steadily decreased from September to March and

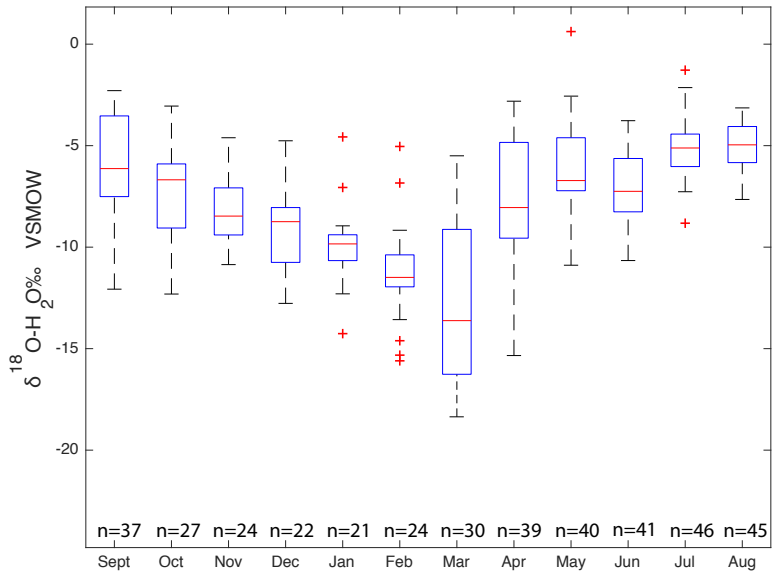

Figure 3.7: Comparison of $\delta^{18}O$ values for each sampling month.

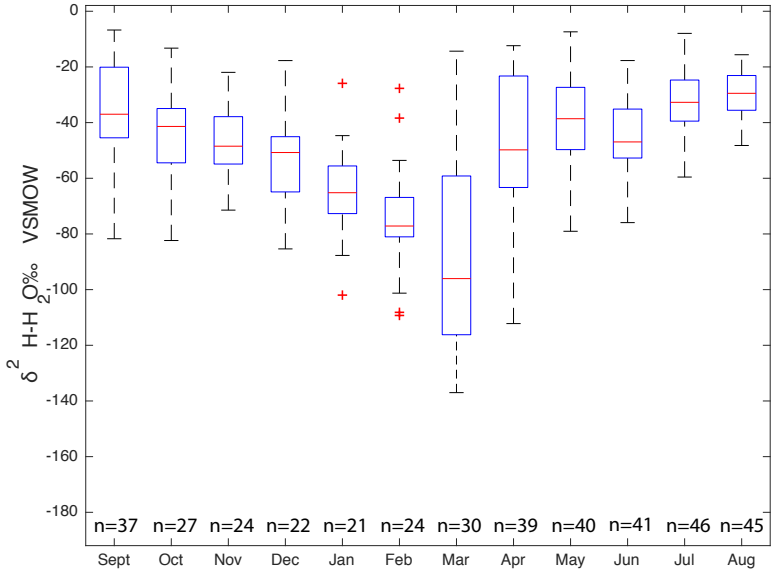

Figure 3.8: Comparison of $\delta^{2}H$ values for each sampling month. These results are almost identical to the $\delta^{18}O$ summary and do not add any additional information.

then drastically increased from March to April where values continued to increase from April to May. Between May and June $\delta^{18}O$ values decreased and then increased from

June to August. Maximum $\delta^{18}O$ values occur during the late summer and early fall months and minimum $\delta^{18}O$ values occur during the late winter and early spring months, specifically March.

These maximum and minimum $\delta^{18}O$ values are primarily driven by temperature and moisture source differences. HYSPLIT models were run for one station in each of the climate zones for the month of March and June in 2018, figure 3.9 and figure 3.10.

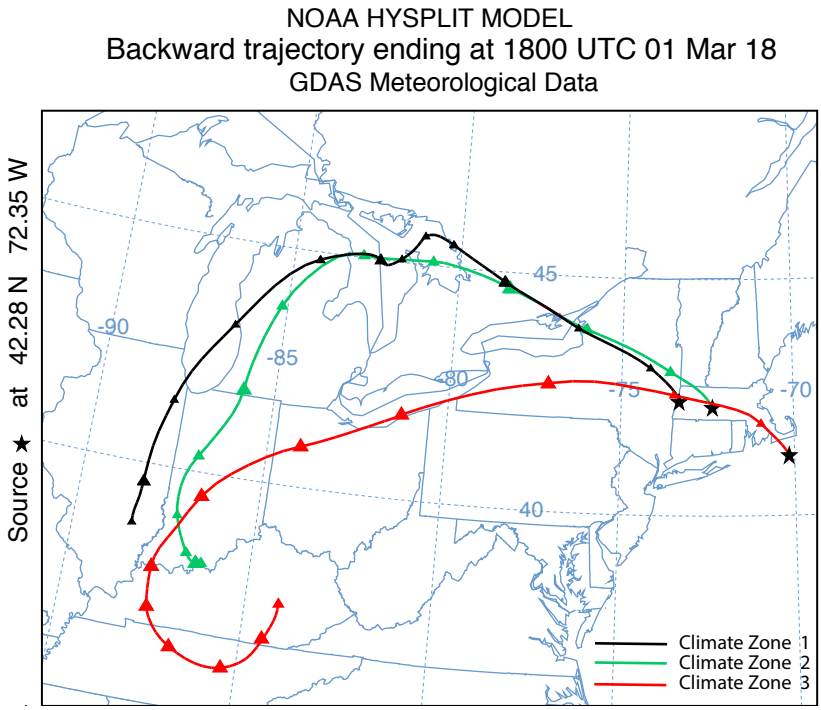

Figure 3.9: Back trajectories for the month of March. Runs showed that all stations had air masses that were a continental source.

These months were chosen as they exhibited the largest difference in $\delta^{18}O$ values. A total of six trajectory analyses were performed. Stations MA-BE-10 (CZ1), BEL314 (CZ2), and MA-NT-1(CZ3) were used for the HYSPLIT models.

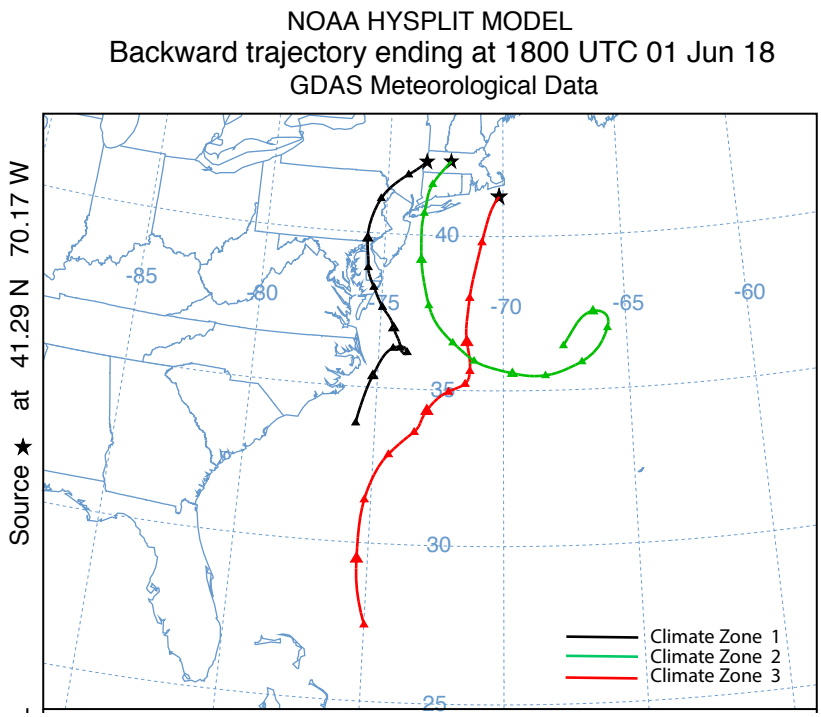

Figure 3.10: Back trajectories for the month of June. Runs showed that all stations had air masses that were sourced from the Mid-Atlantic.

Model results indicate that in March all three stations saw air masses sourced from the continent and in June all stations saw air masses sourced from the Mid-Atlantic, figure 3.9, figure 3.10 respectively.

Average monthly air temperature data was collected from the NOAA National Centers for environmental information, Climate at a Glance: Statewide Mapping from 2017 to 2018 as that time period encompasses the sampling period for the precipitation samples. Two-week weighted monthly $\delta^{18}O$ averages were correlated with temperature and time, figure 3.11 and figure 3.12.

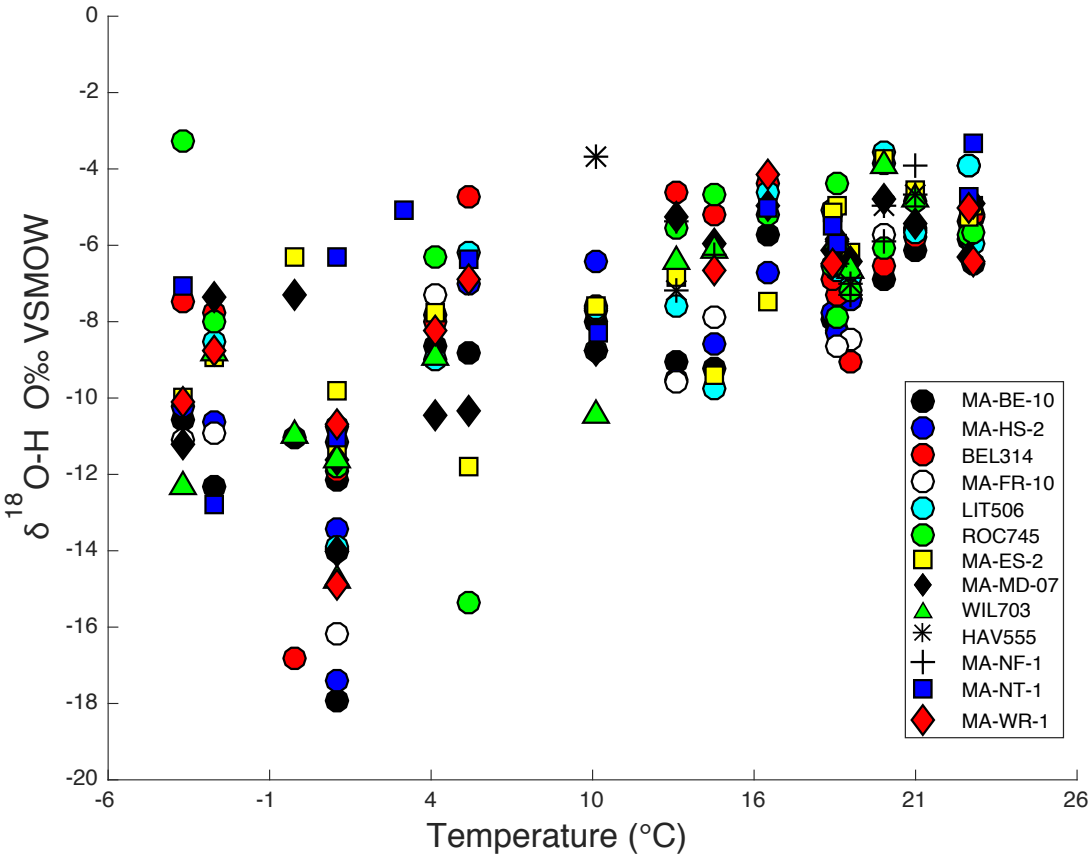

Figure 3.11: Two-week weighted $\delta^{18}O$ averages plotted as a function of monthly average air temperature. As temperature increases $\delta^{18}O$ values become larger.

Figure 3.11 illustrates a positive correlation with $\delta^{18}O$ values and temperature, there is an enrichment as temperature increases. It should be noted that the isotopic values are more variable at cooler temperatures and less variable at warmer temperatures. Figure 3.12 shows a good agreement between time and temperature where temperature follows the same $\delta^{18}O$ temporal pattern.

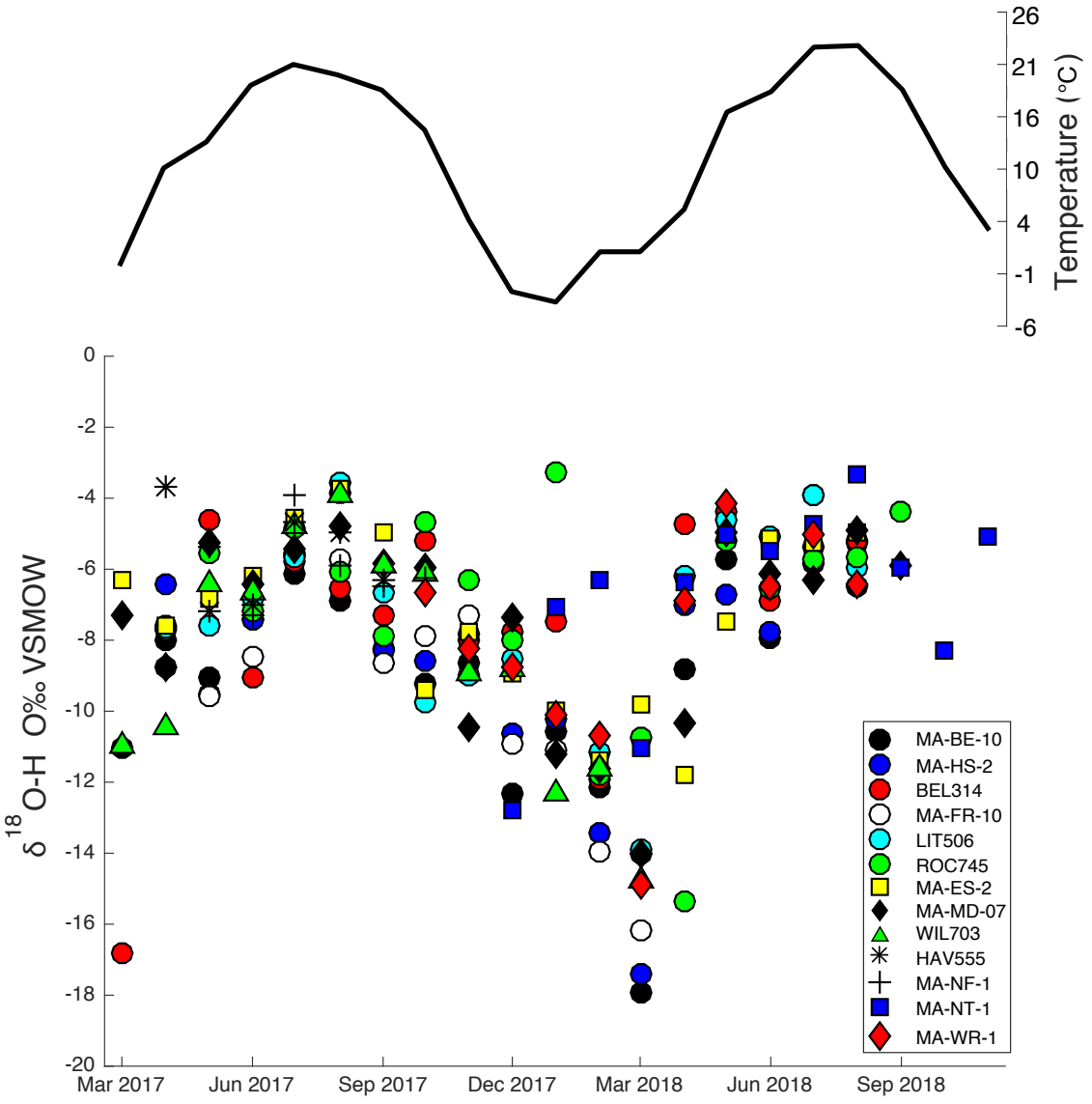

Figure 3.12: Relation of the two-week weighted monthly $\delta^{18}O$ averages for precipitation samples in the isoscape network and monthly air temperature.

3.1.3 Correlation of Environmental Parameters

Using equations 4 and 5, two-week weighted averages were determined for each of the 11 precipitation sampling sites, grouped into their respective climate zones and then related to their respective elevation. Elevations within the sampling sites range from four meters to 331 meters. MA01 (Cape Cod) and MA13 (Boston) from Vachon, 2010

were plotted alongside our sampling sites and categorized into CZ3, to illustrate the accuracy of our precipitation analyses. Sites located at a higher elevation have higher $\delta^{18}O$ values than sites located at a lower elevation. Figure 3.13 illustrates a strong negative correlation with elevation as well as topography.

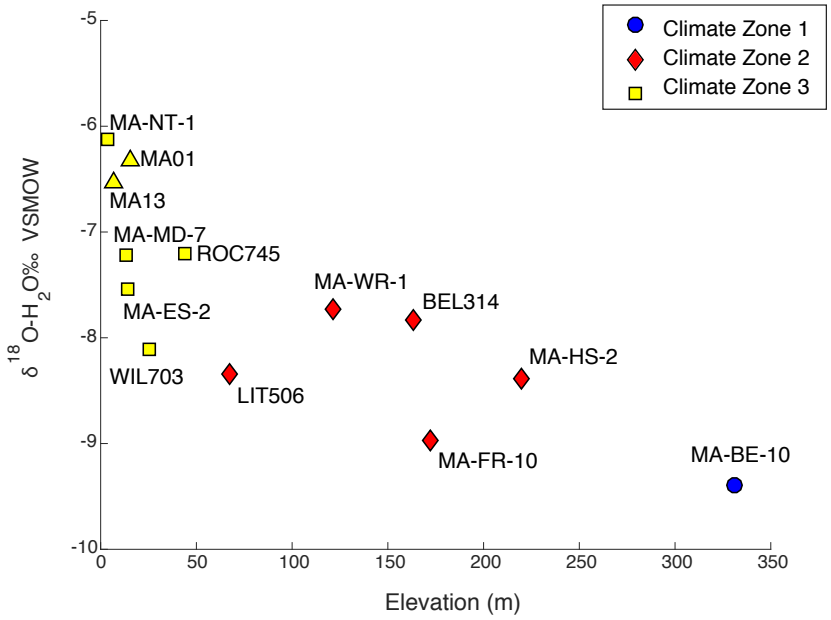

Figure 3.13: Relation of two-week weighted total averages of the 11 volunteer precipitation samples with elevation. Precipitation sites are categorized based on climate zone location. Sample sites from Vachon et al (2010), are illustrated by triangles.

Sampling sites located at a higher elevation and in CZ1 and are more depleted than samples located at a lower elevation CZ3 which are more enriched.

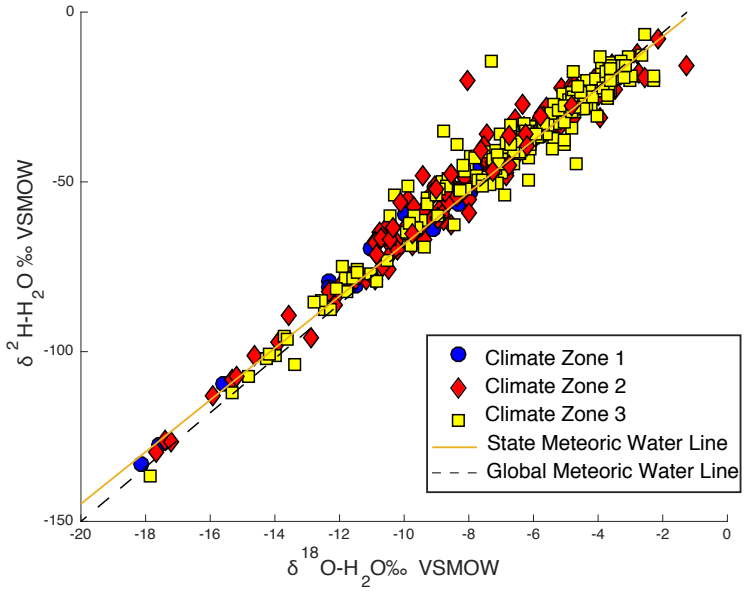

Figure 3.14: Dual isotope plot of precipitation isoscape samples grouped by climate zone.

To determine geographic variability, all precipitation samples were categorized into climate zones. Figure 3.14 illustrates the correlation between climates zones and isotopic composition. Two–week weighted $\delta^{18}O$ values in climate zone 3 range from -18.3 to -4.87‰, two-week weighted $\delta^{2}H$ values range from -132 to -23.0‰, and d-excess values range from 8.86 to 20.93‰. Two–week weighted $\delta^{18}O$ values in climate zone 2 range from -23.6 to -1.28‰, $\delta^{2}H$ values range from -183 to -7.95‰, and d-excess values range from 5.60 to 44.2‰. Two–week weighted $\delta^{18}O$ values in climate zone 1 range from -17.9 to 2.29‰, $\delta^{2}H$ values range from -136.68 to -6.74‰, and d-excess values range from -7.29 to 44.0‰. The average $\delta^{18}O$, $\delta^{2}H$, and d-excess value in climate zone 1 are -9.25 (±3), -59.8 (±27), and 14.2 (±3) ‰ respectively. The average and $\delta^{18}O$, $\delta^{2}H$, and d-excess value in climate zone 2 are -7.90 (±3), -49.2 (±24), and 13.5 (±5)‰ respectively. The average and $\delta^{18}O$, $\delta^{2}H$, and d-excess value in climate zone 3 are -6.92 (±3), -43.0

(±23), and 11.0 (±7) ‰ respectively. Average $\delta^{18}O$ values for each climate zone are shown in figure 3.15 and revelas climate zone 1 is more depleted and has the lowest $\delta^{18}O$ values than climate zone 2 and climate zone 3 which is more enriched and has the highest $\delta^{18}O$ values.

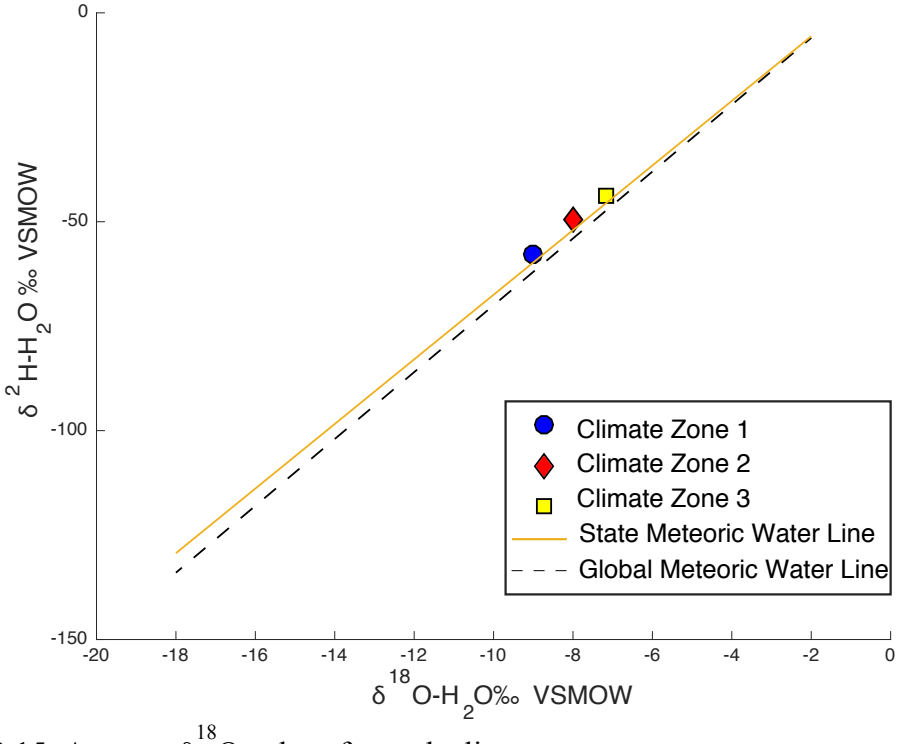

Figure 3.15: Average $\delta^{18}O$ values for each climate zone.

Local meteoric water lines (LMWLs) were calculated for each of the climate zones and plotted, figure 3.16. The climate zone 1 LMWL generated from the 31 samples located in that region is $\delta^{2}H = 7.8*\delta^{18}O + 13$, climate zone 2 LMWL generated from the 186 samples located in that region is $\delta^{2}H = 7.5*\delta^{18}O + 9.3$ and the climate zone 2 LMWL generated from the 178 samples located in that region is $\delta^{2}H = 7.4*\delta^{18}O + 8.1$.

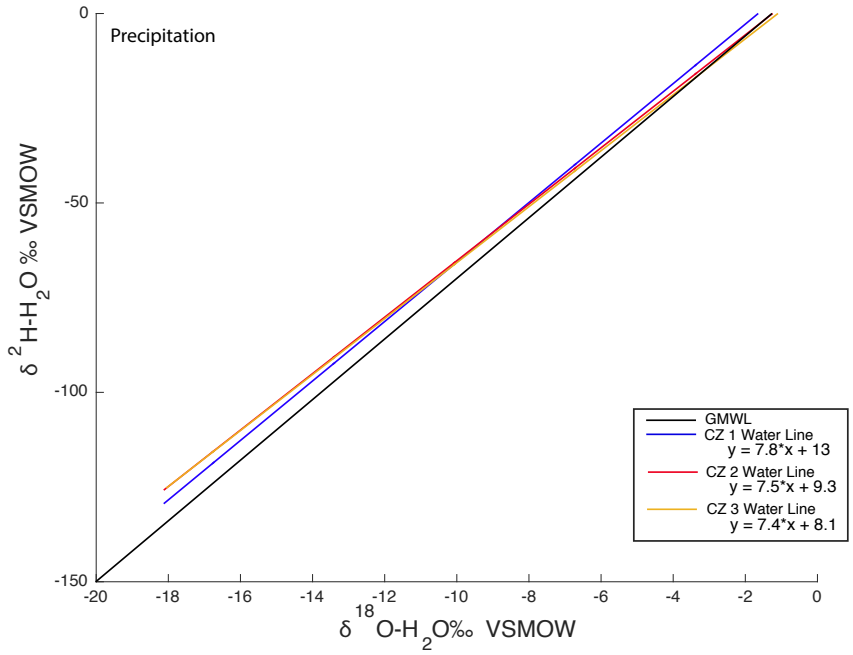

Figure 3.16: Dual isotope plot of calculated climate zone water lines for 394 precipitation samples.

3.1.4 Spatial Distribution of $\delta^{18}O$ and $\delta^{2}H$ values

Average $\delta^{18}O$ values were spatially plotted, figure 3.17, $\delta^{18}O$ values range from -6.82 to -9.42‰. From east to west the $\delta^{18}O$ values of precipitation become depleted. More enriched precipitation samples are located along the coast and western portion, the most enriched sample is located on Cape Cod. More depleted samples are located inland, the most depleted precipitation sample is located near the eastern border of Massachusetts.

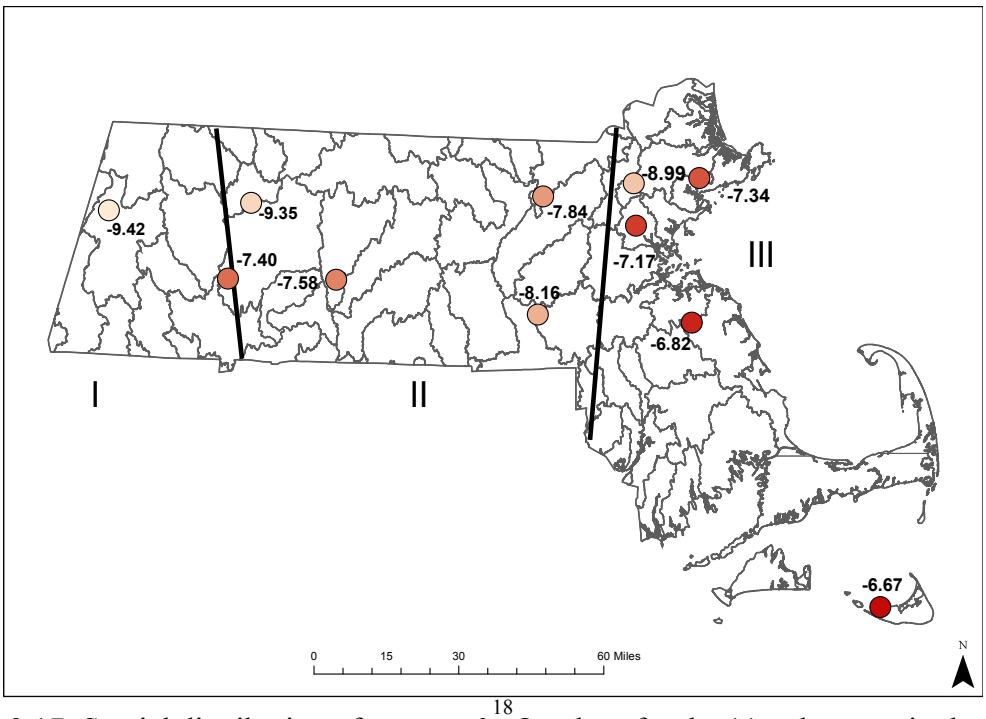

Figure 3.17: Spatial distribution of average $\delta^{18}O$ values for the 11 volunteers in the precipitation sampling network.

CHAPTER 4

SURFACE WATER

4.1 Results

4.1.1 Averages and meteoric water lines

The $\delta^{18}O$ values of the 1,917 surface samples across Massachusetts range from -13.0 to -3.48‰, $\delta^{2}H$ values range from -84.3 to -16.3‰, d-excess values range from -9.72 to 24.9‰, and lc-excess values range from -20.8 to 12.2‰.

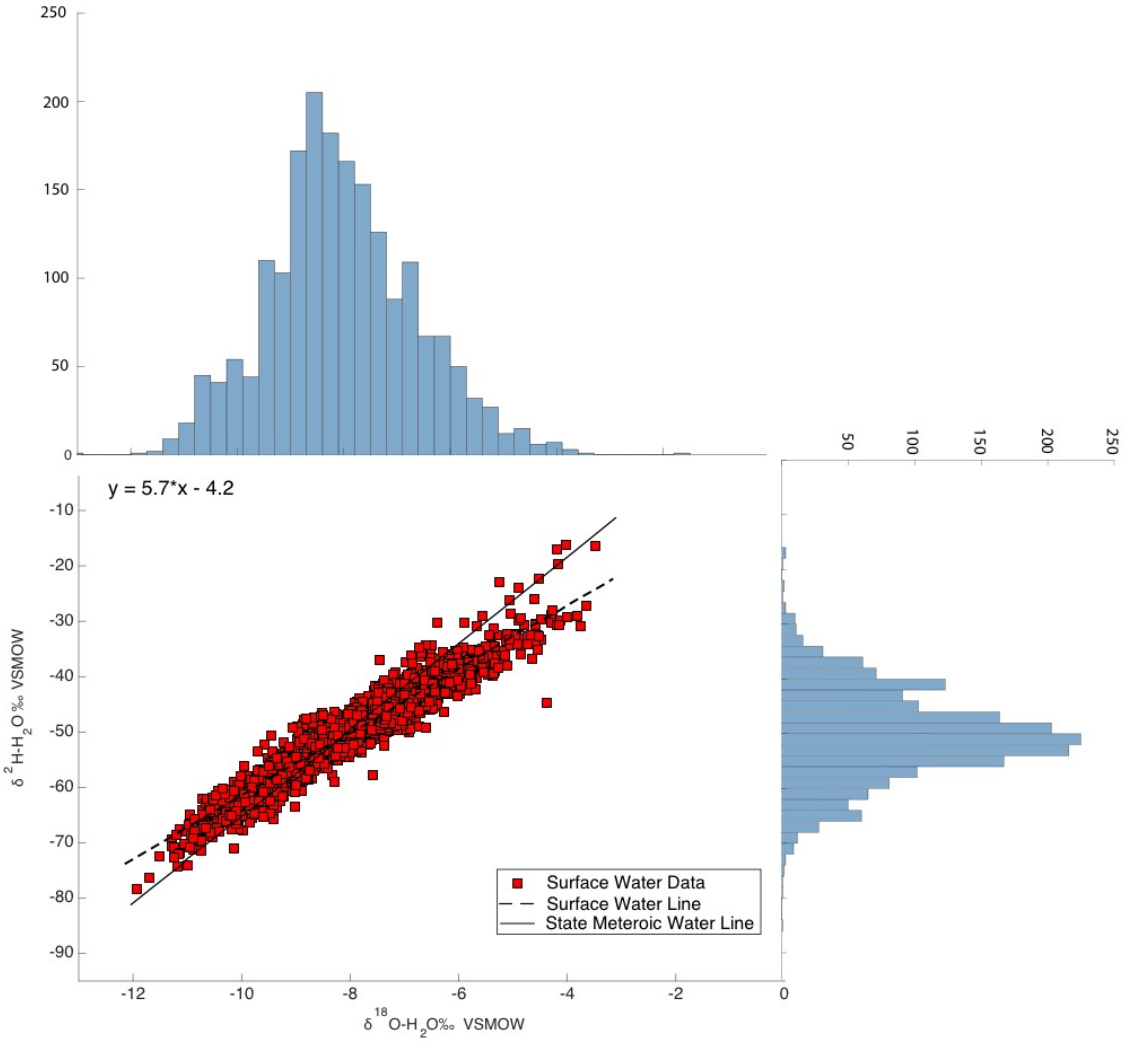

Figure 4.1: Relation between $\delta^{18}O$ and $\delta^{2}H$ surface water values for the entire dataset (1917 surface water samples 556 surface water sites) with histograms of $\delta^{18}O$ and $\delta^{2}H$ on their respective axes.

The dataset forms a flattened ellipse that lies slightly above and angled to the SMWL, figure 4.1 illustrates the isotopic variability. The data points that fall above the SMWL indicate high deuterium excess values and sample points that fall off the SWML, indicate open system enrichment. A histogram for both $\delta^{18}O$ and $\delta^{2}H$ were plotted and juxtaposed with the dual isotope plot of surface water analyses, figure 4.1 to illustrate the distribution and frequency of the $\delta^{18}O$ and $\delta^{2}H$ values. At approximately $\delta^{18}O$ -6‰ and $\delta^{2}H$ -45‰ there is an increase in the number of surface water samples, indicating where surface water samples start to plot off the SMWL. Average $\delta^{18}O$, $\delta^{2}H$ and d-excess values for surface water are 8.0 (±1), 50.0 (±8), and 14.1 (±4) ‰ respectively. The Surface Water Line (SWL), which is the unweighted linear regression generated from the 1,917 surface water samples is $\delta^{2}H = 5.7*\delta^{18}O - 4.2$.

4.1.2 Seasonal Patterns

To determine seasonal variability and its effect on surface water, samples were grouped by sampling month. Medians, minimum, maximum, 25^{th} and 75^{th} percentile, and 1% interquartile ranges were determined for each of the 12 months. Figure 4.2 illustrates that the $\delta^{18}O$ values of surface water experiences seasonal variability where samples experience a depletion and enrichment throughout a hydrologic year. A similar plot for $\delta^{2}H$ was determined to be invaluable as it showed a similar pattern as the $\delta^{18}O$ plot and did not provide any new information.

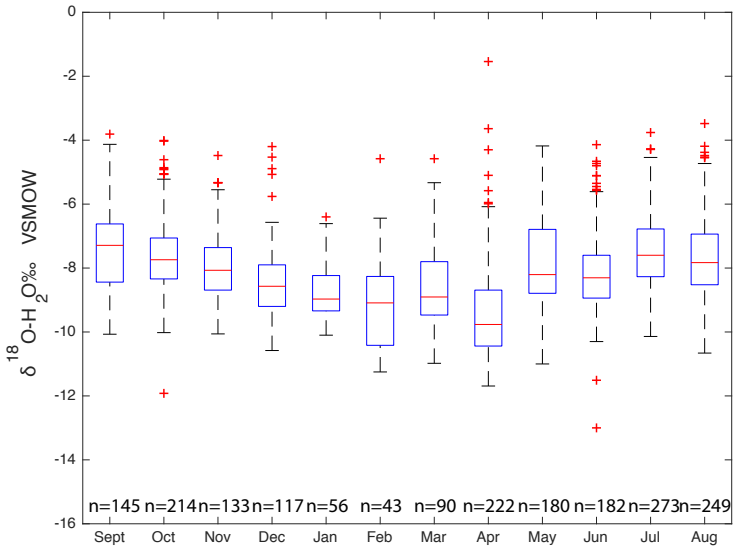

Figure 4.2: Comparison of $\delta^{18}O$ values (1917 samples) for each sampling month.

From September to February the $\delta^{18}O$ median values decrease and then slightly increase in March and decreases again in April. From April to August $\delta^{18}O$ values slowly increase. It should be noted that because each sampling did not have a consistent number of samples there will be an inherent bias between months with a larger number of samples and those with a smaller number of samples. From September through August 145, 214, 133, 117, 56, 43, 90, 222, 180, 182, 273, and 249 samples were taken respectively. Following the methods as described in *section 3.1.2* a sine-wave was fit through the reported surface water isotope values sampled from 2016 to 2018 as most of the surface water sampling took place during this time. A sine wave fit was used to better describe the seasonal isotope cycles: $Cp(t) = -0.45 \cos 2\pi \times \frac{1}{365}x \times -1.03 \sin 2\pi \times \frac{1}{365}x + -8.48$. Using equation 8, we found the amplitude of the sine curve to be 1.13‰, illustrated in figure 4.3. Surface water experiences a seasonal range of 2.26‰.

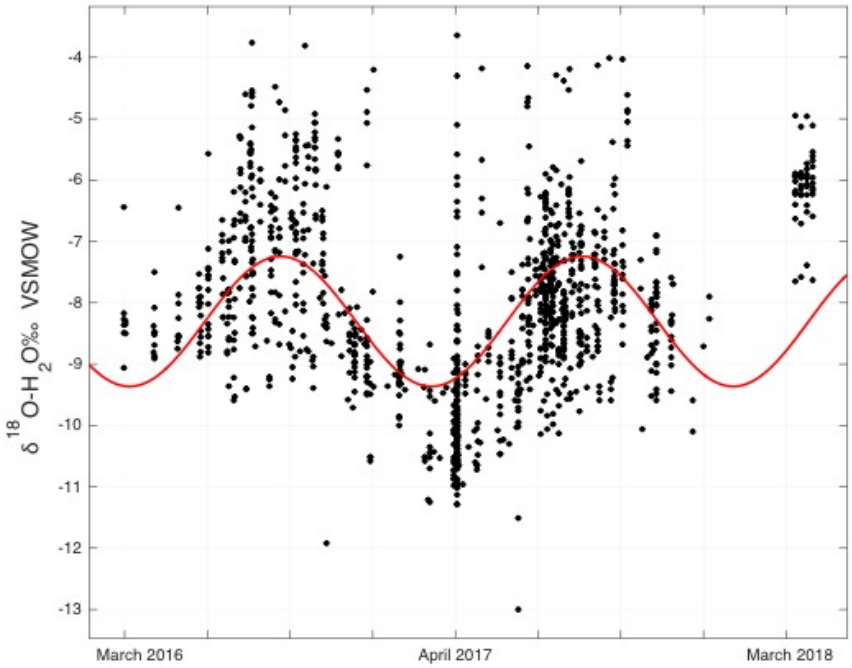

Figure 4.3: Time series of surface water isotopic analyses with a seasonal fitted red line using nonlinear least squares method where the amplitude is 1.13‰.

4.1.3 Hydrologic Effects and Environmental Parameters

As discussed earlier, there are a variety of parameters that effect the $\delta^{18}O$ values of surface water including waters in an open or closed system, latitude, and geographic location. To determine the hydrologic effects on the isotopic composition of surface water, all surface water samples were sorted and grouped by the type of surface water sample (i.e. river/stream, reservoir/lake, and spring/seepage). 1603 samples were categorized as river/stream, 227 samples were categorized as reservoir/lake, and 20 were grouped into the spring/seepage category, figure 4.5. Sixty-seven samples were unknown. Medians, 25th and 75th percentile, and 1% interquartile ranges were determined for each of the surface water type, figure 4.4. Surface water sites that had

multiple samples were averaged and the average value was used in the comparison plot, figure 4.4. Variability is noted between the three groups of surface water type. Though between the three groups, there is more isotopic variability in reservoir/lake. The range for each surface water type differ between 1.32 to 1.09‰. The minimum and maximum for river/stream, spring/seepage, and reservoir/lake of water are -11.7 and -3.48‰, -10.6 and 4.18‰, and -11.9 and -4.01‰ respectively.

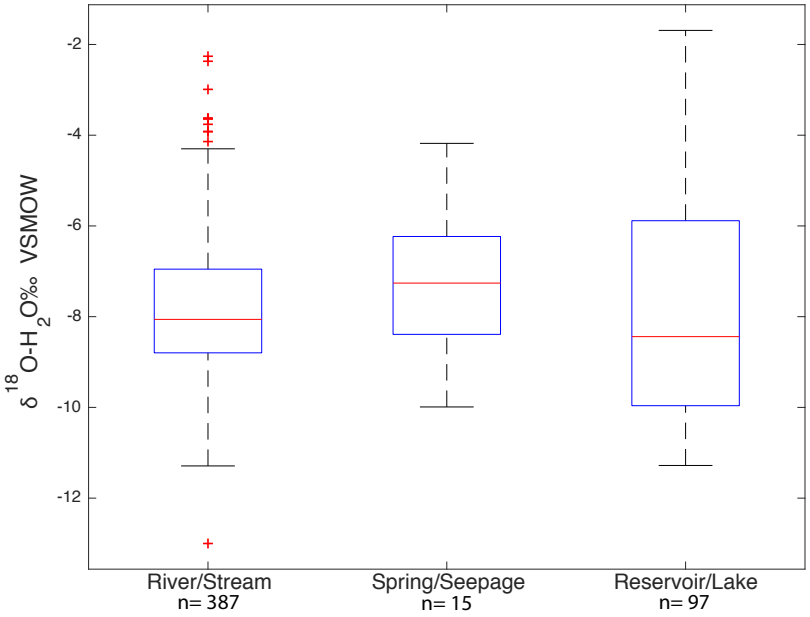

Figure 4.4: Box plot of sample average surface water type.

Surface water type dynamics on the isotopic compositions of said samples are illustrated in the dual isotope plot seen in figure 4.5. The average $\delta^{18}O$, $\delta^{2}H$, d-excess, and lc-excess for moving bodies of water are -8.13 (±2), -50.8 (±10), 14.3 (±5), 2.03 (±4) ‰ respectively. The average $\delta^{18}O$, $\delta^{2}H$, d-excess, and lc-excess for spring/seepage are -8.43 (±2), -45.2 (±11), 14.2 (±4), -3.52 (±4) ‰ respectively. The average $\delta^{18}O$, $\delta^{2}H$, d-

excess, and lc-excess for stagnant bodies of water are -7.61 (±2), -48.1 (±13), 12.9 (±6), -4.03 (±5) ‰ respectively.

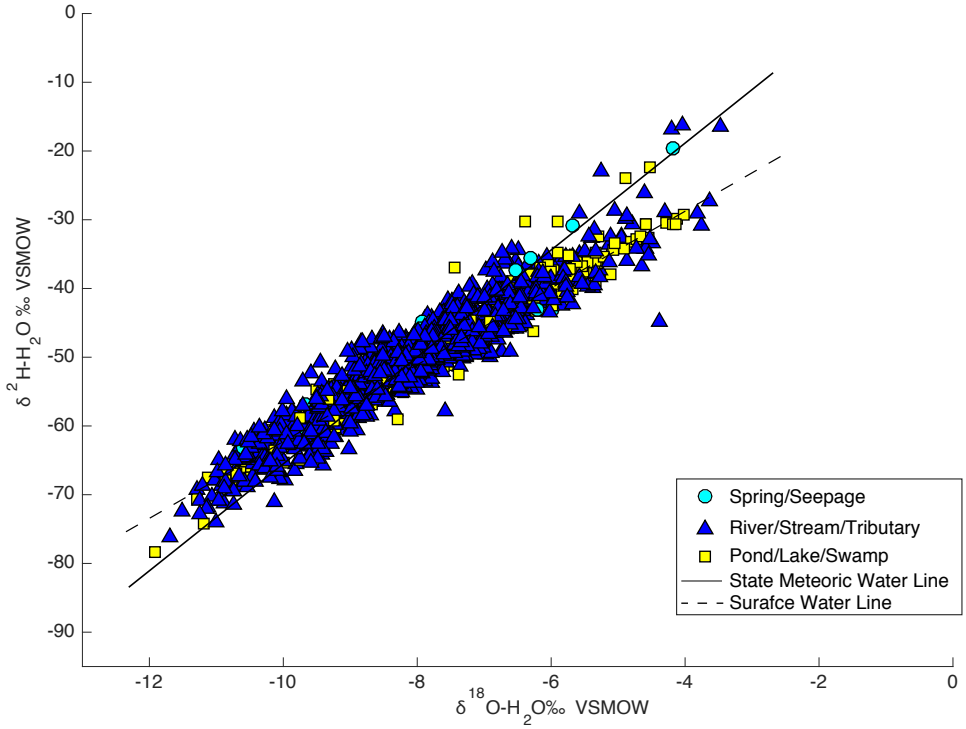

Figure 4.5: Dual isotope plot categorized based on the type of surface water sample.

To compare environmental parameters and their effects on the $\delta^{18}O$ values of surface water, sample analyses were compared to their orientation i.e. latitude and longitude. Figure 4.6 exhibits a negative relationship between $\delta^{18}O$ values and latitude. Figure 4.7 shows a positive relationship between $\delta^{18}O$ values and longitude. The r^2 values for latitude and longitude are 0.0001 and 0.0007 respectively. Although the r^2 values are not informative, they are rather used to illustrate the correlation between $\delta^{18}O$ values and latitude and longitude.

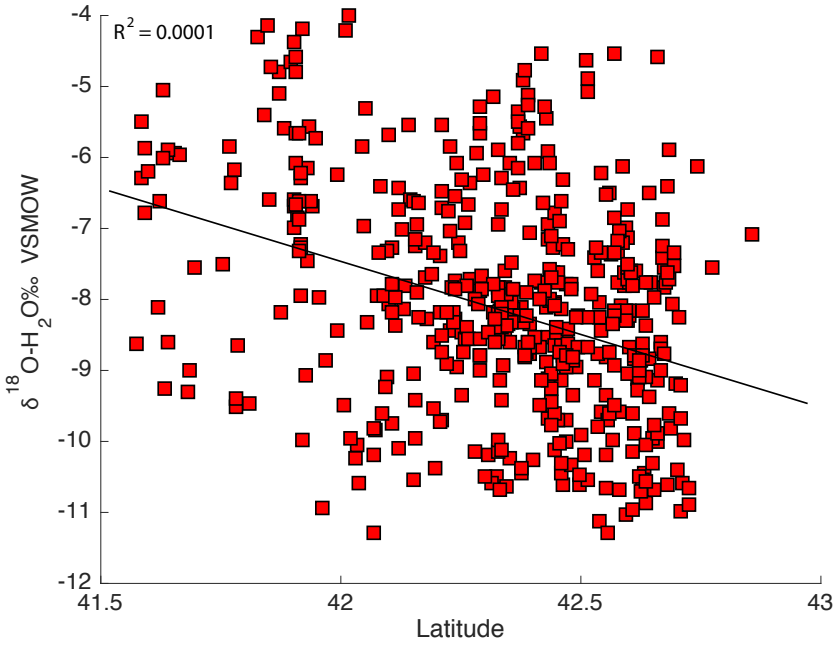

Figure 4.6: Relations between latitude and $\delta^{18}O$ values in surface water.

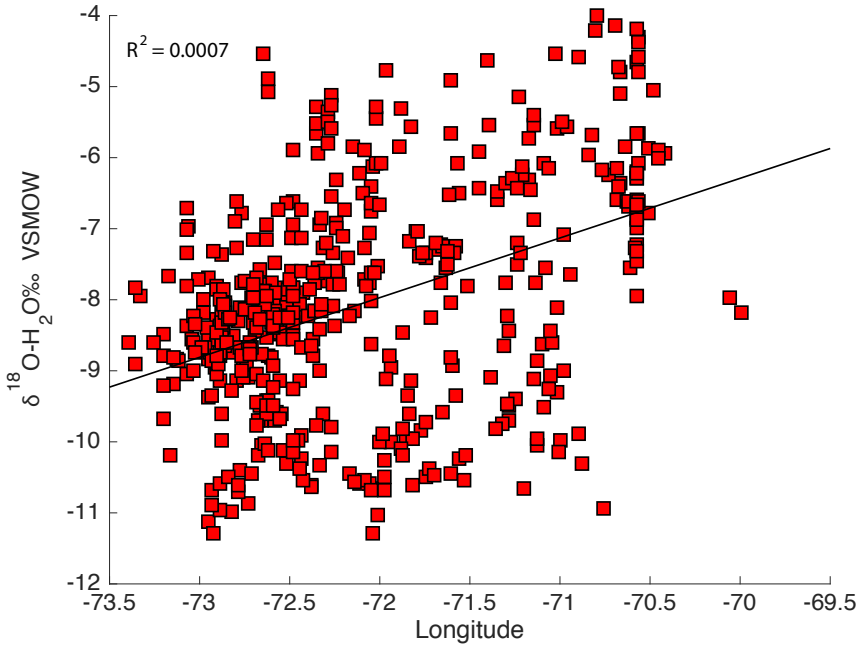

Figure 4.7: Relation between longitude and $\delta^{18}O$ values in surface water.

4.1.4 Spatial Distribution of $\delta^{18}O$ and $\delta^{2}H$ values

Figure 4.8 illustrates the number of samples taken in each HUC within Massachusetts. We determined that 21 HUCs did not contain any sampling sites and were disregarded from the spatial plot.

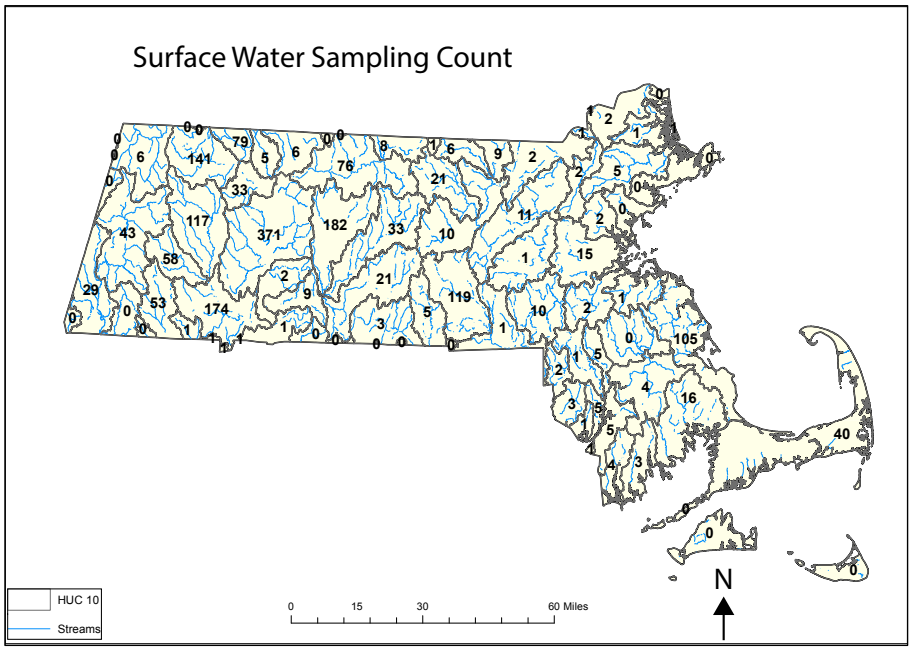

Figure 4.8: The locations of watershed basins are defined by a HUC10 and are illustrated by a black line. The number of surface water samples taken within each HUC are indicated.

The HUC10 average weighted $\delta^{18}O$ and $\delta^{2}H$ values were spatially plotted to produce figure 4.9. A spatial plot is not shown for $\delta^{2}H$ as this spatial distribution had similar patterns to $\delta^{18}O$ and provided no additional information. Average HUC10 $\delta^{18}O$ values ranged -11.29 to -3.76‰. Figure 4.9 exhibits an isotopic depletion from east to west. Surface water samples become increasingly more negative from CZ1 to CZ3. Moving across Massachusetts from CZ3 to CZ1, surface water becomes isotopically depleted from east to west. Highest $\delta^{18}O$ averages are located along the coast and in Cape Cod. Lowest $\delta^{18}O$ average are located western Massachusetts where the lowest $\delta^{18}O$ average is

located just east of the Berkshire mountains. Because each HUC did not have the same number of surface water samples, there is a bias between HUCs with more sampling points than HUCs with fewer sampling points.

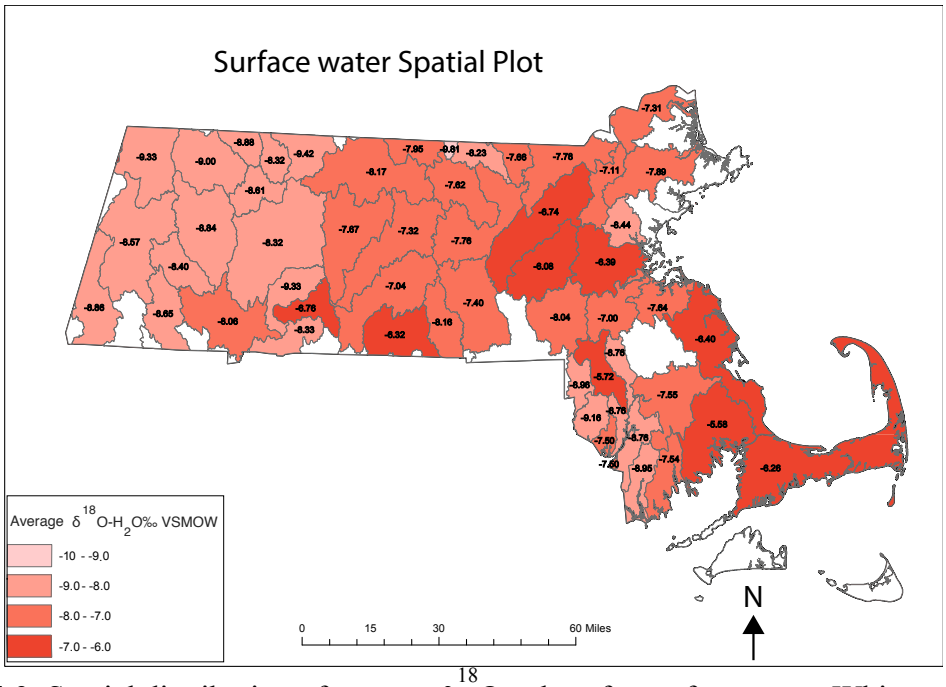

Figure 4.9: Spatial distribution of average $\delta^{18}O$ values for surface water. White spaces indicate that no samples were taken in that watershed.

In 2011 Bowen et al. created a geographic information system based model to predict long term annual average surface water isotope ratios across the contiguous United States where gridded precipitation isotope maps that takes into account elevation and incorporates precipitation-evapotranspiration monthly variability was used as model input. Residual hydrogen and oxygen from the model were used to create an enhanced prediction map for U.S. surface water $\delta^{18}O$ and $\delta^{2}H$ values. Using the residual corrected spatiotemporal H and O isotope ratio model results for surface waters across the contiguous USA, we compared our observed surface water data to these model results to determine the simulated and observed differences in both the H and O isotope ratios,

figure 4.10 and 4.11 respectively. A one to one line was placed in both graphs to better compare simulated versus observed data and will be further discussed in *section 6.2.2*.

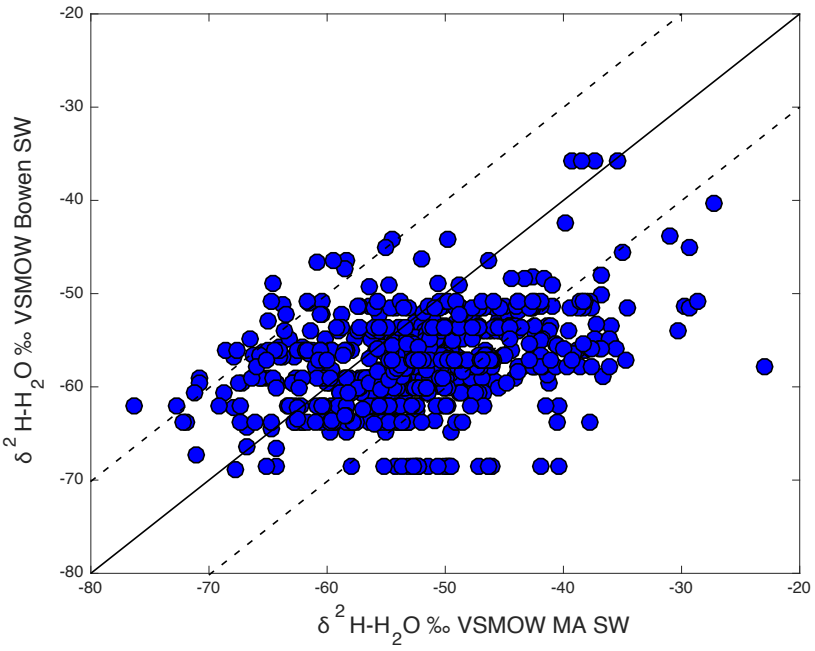

Figure 4.10: Observed versus residual corrected δ^2H ratios as compiled and determined by Bowen et al. 2011. The solid lines represent the one to one line and the dashed lines represents the amplitude of seasonal variability.

A GIS raster for both hydrogen and oxygen were downloaded from http://www.waterisotopes.org. All data was imported into ArcMAP and projected onto the Lambert Azimuthal Equal Area projection for North America.

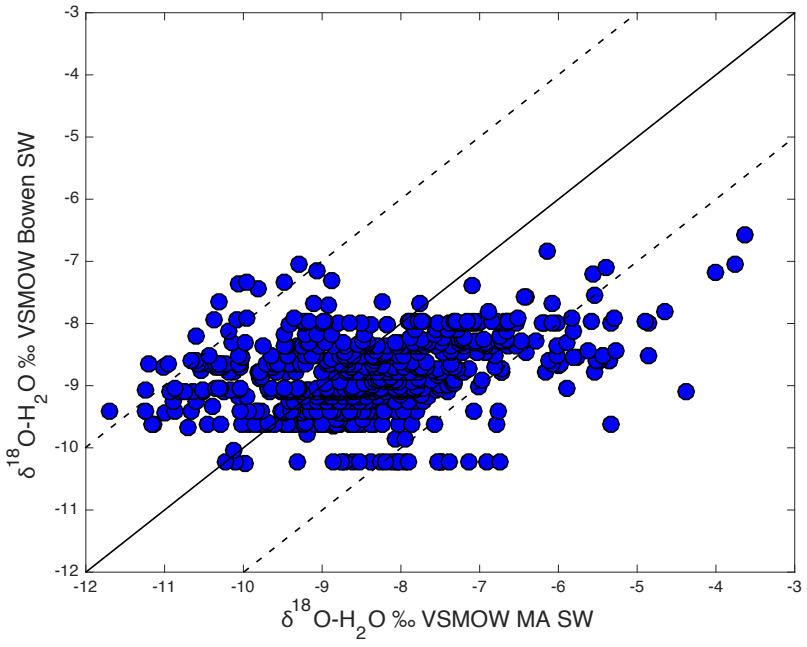

Figure 4.11: Observed versus residual corrected $\delta^{18}O$ ratios as compiled and determined by Bowen et al. 2011. The solid lines represent the one to one line and the dashed lines represents the amplitude of seasonal variability.

Observed isotopic compositions were then extracted from each grid cell that corresponds to a simulated $\delta^{18}O$ or $\delta^{2}H$ value and then the root mean square error (RMSE) were calculated for both H and O. When calculated, the $\delta^{2}H$ RMSE for our data was 52.4 and the RMSE for the data compiled by Bowen et al., 2011, was 57.4. The RMSE calculated for $\delta^{18}O$ for our data and data compiled by Bowen et al., 2011, was 8.47 and 8.83 respectively. From Figure 4.11, it can be determined that 9.7% of $\delta^{18}O$ variability is due to open system enrichment and that roughly 90.3% of $\delta^{18}O$ variability is due to precipitation-evapotranspiration. This percentage was calculated by determining how many sample points fell outside of the and then dividing it by the total number of sampling points.

4.1.5. Climate Zones and its effects on $\delta^{18}O$ values

Surface water samples were grouped by climate zones to determine geographic effects on the isotopic variability of surface water. Topographic dynamics between climate zones are illustrated by the dual isotope plot in figure 4.12. Based on the plot, CZ3 plots higher on the SMWL while CZ1 and CZ2 plot lower on the SMWL. The average $\delta^{18}O$ value of CZ1, CZ2, and CZ3 are -8.69 (±1), -8.03 (±1), and -6.65 (±1) ‰. The average $\delta^{2}H$ value of CZ1, CZ2, and CZ3 are -54.2 (±7), -50.3 (±8), and -41.4 (±8) ‰ and the average d-excess of CZ1, CZ2, and CZ3 are 15.4 (±3), 14.0 (±4), and 11.8 (±4) ‰.

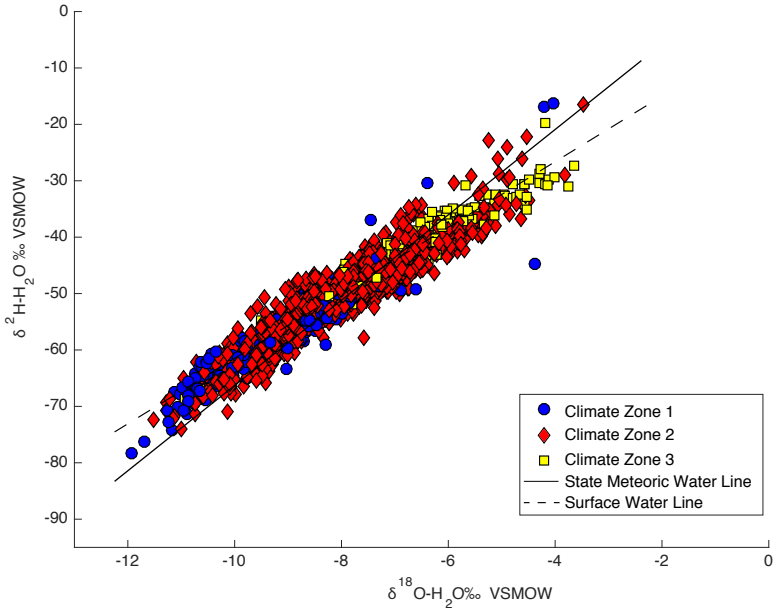

Figure 4.12: Dual isotope plot categorized based on climate zone.

Average $\delta^{18}O$ values for each climate zone were compared to better illustrate the isotopic differences between CZ1, CZ2, and CZ3. These averages are shown in Table 6.2. From figure 4.13, CZ3 is more enriched than CZ1 and CZ2. CZ1 is more depleted than CZ2

and CZ3. This same relationship is seen in the average $\delta^{18}O$ and $\delta^{2}H$ values for precipitation.

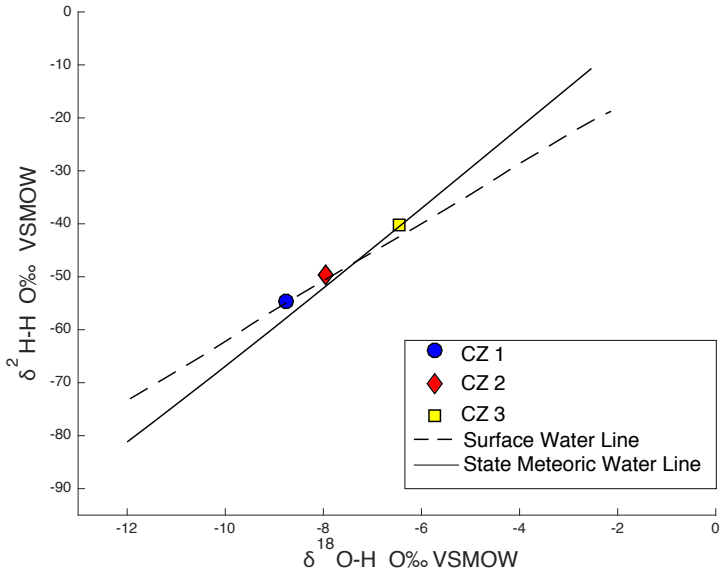

Figure 4.13: Average surface water $\delta^{18}O$ and $\delta^{2}H$ were determined for the three climate zones.

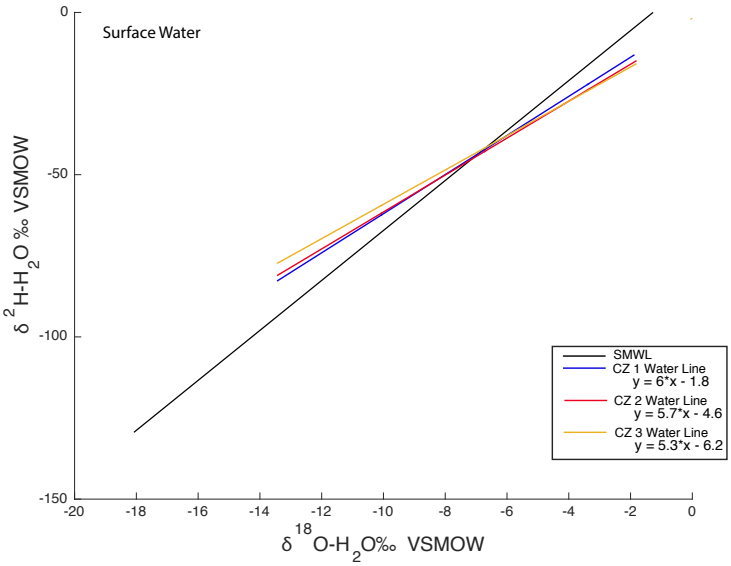

Figure 4.14: Dual isotope plot of calculated climate zone water lines for all surface water samples.

Local meteoric water lines (LMWLs) were calculated for each of the climate zones and plotted, figure 4.14. CZ 1 LMWL generated from 501 samples is $\delta^{2}H = 6.0*\delta^{18}O - 1.8$, CZ 2 LMWL generated from 1,143 samples is $\delta^{2}H = 5.7*\delta^{18}O - 4.6$ and the CZ 3 LMWL generated from the 225 samples is $\delta^{2}H = 5.3*\delta^{18}O - 6.2$.

4.1.6. Acid Rain Monitoring Network

In 1983 the University of Massachusetts Water Resources Research Center started the Acid Rain Monitoring Project. The project's mission was to develop a comprehensive illustration of the sensitivity of surface waters in Massachusetts to acid deposition, and eventually create a long-term trend of this. In 2001 surface water samples were collected three times a year at roughly 150 lakes and ponds and a few streams, in 2011 sampling was reduced to once a year. In 2017 and 2018 we asked to receive samples during their April sampling period. These samples are beneficial as they provide a quick snapshot of surface waters during the time of sampling. Throughout this paper samples from the Acid Rain Monitoring with be referred as ARM 2017 and ARM 2018, the year indicating time of sampling. ARM 2017 and ARM 2018 sampling locations can be seen in figure 4.19 and 4.20.

A dual isotope plot, figure 4.15, was created for ARM 2017 and ARM 2018. ARM 2017 $\delta^{18}O$ values range from -11.3 to -1.69‰, $\delta^{2}H$ range from -70.7 to -17.3‰ and lc-excess range from -17.8 to 7.05‰. For ARM 2018 $\delta^{18}O$ range from -11.6 to -3.57‰, $\delta^{2}H$ range from -76.2 to -32.2‰ and lc-excess range from -16.9 to 4.35‰.

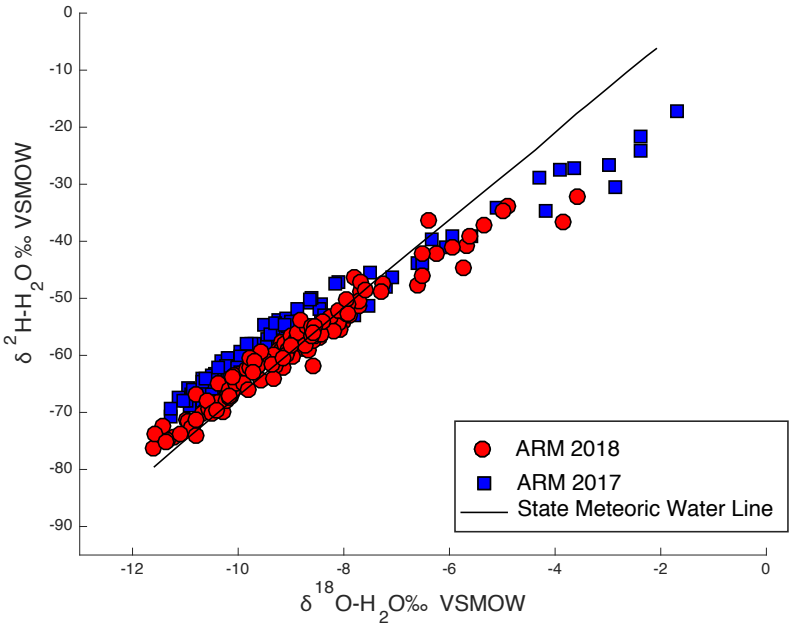

Figure 4.15: Dual isotope plot of 2018 ARM (130) and 2017 ARM surface water samples (120).

Following the same procedures performed on the surface water samples, ARM 2017 and 2018 samples were correlated with surface water type. Figure 4.16 shows that for both ARM 2017 and 2018, all samples that fall onto the evaporative enrichment line are from stagnant bodies of water indicating variability due to open water enrichment. Bodies are water that are stagnant experience more evaporation which will cause that body of water to be more enriched than moving bodies of water.

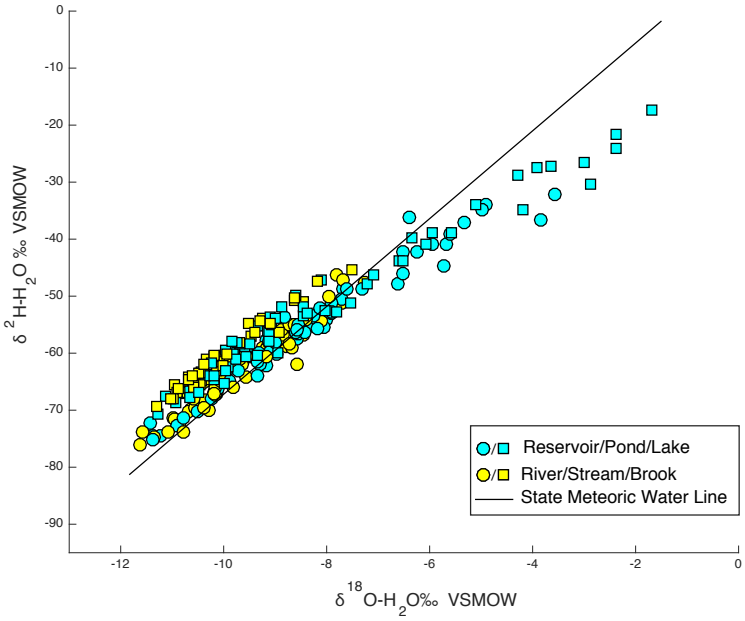

Figure 4.16: 2018 (circle) and 2017 (square) ARM surface water samples categorized by surface water type.

ARM 2017 and 2018 samples were then correlated with geographic located in terms of climate zones. Figure 4.17 illustrates the average $\delta^{18}O$ and $\delta^{2}H$ values for ARM 2017 and 2018 for CZ1, CZ2, and CZ3.

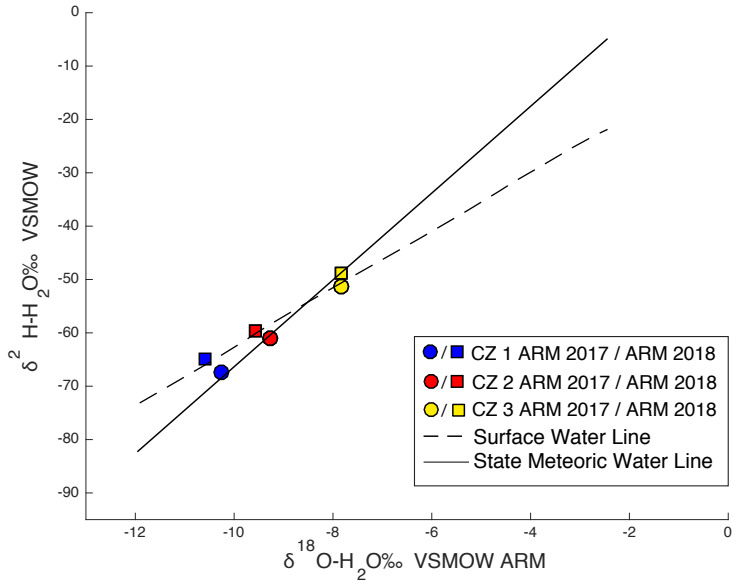

Figure 4.17: Average $\delta^{18}O$ value for ARM 2017 (square) and ARM 2018 (circle).

Average ARM 2017 $\delta^{18}O$ and $\delta^{2}H$ values for CZ1, CZ2, and CZ3 are -10.6 (±0.5) and -64.8 (±3) ‰, -9.56 (±2) and -59.6 (±8) ‰ and -7.83 (±2) and -48.7 (±9) ‰ respectively. Average ARM 2018 $\delta^{18}O$ and $\delta^{2}H$ values for CZ1, CZ2, and CZ3 are -10.3 (±2) and -67.4 (±8) ‰, -9.28 (±1) and -61.0 (±7) ‰ and -7.84 (±3) and -51.2 (±9) ‰ respectively.

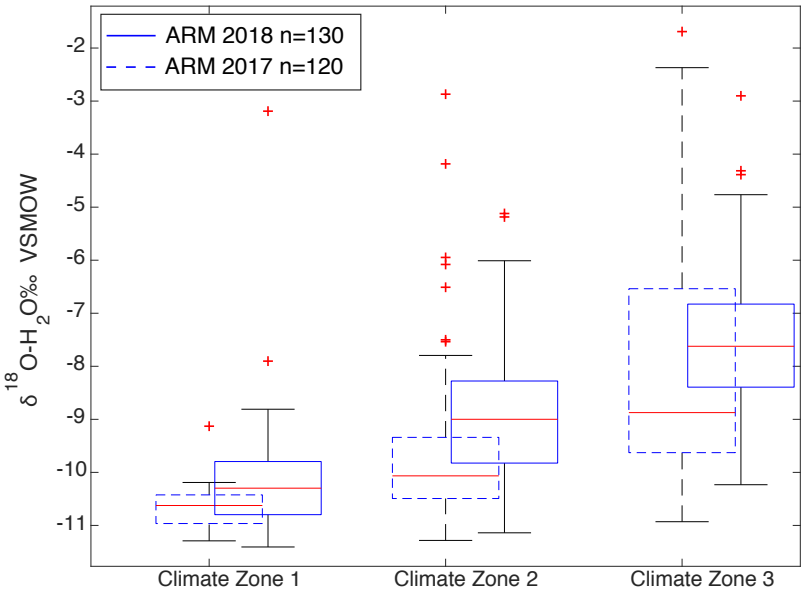

Figure 4.18: Box plot of ARM 2018 and 2017 samples grouped by geographic location.

Median, 25th and 27th percent quartile ranges were determined for CZ1, CZ2, and CZ3 for ARM 2017 and ARM 2018 samples, figure 4.18. ARM 2018 CZ1, CZ2, and CZ3 had 25, 65, and 40 samples in each zone respectively. ARM 2017 for CZ1, CZ2, and CZ3 had 13, 66, 41 samples in each zone respectively. CZ3 is isotopically more variable in 2017 and 2018, which may be due to the fact that outwash aquifers are located in this zone and due to hydrologic characteristics, there is a greater surface water groundwater interaction.

It is noted that the median ARM 2018 $\delta^{18}O$ in each climate zone is consistently higher than ARM 2017. Climate scientists at the University of Massachusetts-Amherst observed that 2018 was the wettest year ever recorded at the Blue Hill Observatory in Milton. This meteorological observation could have had an impact on the surface water variability between 2017 and 2018. Further work on the moisture source of 2018 precipitation events would have to be performed in order to determine if this parameter could have had an effect on the isotopic variability seen in 2017 and 2018.

Both ARM 2017 and ARM 2018 sampling sites and their respective unweighted $\delta^{18}O$ values were spatially plotted. Figure 4.19 and 4.20 show the spatial distribution of ARM 2017 and ARM 2018 respectively and both exhibit an east to west depletion.

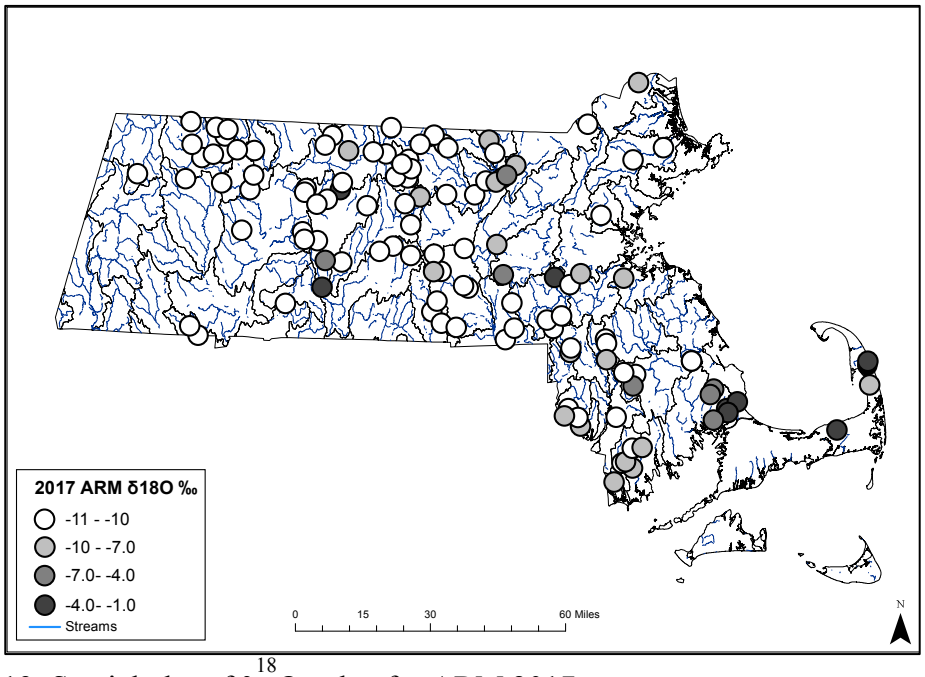

Figure 4.19: Spatial plot of $\delta^{18}O$ value for ARM 2017.

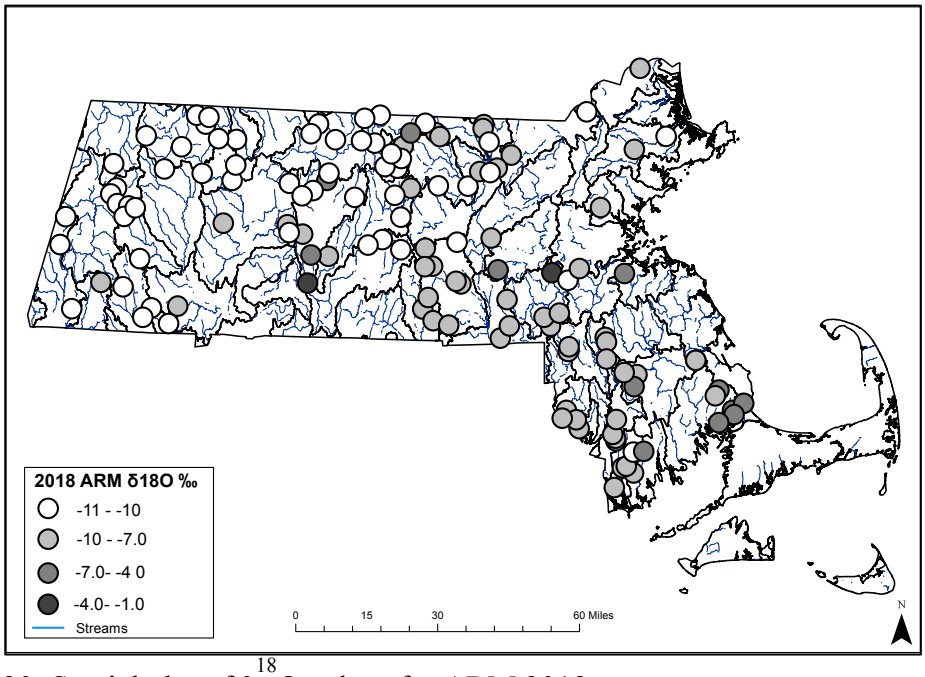

Figure 4.20: Spatial plot of $\delta^{18}O$ values for ARM 2018.

CHAPTER 5

GROUNDWATER

5.1 Results

5.1.1 Averages and meteoric water lines

The $\delta^{18}O$ values of the 1405 groundwater samples across Massachusetts range from -12.2 to -5.07‰, $\delta^{2}H$ values range from -80.1 to -35.5‰, and d-excess values range from -0.2 to 35.2‰. The dataset forms a flattened ellipse that lies slightly angled to the SMWL, figure 5.1 with a higher percentage of points plotting off the SMWL and a few plotting off onto the evaporative enrichment line.

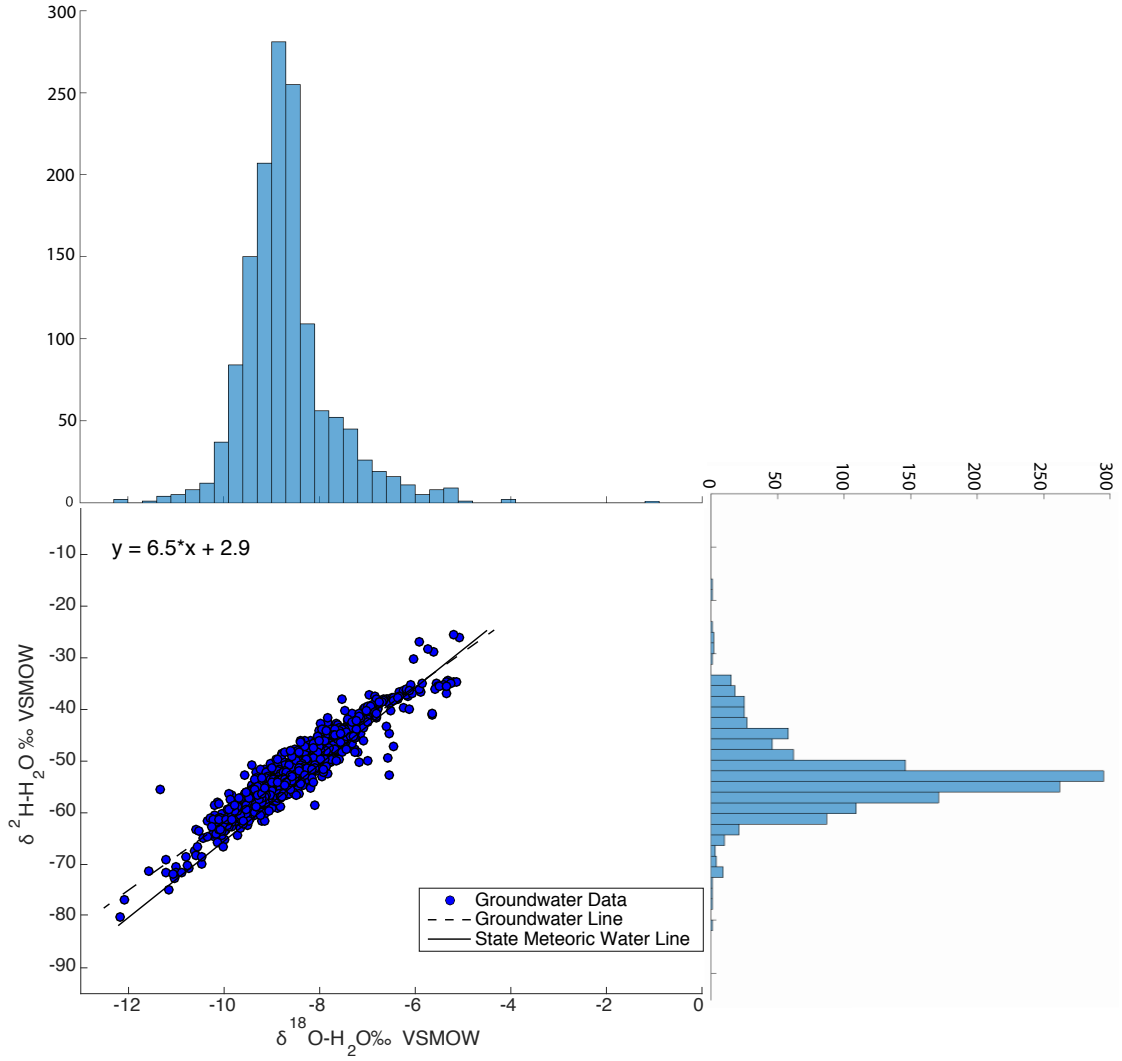

Figure 5.1: Relation between $\delta^{18}O$ and $\delta^{2}H$ groundwater values for the entire dataset (1405 groundwater samples and 409 groundwater sites) with histograms of $\delta^{18}O$ and $\delta^{2}H$ on their respective axes.

Average $\delta^{18}O$, $\delta^{2}H$ and d-excess values for groundwater are 8.7 (±1), 53.3 (±6), and 16.3 (±4) ‰ respectively. In order to better show the isotopic variability in groundwater, a histogram, which shows the frequency and distribution for both $\delta^{18}O$ and $\delta^{2}H$ were plotted and placed on appropriate axes with the dual isotope plot of groundwater analyses. At approximately $\delta^{2}H$ -45‰ there is slight increase in the number of

groundwater samples, this indicates where on the dual isotope plot groundwater samples start to fall off the SMWL and onto the evaporative enrichment line.

The Groundwater Water Line (GWL), which is the unweighted linear regression generated from the 1405 groundwater analyses is $\delta^{2}H = 6.5*\delta^{18}O + 2.9$. The slope of the GWL equation is 6.5 and the y-intercept of intercept is 2.9.

5.1.2 Seasonal Patterns

To visually represent seasonal variability of groundwater, the unweighted $\delta^{18}O$ and $\delta^{2}H$ values of the groundwater samples were compared with the time of sampling. Medians, minimum, maximum, 25^{th} and 75^{th} percentile, and 1% interquartile ranges were determined for each of the 12 months, figure 5.2. Figure 5.2 illustrates little isotopic variability between the medians of each month and indicates relatively homogenous seasonal variations in the unweighted $\delta^{18}O$ values.

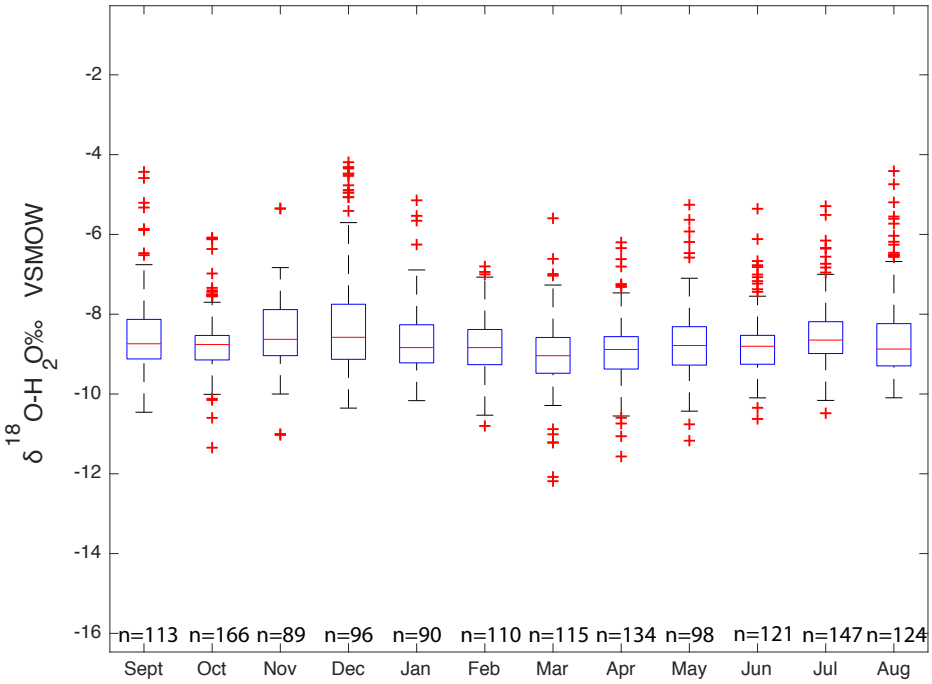

Figure 5.2: Comparison of $\delta^{18}O$ values (1405 samples) for each sampling month.

Following the methods as described in *section 3.1.2* a sine-wave was fit through the reported groundwater isotope values to better describe the seasonal isotope cycles: $Cp(t) = 0.05\cos 2\pi \times \frac{1}{365}x \times -0.04\sin 2\pi \times \frac{1}{365}x + -8.79$. Using equation 8, we found the amplitude of the sine curve to be 0.07‰, illustrated in figure 5.3. Figure 5.3 shows that groundwater experiences very little variability, with a seasonal range of 0.14‰.

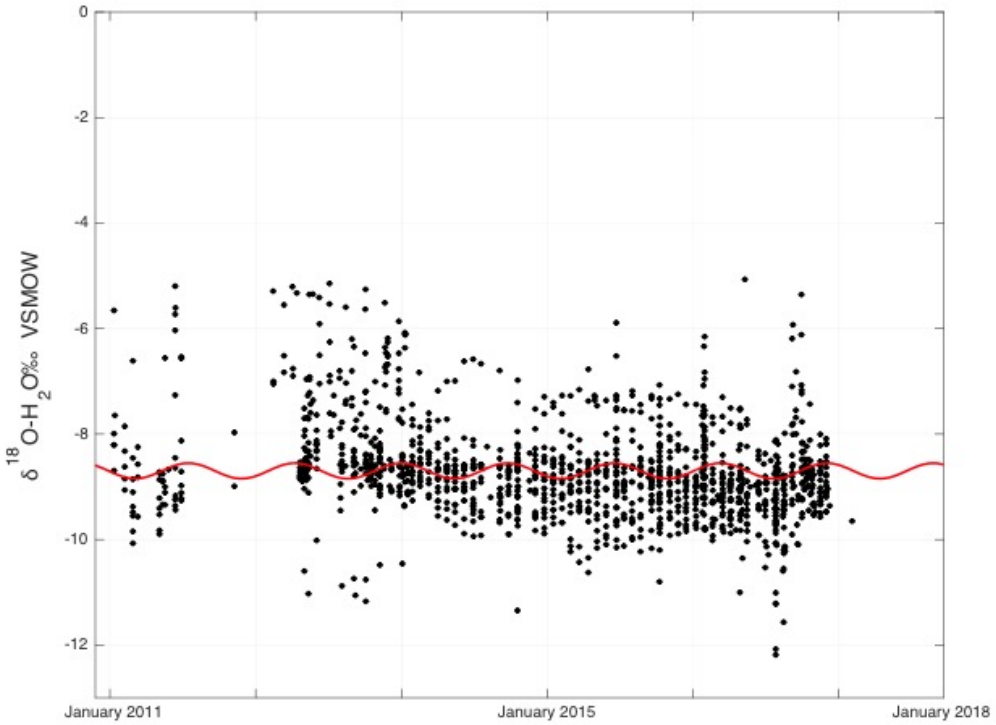

Figure 5.3: Time series of groundwater $\delta^{18}O$ with a sine-wave fitted through data.

5.1.3 Climate Zones and its effects on $\delta^{18}O$ values

Groundwater samples were grouped by geographic location in terms of climate zone, figure 5.4. Based on this figure CZ3 is more enriched than CZ1 and CZ2, while CZ1 is more depleted than CZ2 and CZ3. Average $\delta^{18}O$ values for each climate zone were determined and compared in figure 5.5. The average $\delta^{18}O$ values of CZ1, CZ2, and CZ3 are -9.11‰ (±0.6‰), -8.71‰ (±0.9‰), and -7.20‰ (±1‰) respectively. The average $\delta^{2}H$ values of CZ1, CZ2, and CZ3 are -56.3‰ (±5‰), -53.3‰ (±7‰), and -43.0‰ (±7‰) respectively. The average d-excess values of CZ1, CZ2, and CZ3 are 16.5‰ (±2‰), 16.4‰ (±2‰), and 15.0‰ (±3‰) respectively.

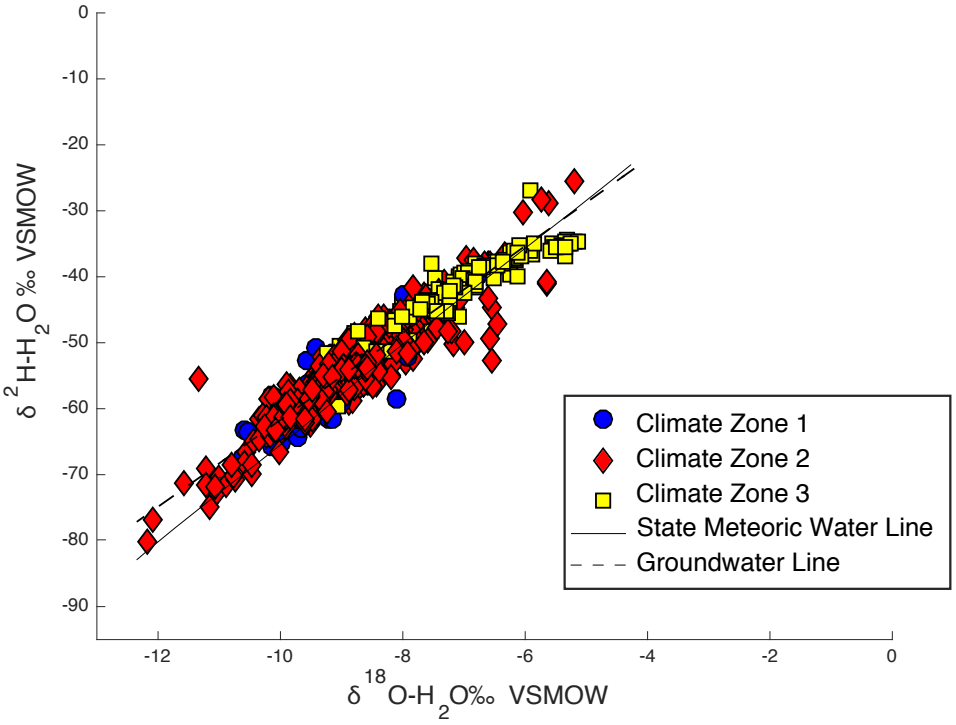

Figure 5.4: Dual isotope plot as a function of climate zones.

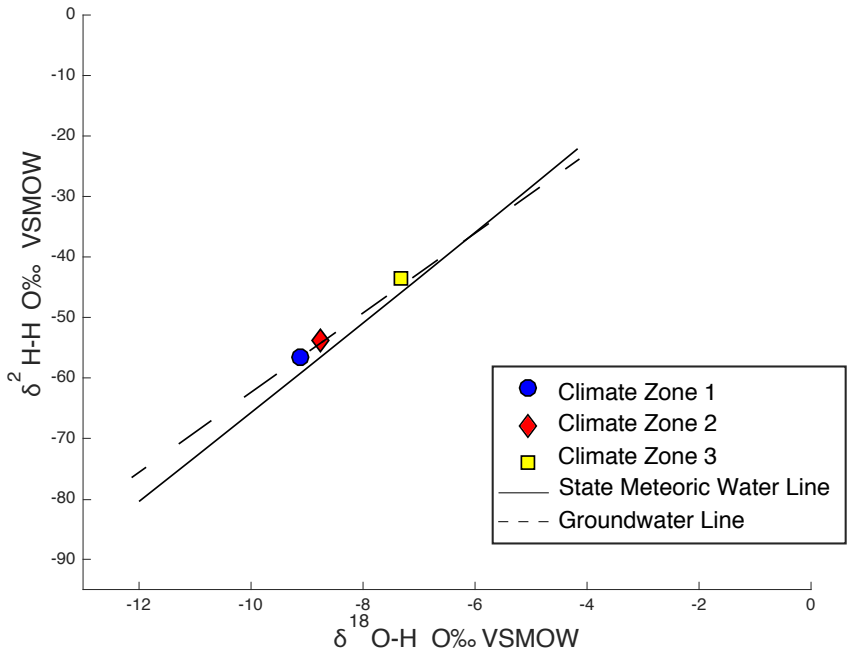

Figure 5.5: Dual isotope plot correlating average $\delta^{18}O$ for each climate zones.

Groundwater sees the same relationship between climate zones and isotopic differences as noted in surface water and precipitation, where CZ 3 is the most enriched and CZ1 is most depleted.

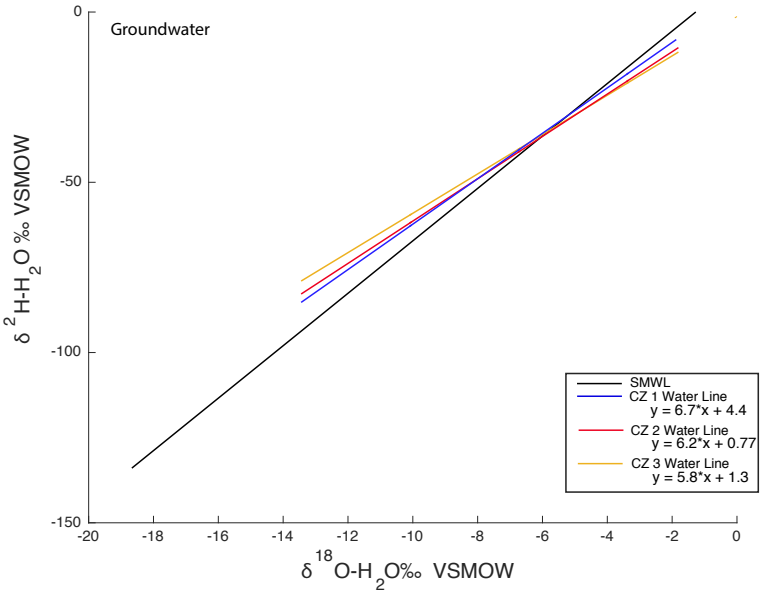

Figure 5.6: Dual isotope plot of calculated climate zone water lines for all groundwater samples.

Local meteoric water lines (LMWLs) were calculated for each of the climate zones and plotted, figure 5.6. CZ1 LMWL generated from 319 samples is $\delta^{2}H = 6.7*\delta^{18}O + 4.4$, CZ2 LMWL generated from 908 samples is $\delta^{2}H = 6.2*\delta^{18}O + 0.7$ and the CZ3 LMWL generated from the 144 samples is $\delta^{2}H = 5.8*\delta^{18}O + 1.3$.

5.1.4 Hydrogeologic Effects and Environmental Parameters

Hydrogeologic effects such as aquifer characteristics are on important parameter that can be used to determine groundwater-surface water interaction and its effects on the isotopic variability of groundwater. Groundwater samples were grouped based on the

aquifer they were sampled in: glacial till, outwash plain, bedrock, and glacial fluvial. Out of the 1,405 groundwater samples the aquifer for 44 of the samples were unknown. Aquifer dynamics of the groundwater isotopic compositions are shown in the dual isotope plot, figure 5.7.

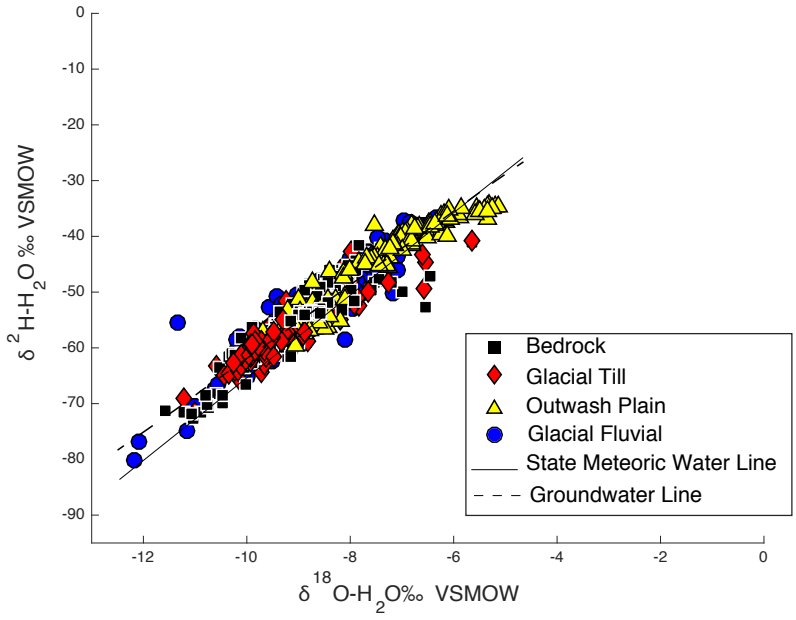

Figure 5.7: Dual isotope as a function of aquifer type.

The $\delta^{18}O$ of till ranges from -11.2 to -5.65 (±1)‰, $\delta^{2}H$ range from -71.5 to -39.9 (±5)‰, and d-excess range from 6.45 to 35.2(±3)‰, $\delta^{18}O$ of bedrock range from -11.7 to -5.63(±1)‰, and $\delta^{2}H$ range from -72.5to -41.0(±5)‰, and d-excess range from -0.22 to 22.8(±2)‰, $\delta^{18}O$ of outwash plains range from -9.69 to -5.14(±1)‰, and $\delta^{2}H$ range from -59.6 to -34.3(±7)‰, and d-excess range from 5.90 to 22.3(±3)‰, $\delta^{18}O$ of glacial fluvial range from -12.2to -5.93(±1)‰, and $\delta^{2}H$ range from -80.1 to -27.0(±5)‰, and d-excess range from 6.46 to 35.2(±2)‰. Samples located in outwash plains with a few samples from glacial fluvial aquifers plot off the SMWL. Average $\delta^{18}O$ values were determined

for the till, outwash plain, bedrock, and glacial fluvial aquifers. The average $\delta^{18}O$ and $\delta^{2}H$ values of waters located in a bedrock aquifer are -9.0 and -55‰ respectively. Average $\delta^{18}O$ and $\delta^{2}H$ values of waters located in a till aquifer are -8.9 and -55‰ respectively. Average $\delta^{18}O$ and $\delta^{2}H$ values of waters located in a glacial fluvial aquifer are -8.7 and -54‰ respectively. Average $\delta^{18}O$ and $\delta^{2}H$ values of waters located in an outwash plain aquifer are -7.3 and -44‰ respectively. Figure 5.8 illustrates these averages. Outwash fluvial, and bedrock aquifers are isotopically very similar, while outwash plains are the most enriched.

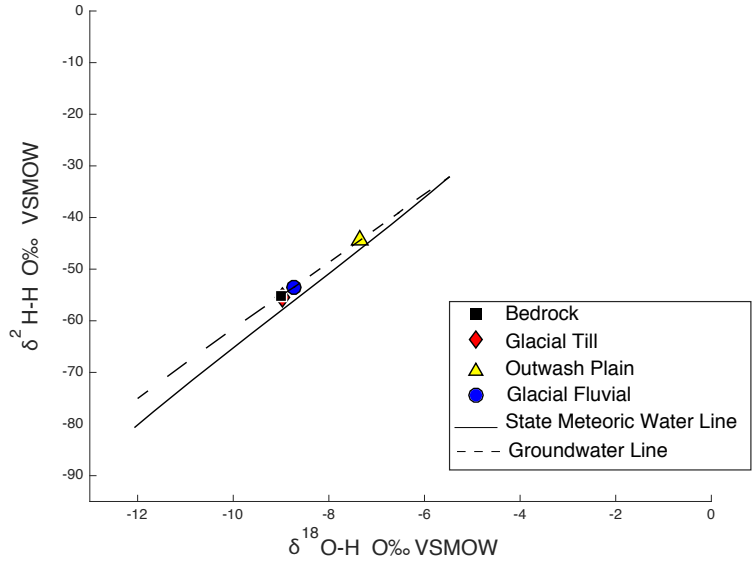

Figure 5.8: The average $\delta^{18}O$ values were calculated for each of the aquifer.

Medians, 25th and 75th percentile, and 1% interquartile ranges for the unweighted $\delta^{18}O$ values were determined for each of the aquifer type. Groundwater sites that had multiple samples were averaged and averaged $\delta^{18}O$ values were used in the aquifer comparison, figure 5.9.

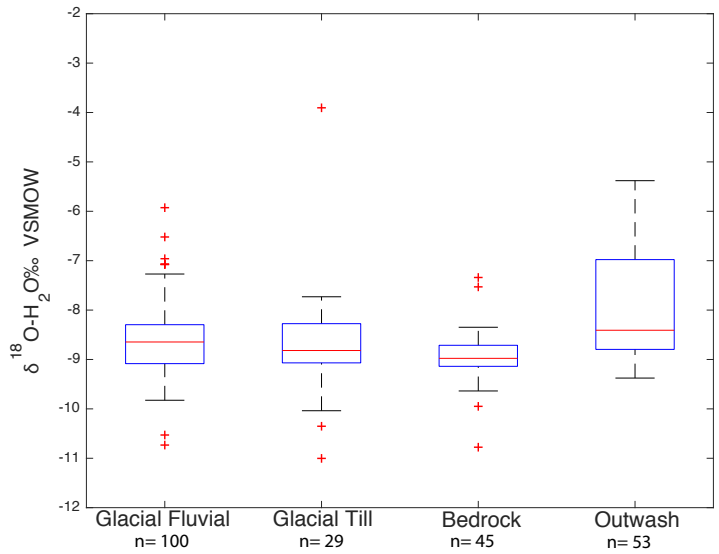

Figure 5.9: $\delta^{18}O$ box plot of sample average aquifer type where the red plus signs indicate outliers.

100, 29, 45, and 53 samples were grouped as glacial fluvial, glacial till, bedrock, and outwash plains respectively. Figure 5.9 illustrates outwash plains have the highest amount of isotopic variability while bedrock has the least amount of variability. The median for each of the aquifer type are relatively similar with each other, with outwash plain having the highest median by approximately 0.5‰.

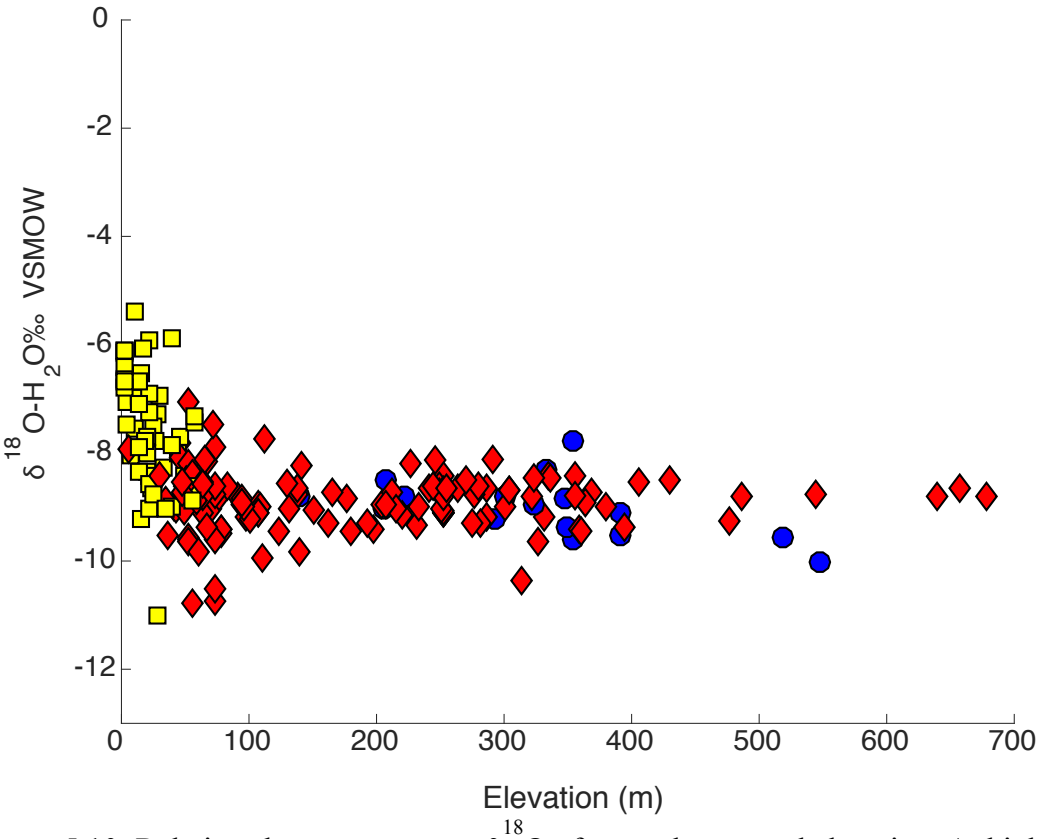

Figure 5.10: Relations between average $\delta^{18}O$ of groundwater and elevation. At higher elevation groundwater is more enriched than groundwater at a lower elevation. Samples are color coded based on climate zone.

Sample average $\delta^{18}O$ values were plotted as a function of elevation to determine elevation effects, figure 5.10. Samples were also color coded by climate zones. The elevation of groundwater samples ranges from 22 to 677 meters. Figure 5.10 indicates that groundwater samples located at a lower elevation are more enriched than samples located at a higher elevation which are depleted. From 22 to 100 meters, $\delta^{18}O$ values decrease from -3 to approximately -10‰. From 100 meters to 700 meters, $\delta^{18}O$ values show some variability but are relatively constant at around -9‰.

Groundwater sample analyses were then compared to their respective latitude and longitude. Figure 5.11 illustrates a negative relationship between $\delta^{18}O$ values and latitude and figure 5.12 shows a positive relationship between the $\delta^{18}O$ values and longitude.

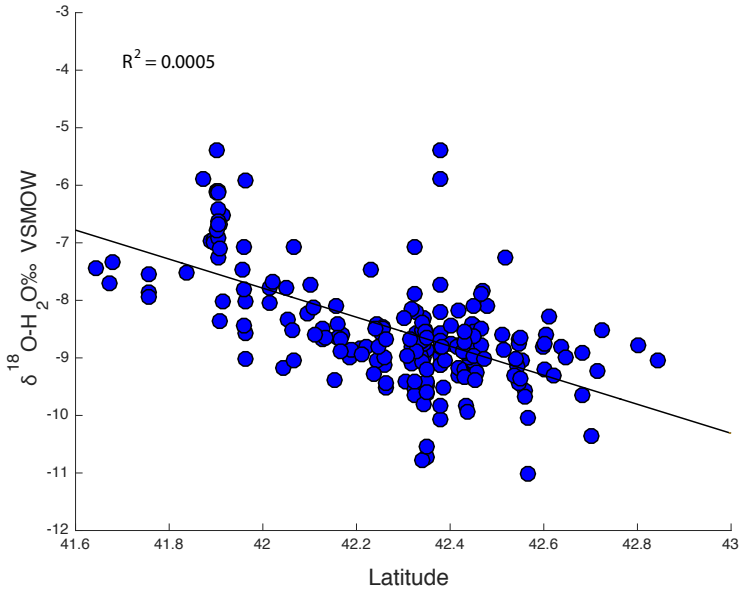

Figure 5.11: Relation between $\delta^{18}O$ values of groundwater and latitude.

The r^2 values for latitude and longitude are 0.0005 and 0.00008 respectively. Same with surface water, the r^2 values are not informative, they are rather used to show the correlation between $\delta^{18}O$ values and latitude and longitude.

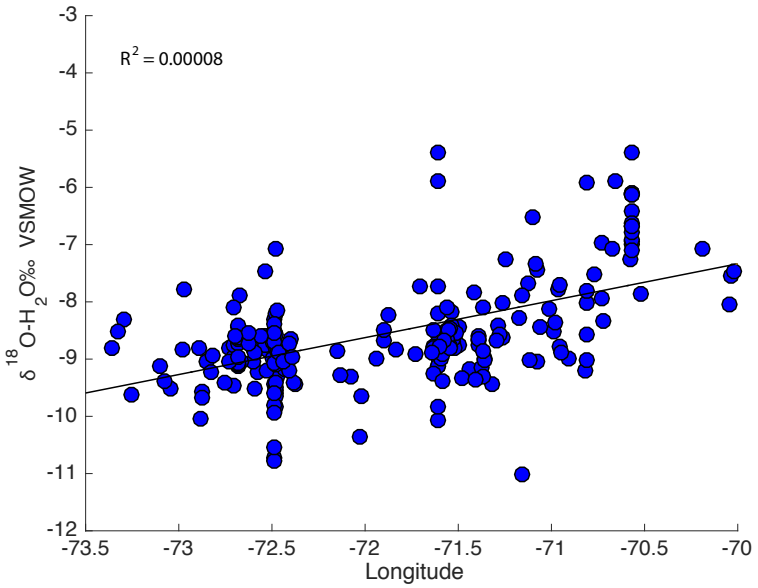

Figure 5.12: Relation between $\delta^{18}O$ values of groundwater and longitude.

5.1.5 Spatial Distribution of $\delta^{18}O$ and $\delta^{2}H$ values

Figure 5.13 shows the number of samples taken in each HUC. We determined that 33 HUCs did not contain any sampling sites and were disregarded from the spatial plot.

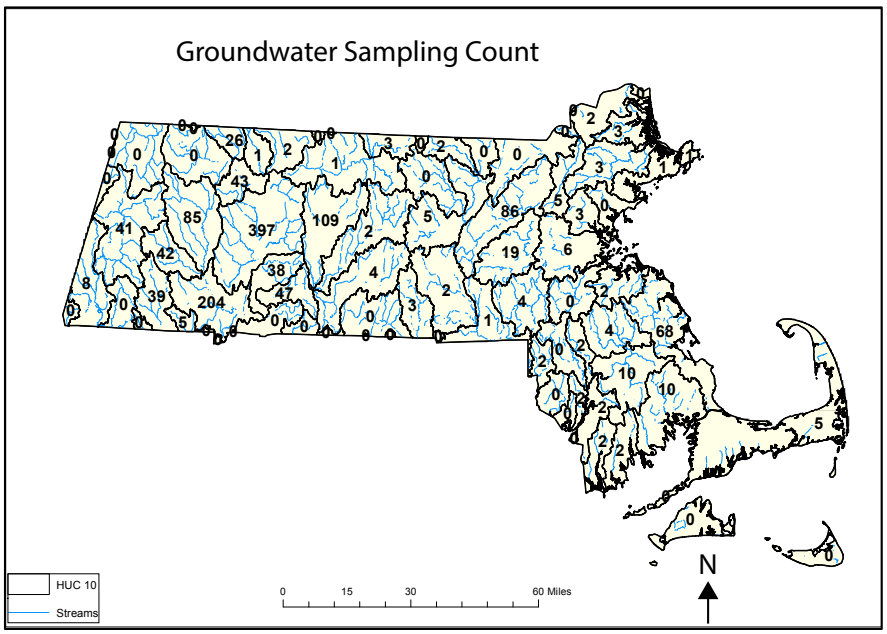

Figure 5.13: The locations of watershed basins are defined by a HUC10 and are illustrated by a black line. The number of samples taken within each HUC are indicated.

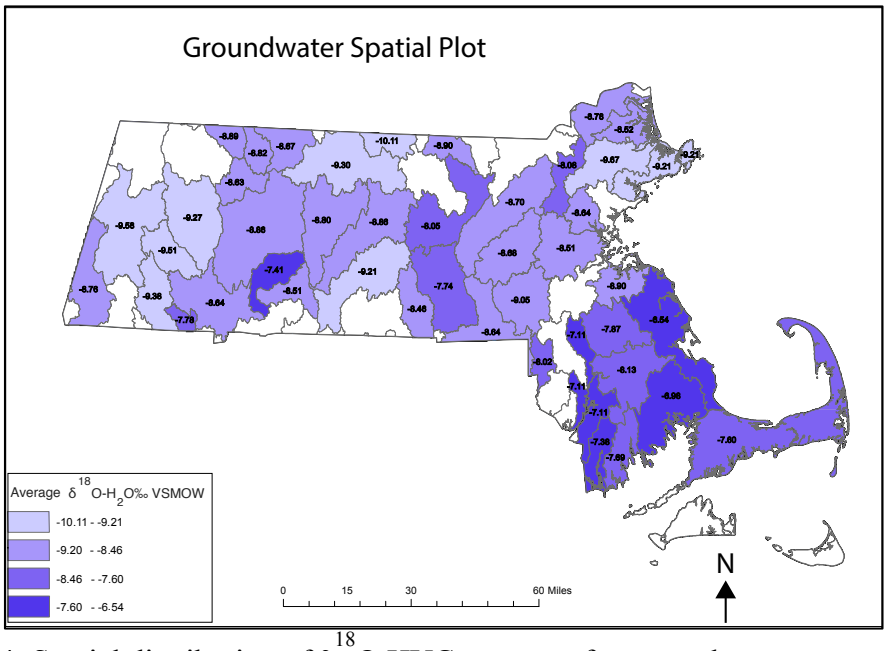

Figure 5.14: Spatial distribution of $\delta^{18}O$ HUC averages for groundwater across Massachusetts.

The HUC10 average weighted $\delta^{18}O$ and $\delta^{2}H$ values were spatially plotted to produce figure 5.14. A spatial plot was not created for $\delta^{2}H$ as this spatial distribution plot was similar to $\delta^{18}O$ and provided no new additional information. Moving across Massachusetts from CZ3 to CZ1, east to west, there is an isotopic depletion of $\delta^{18}O$ values with higher $\delta^{18}O$ values in CZ3 and lower $\delta^{18}O$ values in climate CZ1. This same pattern is seen in both the precipitation and surface water $\delta^{18}O$ values.

CHAPTER 6

DISCUSSION

6.1 Comparison of SMWL, SWL, and GWL and Isotopic Variability

Important differences in the isotopes were observed between precipitation, surface water, and groundwater, Table 6.1. The SMWL is $\delta^{2}H = 7.7*\delta^{18}O + 9.8$, the SWL is $\delta^{2}H = 5.7*\delta^{18}O - 4.2$, and the GWL is $\delta^{2}H = 6.5*\delta^{18}O + 2.9$, each line having its own unique slope and y-intercept. Figure 6.1 illustrates the comparison between the SMWL, SWL and GWL and includes the 95th percent confidence interval for all three which was calculated using the curve fitting tool in MATLAB. The 95th percent confidence interval illustrates the minimum, maximum values and the range of variability for precipitation, surface water, and groundwater. These values and ranges allow us to compare and determine how variable the isotopic composition of $\delta^{18}O$ and $\delta^{2}H$ for precipitation, surface water and groundwater samples. The isotopic composition of precipitation across Massachusetts is more variable than groundwater and surface water. Both groundwater and surface water across Massachusetts experience some but smaller isotopic variability.

Both the SWL and the GWL have shallower slopes than the SMWL and have an imbricate nature relative to the SMWL, figure 6.1.

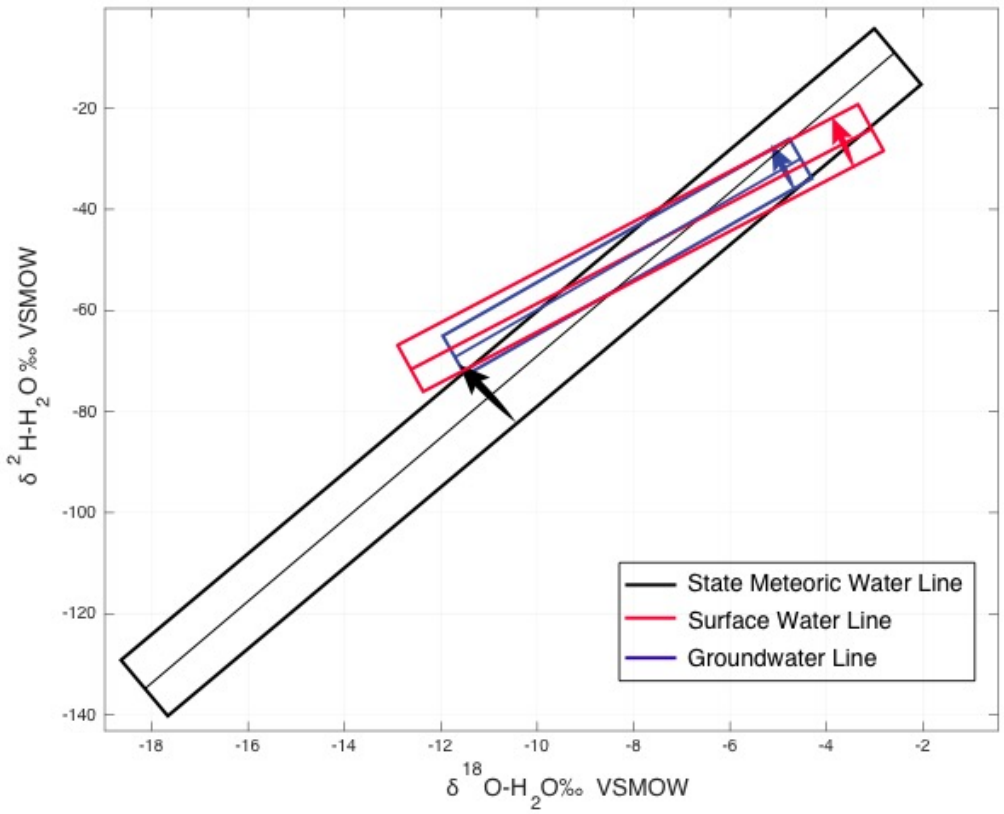

Figure 6.1: 95% confidence interval comparison between the SMWL, SWL and GWL. The arrows indicate low to highest values within the 95% confidence interval polygon.

Variable	Water Line		n	Mean δ^2H	St. Dev	Mean $\delta^{18}O$	St. Dev.	Mean d-excess	St. Dev.
	Slope	Intercept		(‰)		(‰)		(‰)	
Precipitation Network	7.4	8.6	394	-47	24	-7.6	3	12	6
Binned Precipitation from Network	7.7	9.8	31	---	---	---	---	---	---
Total Precipitation Samples	7.5	9.1	558	-50	29	-7.9	4	13	6
Surface Water	5.7	-4.2	1917	50	8	8.0	1	14	4
Groundwater	6.5	2.9	1405	-53	6	-8.7	1	16	4

Table 6.1: Overall summary statistics of precipitation, surface water, and groundwater in terms of spatial variability (std dev).

These differences reflect local precipitation processes but also reveal the correlation between precipitation, surface water and groundwater. Because the slope of the SWL and the GWL are both pulled towards the line of evaporative enrichment, it can be determined that the slope of both these lines are biased by waters in an open water

system. The slope of the GWL is larger than the SWL but smaller than the SMWL. This is telling that groundwater is composed of some fraction of precipitation and surface. Figure 6.3 illustrates the variability of both surface water and groundwater. Although surface water is more variable than groundwater, the isotopic composition of groundwater shows some similarities with the isotopic composition of surface water. Though in order to determine the fraction of surface water to precipitation in groundwater, a data comparison between modeled and observed analyses would have to be performed.

As noted, the slope of the SWL is shallower than both the SMWL and the GWL. The isotopic composition of surface water is affected by both the isotopic composition of precipitation, the isotopic composition of groundwater, and open versus closed water systems. As a result of this, the isotopic composition of surface water will be inherently weighted by precipitation and groundwater (Dutton et al., 2005) and it might be expected for the SWL to be more similar to the SMWL. From Kendall and Coplen (2001) low slopes of the LMWLs may be suggestive of post-rain evaporative enrichment which can be reflected in the surface water. From ARM 2017 and 2018 isotopic analyses, figure 4.16 clearly shows samples that have experienced evaporative enrichment. Most of these samples are from stagnant bodies of water or moving bodies of water (i.e. river, stream, tributary). These samples cause the slope of the SWL to be drawn downward and biased by open water enrichment. In a study performed by Kendall and Coplen in 2001, based on data in Friedman et al. (1992), LMWLs are likely to have slopes as low as 5 to 6 in arid regions where summer rains are primarily derived from the Gulf of Mexico and are the main source of recharge to surface water. Kendall and Coplen (2001) stated that

many of the surface water samples, especially in arid zones, show LMWL slopes less than 6 are indicative of evaporation. Interestingly they found that most of the eastern sites in their study had slopes that range between 7 and 8 and have intercepts that ranged from 5-12‰. The slope of the SWL in Massachusetts is 5.7, which, as suggested by Kendall and Coplen indicates evaporation.

Alternatively, one consideration that hasn't been discussed are anthropogenic affects such as the presence of dams or impoundments, which are present in some of the rivers and reservoirs included in this study. Dams naturally increase evaporation, thus rivers or reservoirs associated with these dams will produce an evaporative signal and cause the $\delta^{18}O$ values of surface waters associated with these dams to be high. This in effect will cause the recycling of surface water that already have high $\delta^{18}O$ values to move through the hydrologic cycle where further enrichment of $\delta^{18}O$ values may take place. Another consideration is the order of the rivers and/or streams and the size of the catchment of the rivers. These will have an effect on the isotopic composition of surface waters and should be considered in future work.

When we compare the slope of the GWL to the SMWL and the SWL, we find that it lies between both the SMWL and the SWL. With the exception of <5% of the groundwater samples, most of the samples lie above the SMWL indicating high d-excess values. Those samples that have $\delta^{2}H$ and $\delta^{18}O$ values that lie below the SMWL and onto the evaporative enrichment line are indicative of samples that have gone through isotopic fractionation, figure 5.1. Most of the groundwater samples that have an evaporative signal are located in CZ 3 where outwash plain aquifers are located and are only found in the southeast portion of Massachusetts. Outwash plains in the southeast portion of

Massachusetts have a high amount of surface water features such as kettles lakes and ponds where ponds are essentially the water table. This could cause a high amount of groundwater surface water variability. From figure 5.4 and figure 5.5 outwash plains are the most enriched and also the most variable. This portion of Massachusetts was located near the terminus of an ice sheet and consists of sandy terminal moraines. Because of the permeable nature of the aquifer, an estimated 45% of the average annual precipitation percolates into the soil and becomes groundwater recharge and an estimated 55% of the precipitation is evapotranspired (Olcott, 1995).

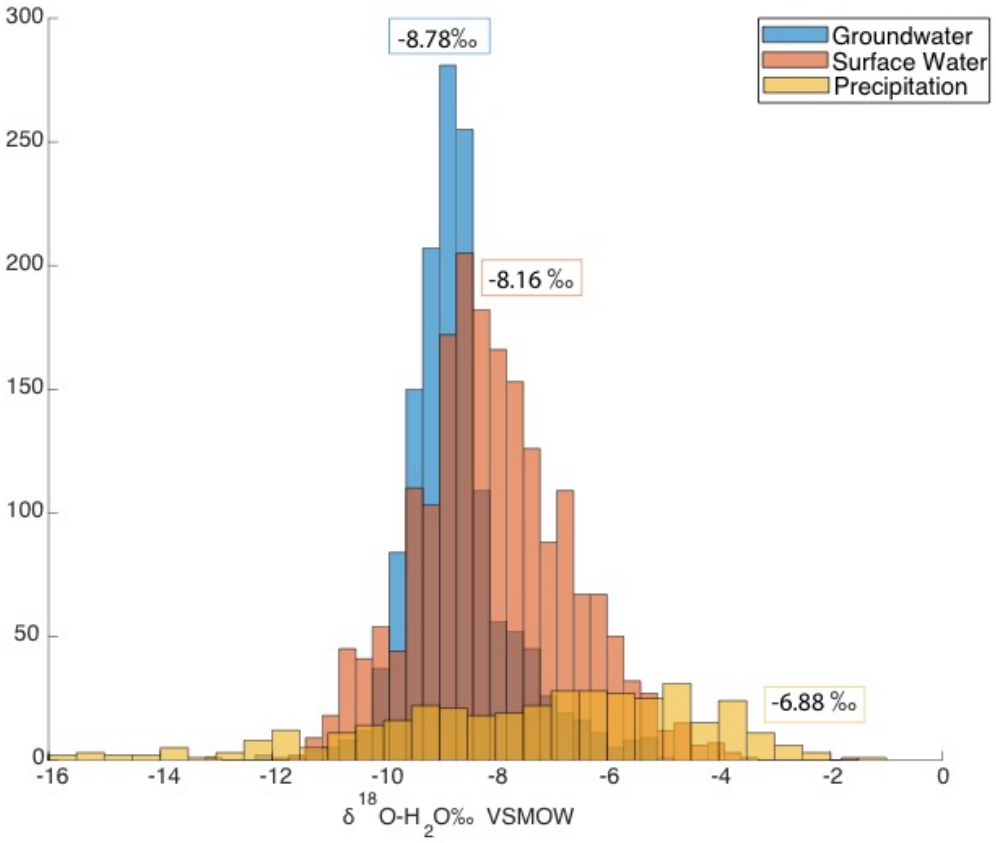

Figure 6.2: Histogram of $\delta^{18}O$ for groundwater (1403 samples), surface water (1917 samples) and precipitation (394 samples).

Figure 6.2 illustrates the distribution and variability of $\delta^{18}O$ values for weighted precipitation, surface water, and groundwater. The median for groundwater, surface water, and precipitation are -8.78, -8.16, and -6.88‰ respectively. It is noted that the tail ends of the surface water and groundwater plot are pulled by the enriched precipitation. This offset reveals that the isotopic signal of precipitation becomes filtered due to recharge infiltration, evaporation, and evapotranspiration and is reflected in the surface and groundwater. The depleted values in both the surface water and the groundwater are suggested to be primarily due to snowmelt and winter events.

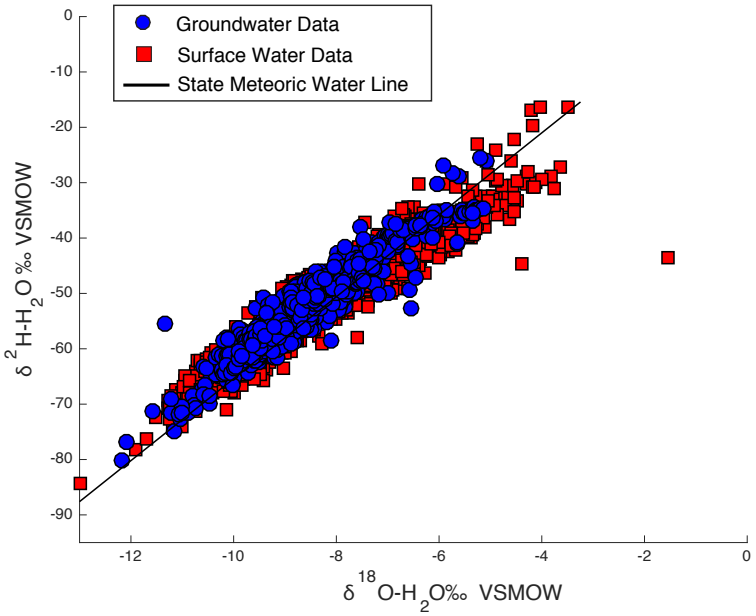

Figure 6.3: Dual isotope plot relating the isotopic composition of groundwater and surface water.

Lc-excess was calculated for both groundwater and surface water to define the number of groundwater and surface water samples that have gone through evaporative enrichment. Negative lc-excess values indicate evaporative enrichment and positive lc-excess values indicate differences in moisture source (Birkel, et al., 2018). From figure 6.4 it can be shown that approximately one quarter and one eighth of surface water and

groundwater samples, respectively, have lc-excess values less than zero. Though it is no surprise that there are more surface water samples with higher lc-excess values than groundwater samples because surface water samples experience more isotopic fractionation than groundwater.

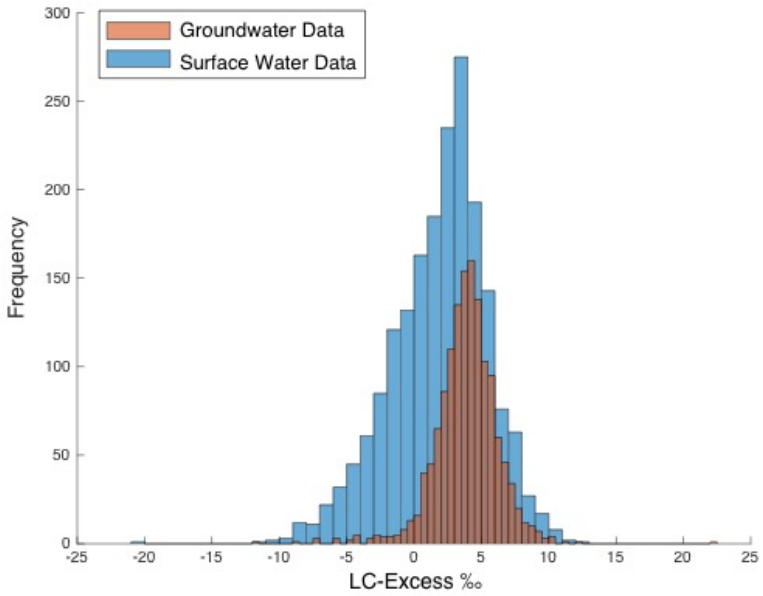

Figure 6.4: Histogram of LC-excess values for both groundwater and surface water.

We found that the SMWL for precipitation to be almost identical to the global meteoric water line. The global meteoric water line (GMWL) is defined as $\delta^{2}H = 8*\delta^{18}O + 10$ and the SMWL is $\delta^{2}H = 7.7*\delta^{18}O + 9.8$. When compared to the GMWL, the slope and y-intercept is less than the GMWL. Differences in slopes could be due to in-cloud processes such as sub-cloud evaporation, evaporation during rainfall, or intensity of rainfall (Ren et al., 2016).

6.2 Seasonal and Hydrologic and Hydrogeologic Effects

6.2.1 Precipitation

Precipitation experiences a seasonal isotopic enrichment and depletion. During the summer and spring months storms are primarily sourced from areas where temperatures are high and the isotopic composition of water vapor are more enriched. The moisture that becomes precipitation is usually sourced from surface water at mid to low latitude oceans where elevation is low and temperatures are high and evaporation occurs from the continents (Welker et al., 2008). During the winter months snow is the primary mode of precipitation. Massachusetts sees Nor'easters, which are storms that are sourced from the Mid-Atlantic and are formed due to the sharp contrast in temperature between the Gulf stream current and the cold air masses from Canada. Due to the formation of these storms, the storms will produce isotopically depleted precipitation. Typically, precipitation events during winter months are sourced from surface water at high latitudes and high elevations where temperatures are cold. For the most part precipitation in the Northeast is sourced from the Gulf of Mexico, Mid-Atlantic, Pacific, Arctic, North Atlantic, and Continental, figure 1.1 (Welker et al., 2000).

Many researchers have determined and documented significant differences between the isotopic compositions of winter versus summer precipitation (Birkel et al., 2018, Freyberg et al., 2018, Dettinger et al., 2000). Birkel et al, 2018 determined the LMWLs for fall, winter, spring, and summer for 22 catchments in Scotland and found that between all the seasons winter had a larger slope than summer. Winter and summer meteoric water line were determined for the 394 precipitation samples in our precipitation isoscape network, figure 3.6. Similar to the findings of Birkel et al., 2018, the slope of the winter meteoric water line is larger than the slope of the summer meteoric water line.

These differences are primarily due to seasonal differences in stormtracks, but can also be due to seasonal changes at the precipitation site (Kendall and Coplen, 2001) and reflect changes in source and temperature during a hydrologic year.

In Massachusetts, there is a seasonal temperature discrepancy between summer and winter months. Average monthly temperatures were collected from the NOAA National Centers for Environmental information, Climate at a Glance: Global Time Series. The average temperature for summer, which is defined as April to September (Jasechko et al., 2014) is 60.8 °F and average winter, which is defined as October to March (Jasechko et al., 2014) temperature is 37.6 °F (NCDC). The temporal dynamics of precipitation $\delta^{18}O$ values are shown in figure 3.11 and figure 3.12. It is documented that air temperature and average two-week weighted monthly $\delta^{18}O$ values have a positive correlation. As temperature increases precipitation becomes isotopically enriched and vice versa. At higher temperatures, the variability is less compared to lower temperatures where there is a larger amount of variability. This is primarily due to seasonal moisture source differences. A comparison of average two-week weighted monthly $\delta^{18}O$ values and average monthly temperature is shown in figure 3.12 as a time series to further exemplify seasonal variability caused by temperature differences. Highest $\delta^{18}O$ values were found during August and the lowest $\delta^{18}O$ values were found during March, figure 3.4.

From March 2018 to July 2018 all 11 precipitation sampling sites experienced a quick-isotopic enrichment, which strayed from the steady, seasonal enrichment and depletion. In order to investigate this quick enrichment seen in all sampling sites, HYSPLIT models, following the methods of Puntsag which are described in *section*

3.1.2., were performed on three sampling sites for the month of March 2018 and June 2018 in CZ1, CZ2, and CZ3: MA-BE-10, BEL314, and MA-NT-1 respectively. Figure 3.9 shows that in the first week of March 2018, all sampling sites experienced precipitation events that originated from a continental source, had a more northerly route and experienced cooler temperatures and more moisture recycling due to the fact that the air mass had a continental pathway.

Figure 3.10 indicates that in the first week of June 2018, sampling sites MA-BE-10, BEL314, MA-NT-1 experienced a precipitation event that originated in the Mid-Atlantic and had a more southerly and direct pathway. Because the air mass stayed over the Atlantic the isotopic signature of the precipitation will be more similar to the GMWL

6.2.2 Surface Water

A seasonal trend was documented for our entire surface water dataset, figure 4.3. Median $\delta^{18}O$ values were determined for each month as shown in figure 4.2. During the summer months (April to September) surface waters experienced isotopic enrichment and during the winter months (October to March) surface waters experienced an isotopic depletion, figure 4.2, figure 4.3. April experienced the lowest $\delta^{18}O$ values while September experienced the highest $\delta^{18}O$ values. Interestingly, as mentioned above summer is defined by the months of April to September and winter is defined by the months of October to March; though it is the month of April that experiences the most isotopic depletion. One possible explanation for this difference is differential recharge or delayed snowmelt (Freyberg et al., 2018). The average temperature of March in Massachusetts is approximately 31°F while the average temperature of April is

approximately 50 °F. This temperature difference could cause snow to melt much later in the winter season and into early spring. Because of the late snowmelt, surface water would experience recharge that has lower $\delta^{18}O$ values. Dettinger and Diaz (2000) found that in the eastern United States the amount of precipitation entering streams is higher during the winter months than the summer months.

Evaporative enrichment via seasonality, surface water type, and precipitation affects the slope the SWL. $\delta^{18}O$ comparisons for each sampling month, figure 4.2, show a large number of surface water samples experience enrichment and plot above the 1% interquartile range. One possible explanation for these outliers are that these samples experienced isotopic fractionation causing sample to become isotopically enriched. Evaporative enrichment either due open water enrichment or a high input of isotopically enriched precipitation. Samples were categorized based on the type of surface water and the $\delta^{18}O$ values of each type were compared (moving bodies of water, stagnant bodies of water, and spring/seepage), figure 4.5. Stagnant bodies of water were more variable than moving bodies of water and spring/seepage, figure 4.4.

In order to investigate whether precipitation or open water enrichment are the primary effects that cause surface water isotopic variability we used the amplitudes calculated from the sine-wave fitted lines in both precipitation and surface water to determine the fraction of young water to precipitation. As defined by Freyberg et al. (2018) the young water fraction is the proportion of catchment discharge that is younger than 2-3 months and can be approximated from the amplitudes of seasonal cycles of stable water isotopes in precipitation and surface water. Young water fractions have been inversely correlated with water table depth and topographic gradients (Jasechko et al.,

2014) and have become a useful value for catchment inter-comparison as well as catchment characteristics as it can be calculated from limited data (Freyberg et al., 2018). By looking at the seasonal isotopic composition of precipitation one can determine the damping and phase shift of the seasonal cycle as it gets propagated through the catchment which can be used to determine the timing of catchments (Freyberg et al., 2018). From Freyberg et al. (2018) higher stream flows will have larger young water fractions as an increase in stream discharge due to rain events will contain more recent precipitation than base flow. Lower stream flows will have smaller young water fractions and will contain more base flow.

From our calculations, the amplitude for precipitation is 2.7 and the amplitude for surface water is 1.13. Using these calculated amplitudes, and following the methods of Freyberg et al. (2018) the young water fraction can be estimated. To calculate the fraction of young water to precipitation we used the following equation below where *Ap* and *As* are the amplitude of precipitation and surface water respectively (Freyberg et al., 2018):

$$\text{Fraction of young water} = As/Ap \tag{10}$$

Using this calculation, we determined the fraction of young water to be 0.4. This value indicates that approximately 40% of total discharge is composed of "young waters" or water that is less than 2-3 months in age.

The young water fraction for groundwater was also determined and calculated to be 0.02‰ which indicates that 2.6% of groundwater is less than 2-3 months in age.

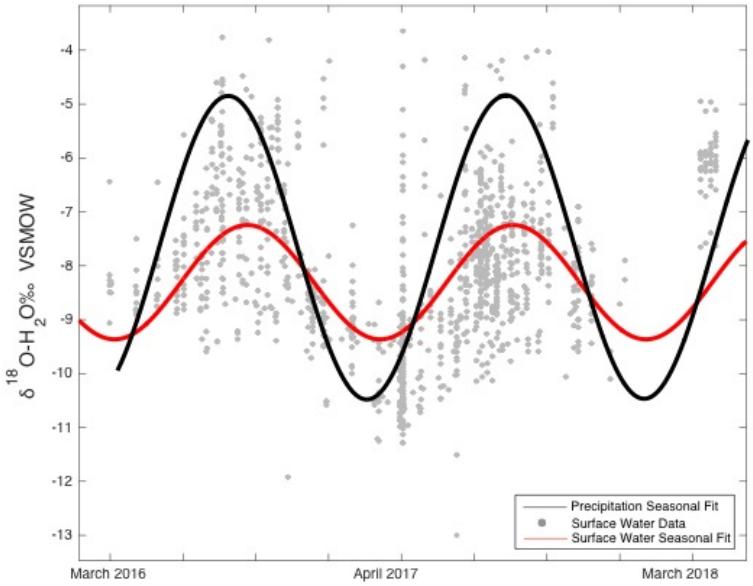

Figure 6.5: Surface water (Red line) and precipitation (black line) seasonal sine wave fitted through the data.

In order to investigate the seasonal relationship between surface water and precipitation, we overlaid the fitted sine wave for both surface water and precipitation, figure 6.5. Figure 6.5 compares seasonal median, minimum, and maximum between precipitation and surface water. Surface water follows the same seasonal enrichment and depletion as precipitation but dampened, with a smaller amplitude. It can also be noted that the phase shift between precipitation and surface water is very small, almost non-existent. From Freyberg et al., 2018, two catchments in Switzerland were correlated, Erlenbach and Dischmabach, where when the seasonal cycles surface water in the Dischmabach watershed experienced a stronger dampening than surface water in the Erlenbach watershed. This is primarily due to a delayed release of depleted winter precipitation from snowpack (Freyberg et al., 2018). A smaller damping also implies a smaller fraction of young water in the stream flow, a smaller proportion of modern water

to base flow (Freyberg et al., 2018). The lack of phase shift between the seasonal cycles of surface water and precipitation along with the calculations to determine the young water fraction, implies that surface water has a higher proportion of modern water to base flow.

Residual corrected model values compiled from Bowen et al, 2011 were compared with our surface water data in order to evaluate how variable our observed values are with modeled isotopic values. Surface water samples and modeled values for both $\delta^{18}O$ and $\delta^{2}H$ were extracted and plotted, figure 4.10 and figure 4.11. A one to one line was used to better compare modeled vs. observed isotopic compositions. Based on our results, our surface water $\delta^{18}O$ and $\delta^{2}H$ values do not agree with the simulated $\delta^{18}O$ and $\delta^{2}H$ values and that samples are biased by higher $\delta^{18}O$ or $\delta^{2}H$ values. From both figures, our surface water $\delta^{18}O$ and $\delta^{2}H$ values are more enriched, than the residually corrected $\delta^{18}O$ and $\delta^{2}H$ values. From figure 4.10 and figure 4.11, many of the data points lie within the seasonal variability range. This further suggests that precipitation-evapotranspiration induced seasonal variability is a primary control on surface water variability. Data points that plot outside of the seasonal range is indicative of open system enrichment (i.e. evaporative enrichment). Our results from figure 4.10 and 4.11 suggests that 90.3% or surface water variability is due to precipitation-evapotranspiration induced seasonality and 9.7% is due to open system induced variability.

6.2.3 Groundwater

In 2014, Jascehko et al. determined the global seasonal groundwater recharge by calculating the seasonal differences in groundwater recharge ratios between the summer and winter seasons at 54 globally distributed locations, one being in eastern Massachusetts. Based on the calculated groundwater recharge ratio, Jasechko et al., 2014, found that groundwater recharge in eastern Massachusetts have winter time groundwater recharge ratios that are consistently higher than summertime recharge ratios. Jasechko et al., 2014 determined that temperate regions, which includes eastern Massachusetts, that a large percent of winter precipitation infiltrates and recharges aquifers relative to summer precipitation. Further work on groundwater recharge should be continued to determine if the groundwater recharge ratios agree with the recharge ratios determined by Jasechko et al., 2014 or if groundwater recharge selectively sees more depleted precipitation events during the non-growing seasons.

Groundwater recharge is affected by aquifer. As mentioned earlier there are four types of aquifers found in Massachusetts: glacial till, glacial fluvial, bedrock, and outwash plains. Each of these aquifers have unique characteristics, properties and isotopic compositions, figure 5.8, figure 5.9. Figure 5.8 and figure 5.9 indicates that outwash plain aquifers have the highest average $\delta^{18}O$ value, glacial till, glacial fluvial, and bedrock have similar average $\delta^{18}O$ values and are the most depleted. It is noted that most of the outliers on figure 5.9 plot higher than the 1% interquartile range, these samples are most likely groundwater that have experienced some sort of fractionation. Outliers that plot below the 1% interquartile range $\delta^{18}O$ value could be representative of the isotopic composition of direct recharge via snow melt. Figure 5.9 shows that

groundwater located in outwash plains are more variable than bedrock, glacial fluvial, and glacial tills. In Massachusetts bedrock aquifers are made up of crystalline rock. They do not recharge quickly as the movement of water is controlled by the existence of secondary openings in the aquifer, which can create long residences time flow paths (Weider and Boutt, 2011). Groundwater in bedrock aquifers have a long residence time because of its low permeability. Till aquifers are located at higher elevations and primarily in recharge areas (Weider and Boutt, 2011). They tend to be thin and consist of unconsolidated material and drain and fill seasonally due to the permeability and porosity of the aquifer material. Stratified glacial fluvial aquifers are found in valleys and areas near streams. They tend to have a larger storage capacity than till aquifers (Weider and Boutt, 2011). In Massachusetts, outwash plains are only found in the south. These hydrogeologic properties as well as their water storage capacity are the determinant factors of groundwater and surface water interaction and may be an implication as to the lack of seasonal variability seen in the groundwater $\delta^{18}O$ values.

Unlike precipitation and surface water, groundwater does not experience a statistically-observable seasonal isotopic enrichment and depletion due to what is known as a reservoir effect which indicates a well-mixed reservoir of groundwater. This lack of seasonal variability can also be due to a small seasonal input which can be further dampened by groundwater residence time being higher than the volume of the groundwater storage. $\delta^{18}O$ values for each sampling month were compared to one another, figure 5.2. In general, the groundwater $\delta^{18}O$ values for each sampling month does not show any significant enrichment or depletion during the summer and winter months respectively, but rather the $\delta^{18}O$ values are fairly constant. This lack of seasonal

variability may suggest that the groundwater in Massachusetts is being dominated by processes occurring in the vadose zone, or local variability due to hydrogeologic properties. Figure 5.3 shows that when a sine-wave line is fit through the groundwater data, there is not a large amount of seasonal variability unlike the variability seen in precipitation and surface water.

Recently there have been studies using the stable $\delta^{18}O$ and $\delta^{2}H$ of mobile and bulk soil water which have suggested an ecohydrological separation of recharge to streams and groundwater, and water used by trees. This has led to what is known as the 'two water worlds' hypothesis which was formulated by McDonnell (2014) (Sprenger et al., 2018; Hervé-Fernández et al., 2016; McCutcheon et al, 2016; Rothfuss and Javaux, 2017). This hypothesis states that mobile water is related to groundwater recharge and sources that sustain streamflow, water that is of a slower flow domain is associated with plant water uptake, bulk water (Sprenger et al, 2018). Soil water dynamics is an important parameter in groundwater isotopic variability as studies have shown that mobile water is isotopically similar to the infiltration of precipitation and bulk soil water reveal an evaporative enrichment signal (Brooks et al., 2009; Goldsmith et al., 2012). Future investigation on site specific monitoring of groundwater and precipitation in Massachusetts will provide more information on the soil water dynamics and water fluxes in the state and to what degree this affects the groundwater isotopic variability.

6.3 Spatial Distribution Average $\delta^{18}O$ values

6.3.1 Precipitation

As mentioned previously, Massachusetts is divided into three climate zones. Samples from the precipitation isoscape network (394 data analyses) were grouped based on geographic location or climate zone Out of our 11 sampling sites only one site was located in CZ1, five sampling sites were located in CZ2 and seven sampling sites were located in CZ3. Average $\delta^{18}O$ values for CZ1, CZ2, and CZ3 were compared with each other, figure 3.15. Based on figure 3.15, average $\delta^{18}O$ values for CZ3 are more enriched than average $\delta^{18}O$ values in CZ1 and CZ2. Average $\delta^{18}O$ values in CZ1 are more depleted than average $\delta^{18}O$ values in CZ2 and CZ3. Recall that this same pattern, where CZ1 is the most depleted and CZ3 is the most enriched is shown in surface water and groundwater. Although our current database has only 11 sampling locations a clear spatial pattern is still visible even with a small database. However, having more sites and a larger database would be more informative and increase the possibility of obtaining more small scale environmental details and the chance to determine more illuminating spatial trends related to local precipitation events and their effects.

The topography of Massachusetts is variable across the state, because of this elevation increases from CZ3 to CZ1. The elevation of CZ3 is 332 meters. The elevation of CZ1 ranges from 67 meters to 223 meters, and the elevation of CZ3 ranges from 4.3 meters to 60 meters. In 1967 Gonfiantini found that elevation and altitude effects isotopic composition and was termed as the 'altitude effect.' As elevation increases δ values decrease. From model simulations, this negative correlation is due to the lowering of temperature and the increase of the condensation rate of atmospheric vapor (Gonfiantini, 1967). Temperate, vertical gradient and the initial relative humidity of the air mass are the parameters that affect the δ values the most.

Two-week weighted averages were determined for each sampling site and compared with its respective elevation. Figure 3.13 indicates that precipitation that fell in CZ1 is the most depleted and precipitation that fell in CZ3 is the most enriched. The one sampling point in CZ1 is located at the highest elevation while sampling sites in CZ3 are located in the lowest elevation. The close $\delta^{18}O$ relationship with elevation, climate zone, moisture source, and temperature, which was previously described, indicate that elevation and topographic location are two parameters that affect the isotopic variability of precipitation. There have been multiple studies that show the altitude effect on a global scale, but this effect is still noticeable on a local scale as seen here.

6.3.2 Surface Water

Along with precipitation, surface water too is inherently subjected to a variety of environmental parameters that affect its stable isotopic composition. By spatially plotting the average $\delta^{18}O$ values in each HUC we find an east to west depletion, where CZ1is more enriched than CZ1 and CZ2. CZ1 is more depleted than CZ2 and CZ3. Average $\delta^{18}O$ for each climate zone was determined and also showed that CZ3 the highest $\delta^{18}O$ value and CZ1 has the lowest $\delta^{18}O$ value. Because the surface water shows the same east to west enrichment, also seen in the precipitation spatial plot, it suggests that surface water reflects the seasonal isotopic variability of precipitation.

Using the ARM 2017 and ARM 2018 dataset, average $\delta^{18}O$ values were determined to further investigate primary controls on the isotopic variability of surface

water. Average $\delta^{18}O$ values for CZ1, CZ2, and CZ3 for ARM 2017, ARM 2018, and precipitation were compared as shown in the dual isotope in figure 6.6.

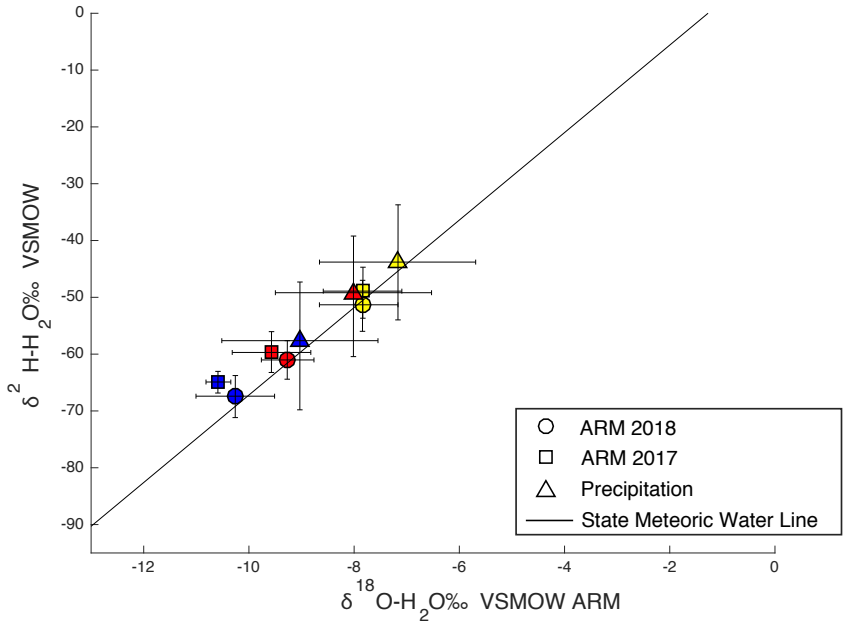

Figure 6.6: Dual isotope plot comparing the average climate zones of ARM 2018 and 2017 samples (130 and 120 respectively) and two-week weighted precipitation isoscape samples (394). Standard deviations for $\delta^{18}O$ and $\delta^{2}H$ are plotted along points. The colors represent the climate zones where CZ1 is blue, CZ2 is red, and CZ3 is yellow.

For all three climate zones, average $\delta^{18}O$ values for precipitation plot higher than the average $\delta^{18}O$ values for ARM 2017 and ARM 2018. Figure 6.6 illustrates that precipitation drives the isotopic variability seen in surface water but also indicates that precipitation is more enriched than surface water in all of the climate zones seen in Massachusetts.

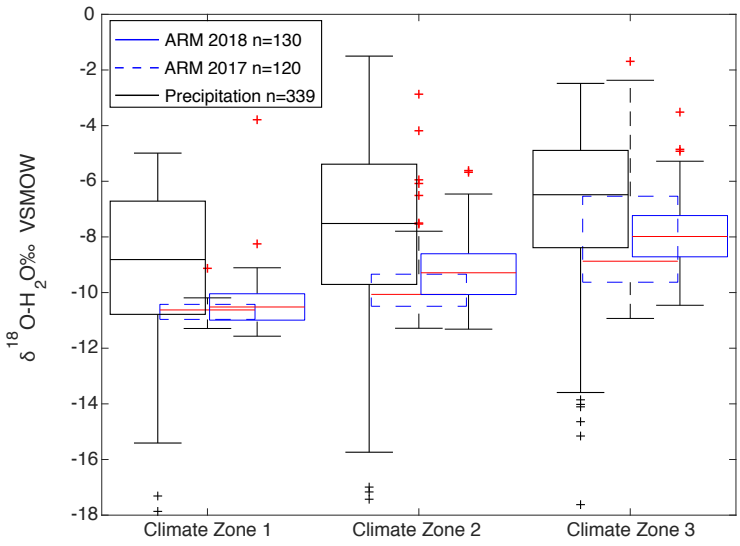

Figure 6.7: Box plot of ARM 2017, ARM 2018, and Precipitation samples grouped by geographic location.

Figure 6.7 shows that the median, minimum, and maximum $\delta^{18}O$ values for precipitation consistently plots higher in CZ1, CZ2, and CZ3 and plots roughly 1-1.5‰ higher than the $\delta^{18}O$ median for ARM 2017 and ARM 2018. The red outliers seen in both ARM 2017 and ARM 2018 are due to samples being in an open water system as seen in figure 4.16. The minimum $\delta^{18}O$ values for precipitation are consistently lower in CZ1, CZ2, and CZ3than ARM 2017 and ARM 2018. This is due to the characteristics of the source of the air mass. Figure 6.7 coupled with figure 6.6 suggests that precipitation is a driver in the surface water isotopic variability.

Average $\delta^{18}O$ values ARM 2017 and 2018 for CZ1, CZ2, and CZ3 were related to the average $\delta^{18}O$ values of precipitation, figure 6.8

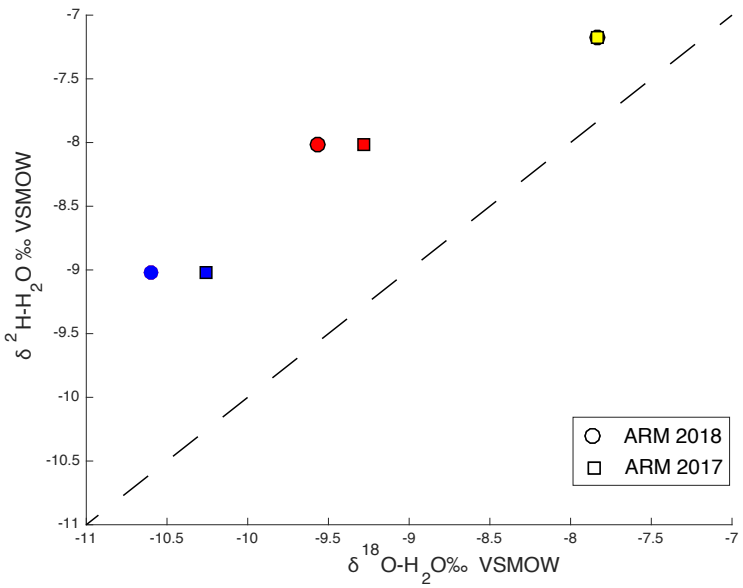

Figure 6.8: $\delta^{18}O$ cross plot of ARM 2018, ARM 2017, and Precipitation. The black dashed line represents the one to one line. The colors represent the climate zones where CZ1 is blue, CZ2 is red, and CZ3 is yellow.

Figure 6.8 shows that all ARM 2017 and ARM 2018 average $\delta^{18}O$ values for CZ1, CZ2, and CZ3 plot above the one to one line, indicating that surface water is being biased by precipitation isotopic variability. This bias causes the surface water to experience seasonal variability as brought on by precipitation. It should be noted that for CZ3, the average $\delta^{18}O$ values for ARM 2018 and ARM 2017 are the same and lie on top of each other.

The $\delta^{18}O$ values were compared as a function of longitude and latitude. From south-north a decreasing trend in $\delta^{18}O$ values is noted, figure 4.7. This depletion is attributed to a temperature gradient. It was observed that when a best fit line was fitted into the dataset, $\delta^{18}O$ values exhibit a positive correlation with increasing latitude. The $\delta^{18}O$ values on figure 4.6 increase as latitude decreases, where the lower latitudinal values represent the western region of Massachusetts and the higher latitudinal values

represent the eastern region of Massachusetts. This relation is most likely due to elevation differences from east to west. This scatter is representative of the isotopic variability of surface water. Even still, this relationship further proves that the pattern of isotopic enrichment from east to west and is spatially coherent.

Lower elevations are located closer to the coast and higher elevations are located further inland. The enrichment from CZ3 to CZ1 may reflect the differences in elevation and temperature gradients between areas located at higher elevations versus areas at lower elevations.

6.3.3 Groundwater

Spatial plots of average $\delta^{18}O$ in each HUC where groundwater samples were taken illustrates similar patterns seen in the spatial plots of precipitation and surface water, figure 5.14. There is an east to west depletion where CZ3 is the most enriched and CZ1 is the most depleted. Figure 5.14 shows the most enriched HUCs are located along the southern coast of Massachusetts where outwash plains are located, based on figure 5.8 and figure 5.9, groundwater in outwash plains are also the most enriched and variable than the other aquifers found in Massachusetts. Figure 5.8 illustrates that average $\delta^{18}O$ value for climate zone 3 is higher than average $\delta^{18}O$ value for CZ1 and CZ2 and average $\delta^{18}O$ value for CZ1 is smaller than average $\delta^{18}O$ values for CZ2 and CZ3.

Based on figure 5.9, because it was noted that samples located in an outwash plain aquifer have the highest amount of variability, the medians, 25^{th} and 75^{th} percentile, and 1% interquartile ranges were determined for each of the aquifer type in CZ1, CZ2, an CZ3, figure 6.9.

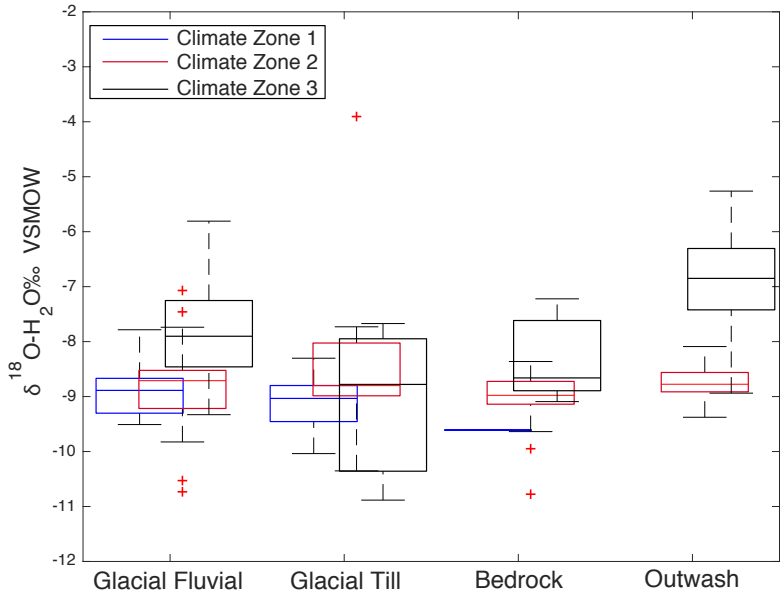

Figure 6.9: Box plot comparison of $\delta^{18}O$ values of aquifers in each climate zone.

Sample $\delta^{18}O$ averages were used for the aquifer versus climate zone comparison. In CZ1, 8, 7, 1, and 0 samples were grouped into glacial fluvial, glacial till, bedrock, and outwash plains. Because of the small number of samples in climate zone 1 it is hard to speculate how much variability is due to aquifer characteristics. Though figure 5.14 does illustrate that glacial fluvial is slightly more enriched than glacial till and bedrock. For CZ2, 68, 19, 37, and 27 samples were grouped into glacial fluvial, glacial till, bedrock and outwash plains. Glacial till is more variable than the other aquifers while outwash plain are the least variable. The median for all of the aquifers are very similar to each other and differ by roughly .3‰. For CZ3, 24, 3, 7, and 26 samples were grouped into glacial fluvial, glacial till, bedrock and outwash plains. Outwash plains and glacial fluvial are the most variable while bedrock is the least variable. It is also noted that glacial fluvial has the highest median and glacial till and bedrock have the lowest.

Between all three climate zones, the $\delta^{18}O$ values are more variable in climate zone 3 though it can be determined that aquifer characteristics plays a role in the isotopic variability of groundwater. Because each climate zone did not have equal number of groundwater samples for each aquifer type there will be bias between aquifers and climate zones that had more samples than those that had fewer.

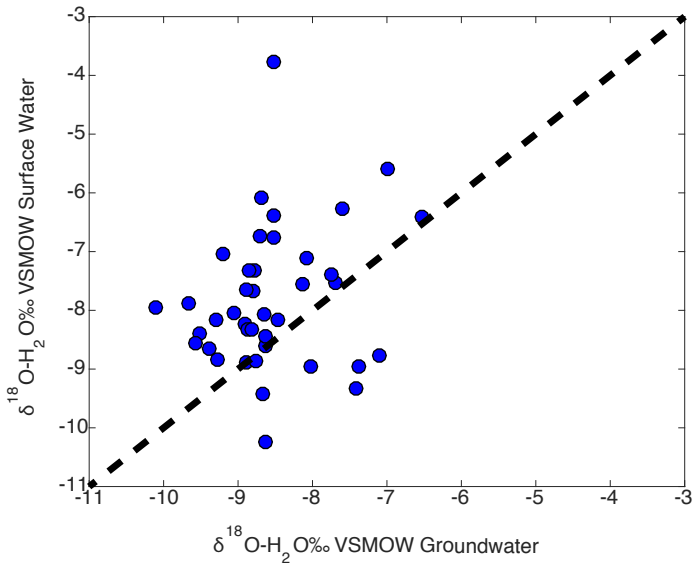

Figure 6.10: $\delta^{18}O$ cross plot of groundwater and surface water. 17.5% of the points lie off the 1:1 line. Surface Water dominates HUC averages.

We also speculated that this spatial variability is due to a high surface water to groundwater interaction which may be attributed to aquifer characteristics. To investigate this, we determined which HUCs had both groundwater and surface water sample sites. We then calculated the ratio of each average HUC $\delta^{18}O$ value of surface water to each average HUC $\delta^{18}O$ value of groundwater, figure 6.10, using the equation below:

$$\text{Ratio} = \frac{\delta_{surface\ water}{}^{18}O}{\delta_{groundwater}{}^{18}O}$$

This allows us to establish whether surface water or groundwater dominance within each HUC. From our calculation, we then compared the $\delta^{18}O$ value for groundwater and surface water, figure 6.10. A one to one line was plotted to determine the percent of points that either plot above or below the line. If the isotopic composition of groundwater and surface water were the same, all points would plot on the one to one line, which, as seen in figure 6.10 is not the case. From figure 6.10, 82.5% of the points lie to the left of the one to one line, which indicates that a majority of the surface water samples are more enriched than the groundwater samples. The points that fall below the line is suggestive of seasonal variability.

Topographically there is an effect on groundwater isotopic signature. From figure 5.7, groundwater samples that are located at higher elevations have lower $\delta^{18}O$ values than groundwater samples located at lower elevations, which may be attributed to source of recharge and the integration of the surface water and precipitation isotopic signatures due to Rayleigh distillation.

Further work into processes occurring in the vadose zone and affects from evapotranspiration can shed more light onto the isotopic variability of groundwater and can further deduce the isotopic composition of groundwater in Massachusetts.

6.3.4 Precipitation, Surface Water, Groundwater Comparison

To better understand the spatial variability between precipitation, surface water, and groundwater, average $\delta^{18}O$ and $\delta^{2}H$ for each climate zone were correlated.

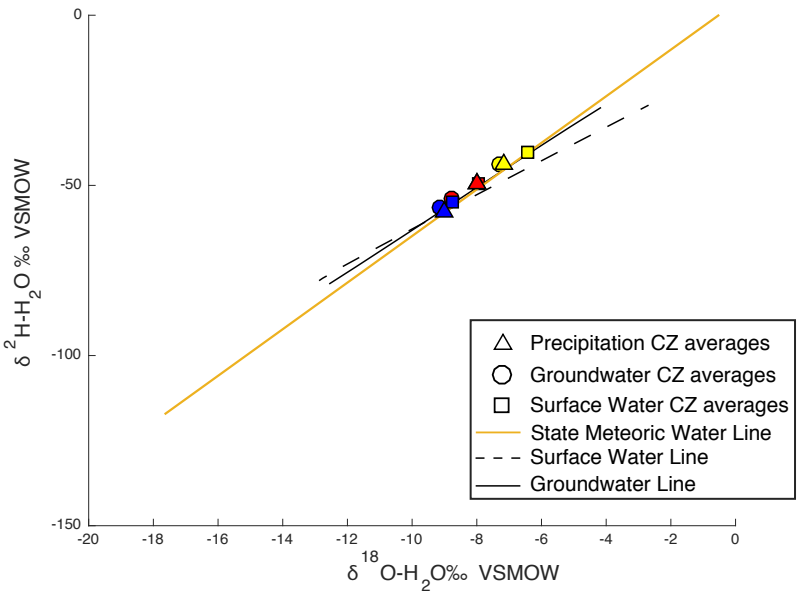

Figure 6.11: Dual isotope plot comparing the average climate zones of precipitation, surface water, and groundwater. The colors represent the climate zones where CZ1 is blue, CZ2 is red, and CZ3 is yellow.

Interestingly when all climate zone averages for precipitation, surface water, and groundwater are plotted together, the average $\delta^{18}O$ and $\delta^{2}H$ values cluster rather well with each other. Values are summarized in Table 6.2.

Variable	Climate Zone 1			Climate Zone 2			Climate Zone 3		
	Mean $\delta^{2}H$ (‰) (st. dev.)	Mean $\delta^{18}O$ (‰) (st. dev.)	Mean d-excess (‰) (st. dev.)	Mean $\delta^{2}H$ (‰) (st. dev.)	Mean $\delta^{18}O$ (‰) (st. dev.)	Mean d-excess (‰) (st. dev.)	Mean $\delta^{2}H$ (‰) (st. dev.)	Mean $\delta^{18}O$ (‰) (st. dev.)	Mean d-excess (‰) (st. dev.)
Precipitation Network	-59.8 (27)	-9.25 (3)	14.2 (3)	-49.2 (24)	-7.9 (3)	13.5 (5)	-43 (23)	-6.92 (3)	11.0 (7)
Surface Water	-54.2 (7)	-8.69 (1)	15.4 (3)	50.3 (8)	8.03 (1)	14.0 (4)	-41.4 (8)	-6.65 (1)	11.8 (4)
Groundwater	-56.3 (5)	-9.11 (.6)	16.5 (2)	-53.3 (7)	-8.71 (0.9)	16.4 (2)	-43.0 (7)	-7.20 (1)	15.3 (3)

Table 6.2: Overall summary of climate zone averages in precipitation, surface water, and groundwater.

The average $\delta^{18}O$ and $\delta^{2}H$ value for groundwater in CZ2 is more depleted than surface water and precipitation. Based on figure 6.11, it is surprising to see average $\delta^{18}O$ and $\delta^{2}H$ for precipitation to be isotopically similar to the averages of groundwater and surface water. Unlike figure 6.6, this comparison of climate zone averages for surface water

takes into account seasonal variability. This likeness between climate zone averages may suggest that there is a high amount of interaction between precipitation, surface water, and groundwater. If the interaction between all three were low, there would be a greater a difference between the averages for each climate zone. As mentioned above, the slope of the GWL is smaller than the slope of the SMWL but larger than the slope of the SWL, figure 6.11 further suggests that because the groundwater averages for CZ1, CZ2 and CZ3 are similar with the averages of precipitation and surface water that groundwater consists of both surface water and precipitation.

When climate zone LMWLs were calculated for precipitation, surface water, and groundwater, figure 3.16, figure 4.14, and figure 5.6, slopes range from 5.3 to 7.8. It is noted that for all three, precipitation, surface water, and groundwater, the slopes from CZ1 to CZ3 gets progressively smaller. The y-intercept for precipitation and surface water becomes progressively larger from CZ1 to CZ3, indicating an increase in d-excess. The y-intercept in groundwater is largest in CZ3 but smallest in CZ2. Similar to the slope of the GWL, the slopes for groundwater in CZ1, CZ2, and CZ3 are smaller than precipitation but larger than surface water. The differences in slopes is most likely to be due to geographic differences between each climate zone.

CHAPTER 7

CONCLUSIONS AND REMARKS

7.1 Conclusions

Isoscapes and isotopic studies are an important tool to better understand hydroclimatic studies and their effects on water resource and water management. The use of stable isotopes has become a low cost, effective tracer mechanism to gain more knowledge on precipitation dynamics, groundwater recharge mechanisms, paleoclimate, and water resource management (Birke et al., 2018). A dataset of 1917 surface water samples, 1405 groundwater samples, and 558 precipitation samples across Massachusetts has been analyzed in terms of seasonal, temporal, spatial, and environmental variability with the aim of determining and explaining the isotopic signature and variability of precipitation, surface water and groundwater for the state of Massachusetts.

A state meteoric water line, surface water line, and groundwater line have been calculated from unweighted precipitation, surface and groundwater analyses. The SMWL is $\delta^{2}H = 7.7\ \delta^{18}O + 9.8$. The SWL is $\delta^{2}H = 5.7\ \delta^{18}O + 4.2$, and the GWL is $\delta^{2}H = 6.6\ \delta^{18}O + 4.0$. SMWL, SWL, and GWL reveal significant differences in slopes and y-intercept, slopes range from 0.9 to 2.0‰. Mean $\delta^{18}O$ and $\delta^{2}H$ values of precipitation vary as a function of moisture source, seasonality, elevation and topographic location. Mean $\delta^{18}O$ and $\delta^{2}H$ values of surface water vary as a function of open vs closed water systems, topographic location, seasonality and precipitation induced seasonality. Mean $\delta^{18}O$ and $\delta^{2}H$ values of groundwater vary as a function of hydrogeologic characteristics and topographic location.

Spatially, $\delta^{18}O$ and $\delta^{2}H$ values for precipitation, surface water, and groundwater illustrate an isotopic separation along an east-west topographic gradient where isotopes are enriched in CZ3, where there is little change in elevation, and depleted in CZ1, where topography varies more, figures 3.17, 4.9, 5.14. This east to west depletion is primarily due to differences in elevation and relative distance from a moisture source. Median $\delta^{18}O$ values from ARM 2017 and ARM 2018 for CZ1, CZ2, and CZ3 were correlated with the median $\delta^{18}O$ values of precipitation. Precipitation median $\delta^{18}O$ values plot consistently higher than both ARM datasets. These results imply that the isotopic signature of precipitation gets filtered due to recharge infiltration, evaporation, and evapotranspiration and is reflected in both the surface water and groundwater.

Following the methods of Freyberg et al., 2018, the calculation of young water fractions for surface waters reveal that roughly 40% of total discharge is composed of water that is less than 2-3 months and that 2.5% of groundwater consists of water that is less than 2-3 months in age. Correlation between river water data that incorporates monthly precipitation isotopic variation for the state Massachusetts, compiled from Bowen et al., 2011 and our surface water analyses illustrate that roughly 90% of our surface water variability is due to precipitation-evapotranspiration induced seasonality and 9% is due to open water system, figure 6.12.

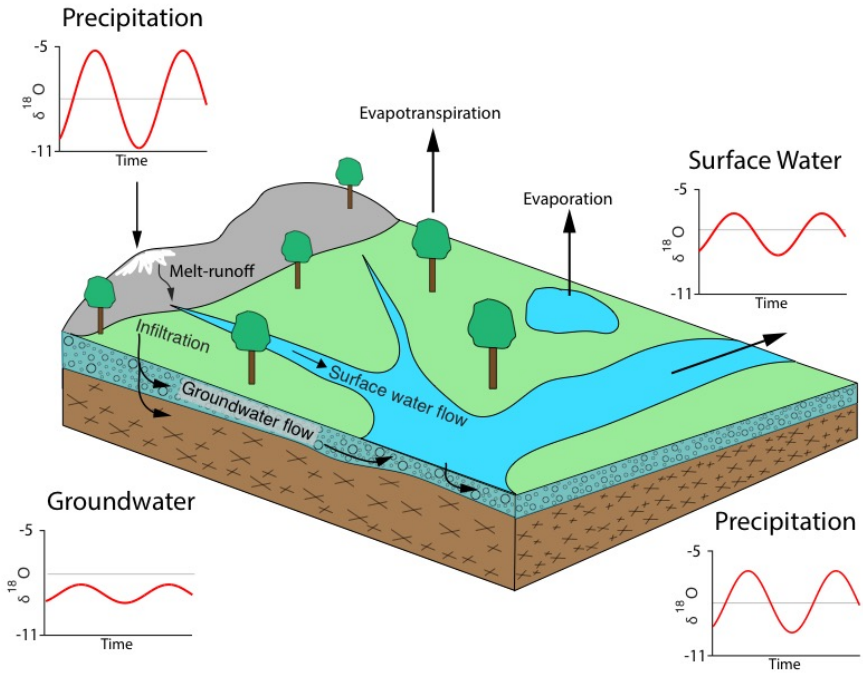

Figure 7.1: Conceptual diagram illustrating the seasonal cycle of precipitation, surface water and groundwater and how surface water and groundwater compares to the amplitude of precipitation which is indicated by the gray line.

In this paper, we have developed a basic characterization and understanding of the isotopic signatures and variability of precipitation, surface water, and groundwater. We have related the interaction between surface water and groundwater and surface water to precipitation and have determined that a large portion of surface water variability is due to precipitation induced seasonality and groundwater variability reflects the dampening of this seasonality, figure 6.12. The good agreement of the spatial patterns in precipitation, surface water, and groundwater will be useful for analyzing the effects of climate change and how these changes are propagated through the hydrological cycle in Massachusetts. Furthermore, by relating the surface water to precipitation and surface waters sensitivity to precipitation isotopic variability it will be useful in analyzing the changes in moisture source and how it is reflected in the stable isotope of surface water. This work has the

potential to answer many more questions about the hydrologic cycle of Massachusetts and how factors such as catchment size, recharge processes in the vadose zone, and climate change can affect the isotopic topic signature of waters throughout the state of Massachusetts. Further work into studying these factors will improve our basic understanding of the hydrological behavior of Massachusetts.

BIBLIOGRAPHY

Ala-aho, P., C. Soulsby, O. Pokrovsky, (2018), Using Stable isotopes to assess surface water source dynamics and hydrological connectivity in a high-latitude wetland and permafrost influenced landscape, Journal of Hydrology, 556, doi: 10.1016/j.jhydrol.2017.11.024.

Akers, P.D., J.M. Welker, (2017), Reassessing the role of temperature in precipitation oxygen isotopes across the eastern and central United States through weekly precipitation-day data, *Water Resources Research*, 53, 7644-7661, doi:10.1002/2017WR020569.

Baskaran, S., T. Ransley, R.S. Brodie, P. Baker, (2009), Investigating groundwater-river interactions using environmental tracers, *Australian Journal of Earth Science,* 56(1):13-19, doi:10.1080/08120090802541887.

Berden, G., R. Peeters, G. Meijer, (2000), Cavity ring-down spectroscopy: Experimental schemes and applications, *Int. Reviews in Physical Chemistry*, 19(4):565-607, doi: 10.1080/01442350075004067.

Botter, G., E. Bertuzzo, A. Rinaldo, (2010), Transport in the hydrologic response: Travel time distributions, soil moisture dynamics, and the old water paradox, *Water Resources Research*, 46(3):1-18, doi: http://dx.doi.org/10.1029/2009WR008371; doi:10.102

Boutt F.D., Assessing hydrogeologic controls on dynamic groundwater storage using long-term instrumental records of water table levels, *Hydrological Processes*, 2017; 31 (7): 1479 doi: 10.1002/hyp.11119.

Bowen, G., C. Kennedy, Z. Liu, J. Stalker, (2011), Water balance model for mean annual hydrogen and oxygen isotope distributions in surface waters of the contiguous United States, *Journal of Geophysical Research*, Vol 38:161-187, doi: 10.1146.

Bowen, G., (2010), Isoscapes: Spatial Pattern in Isotopic Biogeochemistry, *Annual Review of Earth and Planetary Sciences*, Vol 116:1-14, doi: 10.1029/2010JG001581.

Bowen, G. J., J. R. Ehleringer, L. A. Chesson, E. Stange, T. E. Cerling, (2007), Stable isotope ratios of tap water in the contiguous United States, *Water Resources Research,* 43, W03419, doi:10.1029/2006WR005186.

Bowen G. J., J. Revenaugh, (2003), Interpolating the isotopic composition of modern meteoric precipitation, *Water Resources Research,* 39(10), 1299, doi:10.129/2003WR002086.

Brand, W.A., H. Geilmann, E.R. Crosson, C.W. Rella, (2009), Cavity ring-down spectroscopy versus high-temperature conversion isotope ratio mass spectrometry; a case

study on d^2H and $d^{18}O$ of pure water samples and alcohol/water mixtures, *Rapid Commun. Mass Spectrom*, 23: 1879–1884, doi: 10.1002/rcm.4083.
Brooks, J. R., H. R. Barnard, R. Coulombe, J. J. McDonnell, (2009), Ecohydrologic separation of water between trees and streams in a Mediterranean climate, *Nat. Geosci,* 3:100-104doi: 10.1038/ngeo722

Casado, M., A. Cauquoin, A. Landais, D. Israel, A. Orsi, E. Pangui, et al., (2016), Experimental determination and theoretical framework of kinetic fractionation at the water vapour-ice interface at low temperature, *Geochimica et cosmochimica Acta, 174*(Supplement C)*,* 54-69, doi: 10.1016/j,gca.2015.11.009

Celle-Jeanton, H., R. Gonfiantini, Y. Travi, B. Sol, (2004), Oxygen-18 variations of rainwater during precipitation: application of the Rayleigh model to selected rainfalls in Southern France, *Journal of Hydrology*, 289:165-177, doi: 10.1016/j.jhydrol.2003.11.017.

Dansgaard, W., (1964), Stable isotopes in precipitation, *Tellus, A* **16,** 436–468 (1964).

Darling, W.G., A.H. Bath, J.C. Talbot, (2003), The O and H stable isotope composition of freshwaters in the British Isles. 2. Surface water and Groundwater, *Hydrology and Earth System Sciences Discussions*, EGU, 7(2) 183-195.

Dettinger, M. D., H. F. Diaz, (2000), Global Characteristics of Stream Flow Seasonality and Variability, *Journal of Hydrometerology*, 1, 289-310, doi: https://doi.org/10.1175/1525-7541(2000)001<0289:GCOSFS>2.0.CO;2.

Draxler, R. R., G. D. Rolph, HYSPLIT (Hybrid Single-Particle Lagrangian Integrated Trajectory) model access via NOAA ARL
READY website (http://www.arl.noaa.gov/HYSPLIT.php). NOAA Air Resources Laboratory, College Park, MD. NOAA Air
Resources Laboratory (2003).

Dutton, A., B. Wilkinson, J. Welker, et al., (2005), Spatial Distribution and seasonal variation in 18O/16O of modern precipitation and river water across the conterminous USA, *Hydrological Processes*, 19(20): 4121-41446, doi: 10.1002/hyp.5876.

Earman, S., A. R. Campbell, F. M. Phillips, B. D. Newman, (2006), Isotopic exchange between snow and atmospheric water vapor: Estimation of the snowmelt component of groundwater recharge in southwestern United States, *Journal of Geophysical Research*, 111, D09302, doi: 10.1029/205JD006470.

Evaristo, J., S. Jasechko, J. J. McDonnell, (2015), Global Separation of Plant Transpiration from Groundwater and Streamflow, *Nature*, 525(7567): 91-94, doi: 10.1038/nature14983

Fritz, P., R.J. Drimme, S.K. Frape, K. O'Shea, (1987), The Isotopic Composition of Precipitation and Groundwater in Canada, *IAEA,* 299/17: 539-550.

Fetter, C. W., Applied Hydrogeology. Upper Saddle River, NJ: Prentice Hall, 2001. Print. Fitts, Charles R. Groundwater Science. Amsterdam: Academic, 2002. Print.

von Freyberg, J., S.T. Allen, S. Seeger, M. Weiler, J.W. Kirchner, Sensitivity of young water fractions to hydro-climatic forcing and landscape properties across 22 Swiss catchments, *Hydrol. Earth Syst. Sci*., 22, 3841-3861, https://doi.org/10.5194/hess-22-3841-2018, 2018.

Goldsmith, G. R., L. E. Muñoz-Villers, F. Holwerda, J. J. McDonnell, H. Asbjornsen, T. E. Dawson, (2012), Stable isotopes reveal linkages among ecohydrological processes in a seasonally dry tropical montane cloud forest, *Ecohydrology*, 5:779-790, doi: 10.1002/eco.268.

Gonfiantini, R., M. A. Roche, J. C. Olivry, J. C. Fontes, G. M. Zuppi, (2001), The altitude effect on the isotopic composition of tropical rains, *Elsevier*, 181(1-4):147-167, doi: 10.1016/S0009-2541(01)00279-0.

Good, S. P., D. V. Malia, J. C. Lin, G.J. Bowen, (2014), Stable Isotope Analysis of Precipitation Samples Obtained via Crowd sourcing Reveals the Spatiotemporal Evolution of Superstorm Sandy, *PLoS ONE,* 9(3): e91117, doi: 10.1371/journal.pone.0091117.

Hervé-Fernández, P., C. Oyarzún, C. Brumbt, et al., (2016), Assessing the 'two water worlds' hypothesis and water sources for native and exotic evergreen species in south-central Chile, *Hydrological Processes*, 30(23): 4227-4241, doi: 10.1002/hyp.10984.

IAEA, **Environmental isotopes in the hydrological cycle: Principles and applications, Vienna, Austria, 2000.**

Jasechko, S., S. Birks, T. Gleeson, et al., (2014), The pronounced seasonality og flobal groundwater recharge, *Water Resources Research*, 50: 8845-8867, doi: 10.1002/2014WR015809.

Jasechko, S., L. Wassenaar, B. Mayer, (2017), Isotopic evidence for widespread cold-season-biased groundwater recharge and young streamflow across central Canada, *Hydrological Processes*, 31: 2196-2209, doi: 10.1002/hyp.11175.

Kendall, C., T. B. Coplen, (2001), Distribution of oxygen-18 and deuterium in river waters across the United States, *Hydrological processes.,* 15: 1363–1393, doi 10.1002/hyp.217.

Lachniet, M.S., W. P. Patterson (2009) Oxygen isotope values of precipitation and surface waters in northern Central America (Belize and Guatemala) are dominated by

temperature and amount effects, *Earth and Planetary Science Letters*, 284:435-446, doi: 10.1016/j.epsl.2009.05.010

Landais, A., M. Casado, F. Prié et al., (2017), Surface studies of water isotopes in Antarctica for quantitative interpretation of deep ice core data, *Comptes Rendus – Geoscience*, 349(4): 139-150, doi: http://dx.doi.org/10.1016/j.crte.2017.05.003.

Landwehr, J. M., Coplen, T. B., Stewart, D. W., (2014), Spatial, Seasonal, and Source Variability in the Stable Oxygen and Hydrogen Isotopic Composition of Tap Waters throughout the USA, *Hydrological Processes*, 28(21): 5382-5422, doi: 10.1002/hyp.10004.

Lanni, C., McDonnel, J., Hopp, L., Rigon, R., (2014), Simulated effect of soil depth and bedrock topography on near-surface hydrologic response and slope stability, *Earth Surface Processes and Landforms*, 38(2): 146-159, doi: 10.1002/esp.3267.

Lawrence, J. R., S. D. Gedzelman, J. C. White, D. Smiley, P. Lazov, (1982), Storm trajectories in eastern US D/H isotopic composition of precipitation, *Nature,* 296, 638–640.

Lee, J., F. Feng, A. Faiia, et al., (2010), Isotopic evolution of a seasonal snow cover and its melt by isotopic exchange between liquid water and ice, *Chemical Geology*, 270(1-4): 126-134, doi: http://dx.doi.org/10.1016/j.chemgeo.2009.11.011.

Lee, K. S., A. J. Grundstein, D. B. Wenner, et al., (2003), Climate controls on the stable isotopic composition of precipitation in northeast
Asia. *Climate Research,* 23, 137–148, doi: 10.3354/cr023137.

Liu, Z., Bowen G. J., Welker J. M., (2010), Atmospheric Circulation is Reflected in Precipitation Isotope Gradients over the Conterminous United States, *Journal of Geophysical Research Atmospheres*, 115(22): 1-14, doi: 10.1029/2010JD014175.

Maule, C. P., D. D. Chanasyk, K. Muhlenbachs, (1993), Isotopic determination of snow-water contribution to soil water and groundwater, *Journal of Hydrology*, 155:73-91, doi: 10.1016/0022-1694(94)90159-7

McCutcheon, R. J., J. P. McNamara, M. J. Kohn, S. L. Evans, (2016), An evaluation of the ecohydrological separation hypothesis n a semiarid catchment, *Hydrological Processes*, 31:783-799, doi: 10.1002/hyp.11052.

McDonnell, J.J. et al, (2010), How old is stream water? Open questions in catchment transit time conceptualization, modeling and analysis, *Hydrological Process*. 24: 1745-1754, doi: 10.1002/hyp.796.

McGuire, K., J. McDonnell, (2007), Stable isotope tracers in watershed hydrology: in, Michener, R., and Lajtha, K., eds., Stable Isotopes in Ecology and Environmental Science, Blackwell Publishing, Malden, MA.

Munksgaard, N. C., C. M. Wurster, A. Bass, M. I. Bird, (2012), Extreme short-term stable isotope variability revealed by continuous rainwater analysis, *Hydrological Processes*, 26(23), doi: 10.1002/hyp.9505

Penna, D., and 14 others, (2012), Technical Note: Evaluation of between-sample memory effects in the analysis of d^2H and $d^{18}O$ of water samples measured by laser spectroscopes, *Hydrol. Earth Syst. Sci*., 16, 3925–3933, doi: 1-.5194/hess-16-392.

Puntsag, T., M. J. Myron, J. L. Campbell, E. S. Klein, G. E. Likens, W.M. Welker, (2016), Arctic Vortex changes alter the sources and isotopic values of precipitation in northeastern US, *Scientific Report*, 6:22647 doi:10.1038/srep22647.

Reddy, M. M., P. Schuster, C. Kendall, M. B. Reddy, (2006), Characterization of surface and ground water $d^{18}O$ seasonal variation and its use for estimating ground water residence times, *Hydrological Process*, 20: 1753-1772, doi: 10.1002/hpy.5953.

Ren, W., T. Yao, S. Xie, H. You, (2016), Controls on the stable isotopes in precipitation and surface waters across the southeastern Tibetan Plateau, *Journal of Hydrology*, 545: 276-287, doi: 10.1016/j.jhydrol.2016.12.034.

Rodhe, A., L. Nyberg, K. Bishop, (1996), Transit Times for Water in a Small till Catchment from a Step Shift in the Oxygen 18 Content of the Water Input, *Water Resources Research*, 32(12): 3497-3511, doi: 10.1029/95WR01806.

Rothfuss, Y, M. Javaux, (2017), Reviews and syntheses: Isotopic approaches to quantify root water uptake: A review and comparison of methods, *Biogeosciences*, 14: 2199-2224, doi: 10.5194/bg-14-2199-2017.

Satrio, P. S., C. S. Leong, S. Syafalni, (2012), Groundwater Dynamic and Its Interrelationship with River Water of Bandung Basin Using Environmental Isotopes (18-O, 2-H, 14-C), *Modern Applied Sciences*, 6(11):49-59, doi: 10.5539/mas.v6n11p49.

Sjostrom, D. S., J. M. Welker, (2009), The influence of air mass source on the seasonal isotopic composition of precipitation, eastern USA*, Journal of Geochemical Exploration*, 102: 103-112, doi: 10.1016/j.gexplo.2009.03.001.

Smith, G. I., I. Friedman, G. Veronda, C. A. Johnson, (2002), Stable Isotope Composisionts of Water in the Great Bain, United States 3. Comparison of Groundwaters with Modern Precipitation, *Journal of Geophysical Research Atmospheres*, 107(19): 1-15, doi: 10.1029/2001JD000567.

Sprenger, M., H. Leistert, K. Gimbel, et al., (2018), Illuminating hydrological processes at the soil-vegetation-atmosphere interface with water stable isotopes, *Review of Geophysics*, 54(3): 674-704, doi: 10.1002/2015RG000515.

Sprenger, M., D. Tetzlaff, J. Buttle, et al., (2016), Measuring and Modeling Stable Isotopes of Mobile and Bulk Soil Water, *Vadose Zone Journal*, 17(1): 0, doi: https://dl.sciencesocieties.org/publications/vzj/abstracts/17/1/170149.

Stein, A.F., R. R. Draxler, G. D. Rolph, B. J. Stunder, M. D. Cohen, F. Ngan, (2015). NOAA's HYSPLIT atmospheric transport and dispersion modeling system, *Bull. Amer. Meteor. Soc.*, 96, 2059-2077, doi: 10.1175/BAMS-D-14-00110.1.

Stone, B.D., J. R. Stone, M.L. DiGiacomo-Cohen, (2006), Surficial Geologic Map of the Salem-Newburyport East-Wilmington-Rockport 16 Quadrangle Area in Northeast Massachusetts: U.S. Geological Survey Open-File Report 2006-1260B.

Tappa, D. J., M. J. Kohn, S. P. McNamara, S. G. Benner, A. N. Flores, (2016), Isotopic composition of precipitation in a topographically steep, seasonally snow-dominated watershed and implications of variations from the global meteoric water line, *Hydrological Processes*, 30(24), doi: https://doi.org/10.1002/hyp.10940.

Timsic, S., W. P. Patterson, (2014), Spatial variability in stable isotope values of surface waters of Eastern Canada and New England, *Journal of Hydrology*, 511: 594-604, doi: 10.1016/j.jhydrol.2014.02.

Wassenaar, L.I., M. Ahmad, P. Aggarwal, M. van Duren, L. Pöltenstein, L. Araguas, T. Kurttas, (2012), Worldwide proficiency test for routine analysis of d^2H and $d^{18}O$ in water by isotope-ratio mass spectrometry and laser absorption spectroscopy: *Rapid Commun. Mass Spectrom*, 26, 1641–1648, doi: 10.1002/rcm.6270.

Weider, K., and D. Boutt (2011), Heterogeneous water table response to climate revealed heterogeneous water table response to climate revealed by 60 years of ground water data, *Geophysical Research Letters*, 37, doi:10.1029/ 2010GL045,561.

Welker, J. M., (2000), Isotopic ($d^{18}O$) characteristics of weekly precipitation collected across the USA: an initial analysis with application to water source studies. *Hydrological Process*, vol. 14 1449–1464, doi:10.1029/2.

Welker, J. M., (2012), ENSO effects on $\delta^{18}O$, δ^2H and d-excess values in precipitation across the US. using a high-density, long-term network (USNIP). *Rapid Commun. Mass Spectrom.* 15 26(17)**,** 1893–1898, doi: 10.1002/rcm.6298.

West, A. G., E. C. February, G. J. Bowen, Spatial Analysis of Hydrogen and Oxygen Stable Isotopes ('isoscape') in Groundwater and Tap Water across South Africa, *Journal of Geochemical Exploration*, 145: 213-222, doi: http://dx.doi.org/10/1016/j.gexplo.2014.06.009.

Vachon, R. W., J. M. Welker, J. W. C. White, B. H. Vaughn, (2010), Moisture source temperatures and precipitation δ18O-temperature relationships across the United States. *Water Resour. Res.* 46**,** W07523, doi: 10.1029/2009WR008558.

Yeh, H., H. Lin, C. Lee, et al., (2014), Identifying seasonal groundwater recharge using environmental stable isotopes, *Water (Switzerland)*, 6(10): 2849-61, doi: 10.3390/w6102849.